Chemical and structural changes of biomass during pyrolysis and the influence on gasification reactivity in coal-biomass blends

Lihle D Mafu

orcid.org/0000-0001-6817-1277

Thesis submitted in fulfilment of the requirements for the degree *Doctor of Philosophy in Chemistry* at the North-West University

Supervisor:	Prof. H W J P Neomagus
Co-supervisors:	Prof R C Everson
	Prof C A Strydom
	Prof J R Bunt
Graduation:	**19 October 2018**
Student number:	**24873004**

Dedication

This work is dedicated to the loving memory of my beautiful mother, S.C. Mafu. She passed on to be with the Lord on the 27th of July 2006.

Declaration

I, Lihle D. Mafu, hereby declare that this thesis entitled: "**Chemical and structural changes of biomass during pyrolysis and the influence on gasification reactivity in coal-biomass blends**", submitted in fulfilment of the requirements of the degree Ph.D. in Chemistry at the North-West University, is my own work and has not previously been submitted to any other institution in whole or in part.

Signed at Potchefstroom

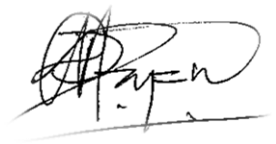

Lihle D. Mafu	18-12-2017
	Date

Preface

Format of thesis

The format of this thesis is in accordance with the academic rules of the North-West University (approved on November 22nd, 2013), where rule A.5.4.2.7 states: "Where a candidate is permitted to submit a thesis in the form of a published research article or articles, or as an unpublished manuscript or manuscripts in article format and more than one such article or manuscript is used, the thesis must still be presented as a unit, supplemented with an inclusive problem statement, a focused literature analysis and integration and with a synoptic conclusion, and the guidelines of the journal concerned must also be included."

Rule A.5.4.2.8 states: "Where any research article or manuscript and/or internationally examined patent is used for the purpose of a thesis in article format to which other authors and/or inventors than the candidate contributed, the candidate must obtain a written statement from each co-author and/or co-inventor in which it is stated that such co-author and/or co-inventor grants permission that the research article or manuscript and/or patent may be used for the stated purpose and in which it is further indicated what each co-author's and/or co-inventor's share in the relevant research article or manuscript and/or patent was."

Rule A.5.4.2.9 states: "Where co-authors or co-inventors as referred to in A.5.4.2.8 above were involved, the candidate must mention that fact in the preface and must include the statement of each co-author or co-inventor in the thesis immediately following the preface."

Format of numbering and referencing

It should be noted that the formatting, referencing style, numbering of tables and figures, and general outline of the manuscripts were adapted to ensure uniformity throughout the thesis. The format of manuscripts which have been submitted and/or published adhere to the author guidelines as stipulated by the editor of each journal, and may appear in a different format to what is presented in this thesis. The headings and original technical content of the manuscripts were not modified from the submitted and/or published versions, and only minor spelling and typographical errors were corrected. The bibliography (reference list) was included at the end of each chapter, and the Appendices.

Supplementary information

Relevant supplementary data, where necessary, were included in Supplementary information subsection(s) after the chapter references.

Nomenclature

The description of the nomenclature (notations/symbols, Greek symbols, and relevant abbreviations) were included in the text following the guidelines of the published and accepted papers, unless stated otherwise. It should be noted that notations/symbols and Greek symbols may vary between chapters, following the format of the published papers.

Letter of consent

To whom it may concern,

The listed co-authors hereby give consent that **Lihle D. Mafu** may submit the following manuscript(s) as part of his thesis entitled: **Chemical and structural changes of biomass during pyrolysis and the influence on gasification reactivity in coal-biomass blends,** for the degree *Philosophiae Doctor in Chemistry,* at the North-West University:

Mafu, L.D., Neomagus, H.W.J.P., Everson, R.C., Carrier, M., Strydom, C.A. and Bunt, J.R., 2016. Structural and chemical modifications of typical South African biomasses during torrefaction. Bioresource Technology. 202, 192–197.

Mafu, L.D., Neomagus, H.W.J.P., Everson, R.C., Strydom, C.A., Carrier, M., Okolo, G.N., Bunt, J.R. 2017. Chemical and structural characterization of char development during lignocellulosic biomass pyrolysis. Bioresource Technology. 243, 941–948.

Mafu, L.D., Neomagus, H.W.J.P., Everson, R.C., Okolo, G.N., Strydom, C.A., Bunt, J.R. 2018. The carbon dioxide gasification characteristics of biomass char samples and their effect on coal gasification reactivity during co-gasification. Bioresource Technology. 258, 70–78.

(This letter of consent complies with rules ***A5.4.2.8 and A.5.4.2.9*** of the academic rules, as stipulated by the North-West University).

06-12-2017

Hein W.J.P. Neomagus — Date

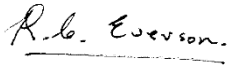

06-12-2017

Raymond C. Everson — Date

06-12-2017

Christien A. Strydom — Date

06-12-2017

John R. Bunt Date

06-12-2017

Marion Carrier Date

04-12-2017

Gregory Okolo Date

List of publications

Journal articles

Mafu, L.D., Neomagus, H.W.J.P., Everson, R.C., Carrier, M., Strydom, C.A., Bunt, J.R., 2016. Structural and chemical modifications of typical South African biomasses during torrefaction. *Bioresource Technology*. 202, 192–197. http://dx.doi.org/10.1016/j.biortech.2015.12.007.

Mafu, L.D., Neomagus, H.W.J.P., Everson, R.C., Strydom, C.A., Carrier, M., Okolo, G.N., Bunt, J.R. 2017. Chemical and structural characterization of char development during lignocellulosic biomass pyrolysis. *Bioresource Technology*. 243, 941–948. http://dx.doi.org/10.1016/j.biortech.2017.07.017.

Mafu, L.D., Neomagus, H.W.J.P., Everson, R.C., Okolo, G.N., Strydom, C.A., Bunt, J.R. 2018. The carbon dioxide gasification characteristics of biomass char samples and their effect on coal gasification reactivity during co-gasification. *Bioresource Technology*. 258, 70–78. https://doi.org/10.1016/j.biortech.2017.12.053.

Conference proceedings

Mafu, L.D., Neomagus, H.W.J.P., Everson, R.C., Carrier, M., Strydom, C.A., **Okolo, G.N.**, Bunt, J.R., 2017. Chemical and structural characterization of char development during lignocellulosic biomass pyrolysis. Presented at the conference on sustainable development of Southern Africa's Energy Resources, Johannesburg, South Africa, November 2017 **(Oral presentation)**.

Mafu, L.D., Neomagus, H.W.J.P., Everson, R.C., Strydom, C.A., Bunt, J.R. 2015. Structural and chemical modifications of typical South African biomasses during torrefaction. Presented at the 20th Southern African Conference on Research in Coal Science and Technology, Potchefstroom, South Africa. November 2015 **(Oral presentation).**

Mafu, L.D., Neomagus, H.W.J.P., Everson, R.C., Strydom, C.A., Bunt, J.R. 2014. The effect of torrefaction on the chemical and structural characteristics of lignocellulosic biomass. Presented at the IEA Clean Coal Technologies. 4th Workshop on co-firing biomass with coal. State College, United States of America, November 2014 **(Oral presentation).**

Mafu, L.D., Neomagus, H.W.J.P., Everson, R.C., Strydom, C.A., Bunt, J.R. 2013. Impact of torrefaction on the fuel characteristics of selected biomass samples. Presented at the 41st SACI convention, East London, South Africa, November 2013 **(Oral presentation).**

Acknowledgements

The author would like to acknowledge and thank the following people/institutions for the various roles played throughout the course of this study"

- My supervisor, Professor Hein Neomagus, for the patience, encouragement and guidance throughout this study. Your belief in my abilities and critical assessment of our work ensured the successful completion of this study,
- My co-supervisors, Professors Ray Everson, Christien Strydom and John Bunt for their valuable input and encouragement throughout the study,
- Dr Marion Carrier for always making herself available for consultations and for the input during manuscript formulation,
- The National Research Fund (NRF) and the North-West University for the financial support,
- My friends in research and outside, Dr Gregory Okolo and Ms Nthabiseng Leokaoke for the lovely interactions, advices and social gatherings during my stay in Potchefstroom.
- The coal research group, Unit of Energy and Technology Systems and the Chemical Resource Beneficiation (CRB) personnel and students for the assistance,
- My family, Muzi, Banele, Lindelwa, Philile, your support and prayers did not go unnoticed; you were a great source of strength for the duration of my studies. Thank you.

The work presented in this Thesis is based on the research financially supported by the South African Research Chairs Initiative of the Department of Science and Technology (DST) and National Research Foundation (NRF) of South Africa (Coal Research Chair Grant No.: 86880, UID85643, UID85632). Any opinion, finding or conclusion or recommendation expressed in this material is that of the author(s) and the NRF does not accept any liability in this regard.

Abstract

In this study, the conversion of biomass for thermochemical energy applications is studied. In the first section, the effect of biomass upgrade, via torrefaction, on the structural and chemical properties of lignocellulosic biomass, was investigated. Three biomass samples; softwood chips (SW), hardwood chips (HW) and sweet sorghum bagasse (SB) were used for this study. SW and HW showed similarities in characteristics in terms of the ultimate and proximate analysis, fibre analysis, X-ray diffraction, solid state ^{13}C nuclear magnetic resonance (NMR) and CO_2 adsorption, whilst these were significantly different for SB. The torrefaction conditions, with a weight loss target of 30%, were determined in a thermogravimetric analyser and then torrefaction experiments were performed in a tube furnace, in a N_2 atmosphere. The torrefaction times, at 260 °C were 110, 100 and 20 minutes for SW, HW and SB respectively. Torrefaction was accompanied by a decrease in the H/C and O/C ratios and a significant increase in the calorific value and fixed carbon. The hemicellulose content was significantly reduced by torrefaction. There were no significant changes for cellulose and lignin amounts after torrefaction. These changes were accompanied by the aromatization of biomass where the net aliphatic fractions were reduced whilst the aromatic fraction increased by approximately 40%, for all biomass samples investigated. The crystallite lattice was also affected by torrefaction, where significant decreases in the crystallite size (L_a) which also resulted in the increases in the micropore volume, were observed. There was a significant micropore surface area increase for SB; from 42 m^2/g for raw SB increasing to 92 m^2/g after torrefaction and insignificant changes were observed for SW and HW after torrefaction. This was as a result of the melting of lignin at torrefaction conditions which were in higher amounts for SW and HW.

The second part of this study included the investigation of the char formation process. Chars were prepared from the torrefied material to final temperatures of 300, 400, 600 and 1100 °C and a holding time of 60 minutes. The progressive decrease in O/C and H/C ratios as temperatures were increased, from torrefaction conditions to 1100 °C, was accompanied by other chemical and structural changes and obtained results were comparable for SW and HW than SB. For all biomass samples, the calorific value (CV) increased from torrefaction conditions (22.3, 22.4 and 23.0 MJ/kg for SW, HW and SB respectively), a maximum observed for chars prepared at 600°C (33.1, 33.7 and 30.1 MJ/kg for SW, HW and SB respectively) and slightly decreased for chars prepared at 1100°C (32.3, 32.1 and 26.6 MJ/kg respectively). This was as a result of the reduction of elemental O (resulted in the initial increase) and then the graphitization of the carbon structure at higher temperatures (resulted in the slight decrease beyond 600°C) This observation was confirmed by wide angle X-ray diffraction carbon fraction analysis (WA-XRD-CFA) data. From WA-XRD-CFA, the increase in crystalline diameter (L_a) was accompanied by decreases in interlayer spacing (d_{002}),

crystalline height (L_c) and the average number of aromatic layers per carbon crystallite (N_{ave}) which was a sign that the carbon lattice was stretchered into sheets as pyrolysis temperature increased. The use of attenuated total reflectance Fourier Transforms infrared (ATR-FTIR) spectroscopy was extended by developing a method of evaluating the aromaticity. Results from this new method were comparable to the well documented ^{13}C NMR method. Data from char samples prepared at 1100 °C did not give any peaks for either method as the bonding between elements was almost completely destroyed. The aromaticity increased from approximately 20% at torrefaction conditions rising to approximately 90 % for chars prepared at 600 °C, for all biomass samples. These findings were accompanied by increases in the degree of aromatic ring condensation $(R/C)_u$ and a decrease in the CH_2/CH_3 ratio and the fraction of amorphous carbon (X_A). As char formation progressed, with increasing pyrolysis temperature, below 600 °C the aromatization process was as a result of the removal of the aliphatic components from the matrix while above 600 °C, the condensation of aromatic bonds was a significant contributor to the aromatization as char forms. From the generated results, correlations between the characteristics were drawn where there were linear correlations between the aromaticity and H/C, $(R/C)_u$ with H/C and a power law could related CH_2/CH_3 with H/C ratio, for all samples with correlation coefficients > 85%.

Chars prepared at 1100 °C were then used to investigate CO_2 gasification under isothermal conditions between 850 and 950 °C in a thermogravimetric analyser. Bituminous coal char samples were prepared at 1100 °C and then gasified for comparison with biomass char. SB had the highest gasification reactivities whilst SW and HW had comparable gasification reactivities while coal char showed the lowest gasification rates. All biomass char gasification resembled catalytic gasification, showing gasification reactivity maximums at conversions above X=0.5. As a result, the gasification reactivities were better predicted by the modified random pore model. It was also observed that the different biomass samples exhibited different values of the structural parameter (ψ), and the empirical constants c and p were similar for all samples whilst the p was varied. The gasification characteristics were related to the char characteristics; surface area, L_a, L_c/d_{002}, H/C and AI_2. The addition of biomass char, to coal char, resulted in increased reactivities (R_i and slightly R_s) for HW and SW compared to coal, however, the addition of SB resulted in an improved gasification reactivity throughout the conversion range (increased R_i, R_s and R_f). The differences in effect, between the woody biomass and SB were a result of the mineral content and the possible interaction between the minerals contributed by coal and biomass.

***Keywords**: Lignocellulosic biomass; biomass upgrade, aromatization, aromatic ring condensation, char formation, co-gasification, modified random pore model.*

Table of Contents

List of Tables

List of Figures

Chapter 1: Introduction

1.1 Background

A stable supply of energy is a critical input factor for socioeconomic development (Herbert and Krishnan, 2016). As a result, with constant efforts to improve the quality of life, combined with the increasing world population, there has been an exponential escalation in energy demand (Baranzini et al., 2013). In the quest to meet the world's energy requirements, the use of fossil fuels for various applications has increased over the years (Gil et al., 2015). However, the conversion of fossil fuels results in the release of CO_2 and other greenhouse gases (GHG) to the atmosphere (Weldemichael and Assefa, 2015). Coal is the most used fossil fuel for energy through gasification, combustion and liquefaction and South Africa is ranked sixth in the world's top consumers of coal (Gupta, 2005; Manoj, 2016; Zhang et al., 2000).

In South Africa, the main coal usage is for electricity generation and coal-to-liquid processes (Alan, 2014; Bunt and Waanders, 2008; Damm and Triebel, 2008). Above 92% of electricity in South Africa is generated through coal combustion processes (Van der Walt et al., 2015) whilst the coal to liquid process is used for the production of synthetic fuels and other chemicals (Dudyński et al., 2015; Ruiz et al., 2013). The use of coal is a significant contributor per capita of CO_2 emissions (Weldemichael and Assefa, 2015), nevertheless the utilisation of coal for energy purposes will continue to play a significant role in the future. With the observed depletion of reserves, increasing environmental pollution by GHGs and stringent international climate change policies, the growing calls for the inclusion of alternative sources of fuel in the energy mix cannot be ignored. As a signatory to the United Nations Framework Convention on Climate Change (UNFCC) and the Kyoto protocol, South Africa, and many SADC countries, is expected to play a significant role in the stabilization of GHG concentrations, amongst other objectives, whilst ensuring a stable supply of energy to its populace (Dalton et al., 2008). To achieve this, renewable energy is a viable option, which is achievable in the short-term.

Renewable energy, which includes wind energy, hydro-power, solar energy as well as biomass energy, is considered to be carbon neutral and low cost (Almeida et al., 2010; Tumuluru et al., 2011). In recent years, research efforts have been dedicated into how the available renewable energy options can be used to reduce CO_2 and other GHG emissions into the atmosphere (Arregi et al., 2016; Masnadi et al., 2015; Wannapeera and Worasuwannarak, 2012). Many countries have invested in renewable energy and this has resulted in regional policies such as the European energy policy which compels all EU member countries to achieve 20% renewable energy mix by

2020 (Langsdorf, 2011). South Africa has also made a commitment to achieve 21% renewables by 2030 (Langsdorf, 2011; Van der Walt et al., 2015). However, to date, current energy generation in South Africa is dominated by non-renewable sources (Figure 1.1) (Alan, 2014; Van der Walt et al., 2015).

Since idle biomass also emits greenhouse gases that are harmful to the environment, the utilisation of forest and agricultural wastes eliminates the release of the gases and reduce emissions during energy production (Sami et al., 2001). Wood and forest residues produced in South Africa are approximately 9.2 Mtons per year whilst sugarcane bagasse accounts for 7.5 Mton per year (Vosloo, 2013, Aboyade et al., 2011).

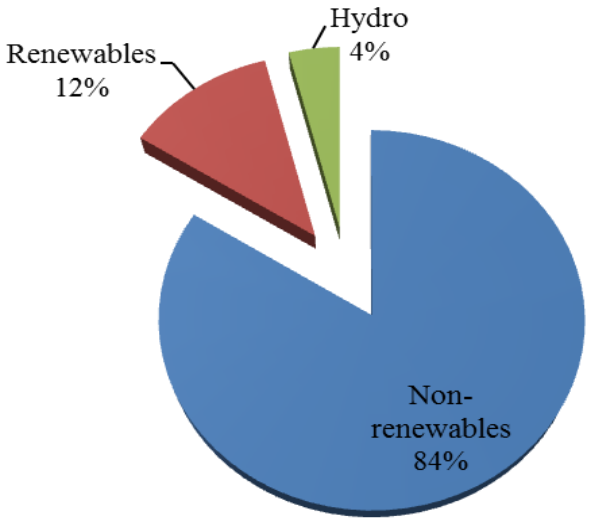

Figure 1-1: The achieved energy mix in South Africa by June 2015 (Adapted from Alan, 2014)

Biomass has emerged as the most important source of energy in several countries (Almeida et al., 2010). Municipal waste, wood waste, agricultural waste and energy crops have been investigated for energy application purposes (Aboyade et al., 2012; Rehrah et al., 2015). All these feedstocks are useful in different applications, based on their characteristics. For instance, agricultural wastes had higher efficiencies in the production of liquid fuels through pyrolysis or digestion (Gunaseelan, 1997; Inyang et al., 2010). Lignocellulosic materials, such as wood chips and bagasse, have found applications through pyrolysis, combustion and gasification to produce useful products (Arregi et al., 2016; Fisher et al., 2012). However, they have low energy density, their chemical and structural characteristics are significantly varying and are available seasonally (Tumuluru et al., 2012; Wikberg and Maunu, 2004). These features of lignocellulosic biomass

present an efficiency problem for stand-alone biomass power generators (Field et al., 2008; Herbert and Krishnan, 2016).

Various pre-treatment methods have been engaged for the upgrade of biomass' fuel properties (Tumuluru et al., 2012). These include washing, steam explosion, hydrothermal carbonization, torrefaction and various densification methods (Dudyński et al., 2015; Liu et al., 2013; Sasaki, 2003; Tumuluru et al., 2012). Torrefaction, often referred to as low temperature pyrolysis, has shown great potential for use a pre-step for thermochemical applications and it significantly improves the mass energy density and hydrophobicity of lignocellulosic biomass (Anupam et al., 2016). The fuel upgrade by torrefaction also results in improved fuel generation efficiencies (Prins et al., 2006). Fuel upgrade of lignocellulosic biomass is accompanied by the degradation of the most heat sensitive fibres; hemicellulose and non-structural carbohydrates which also reduces 'smoking'. The change in fibre composition is accompanied by changes in the characteristics of lignocellulosic biomass (Wannapeera and Worasuwannarak, 2012) which include a decrease in elemental O and H whilst C and the calorific value, increase (Tumuluru et al., 2011; Wannapeera et al., 2011; Wannapeera and Worasuwannarak, 2012). However, techniques such as wide-angle X-Ray diffraction carbon fraction analysis (WA-XRD-CFA) spectroscopy, Nuclear Magnetic Resonance (NMR) spectroscopy and CO_2 adsorption have not been exhaustively employed to monitor the effect of torrefaction on the structure.

The use of ^{13}C NMR spectroscopy and WA-XRD-CFA has been used in various studies for the different carbon functionality quantification and crystalline structure of biomass samples. The study aimed at exploring the use of all these techniques to track the aromatic composition of biomass samples and subsequent changes as chars are prepared. The study also sought to examine the link between ultimate analysis and the advanced structural characteristics as drawn from XRD, ^{13}C NMR and CO_2 adsorption to allow an estimation of certain characteristics (aromaticity, fraction of amorphous carbon and etc) from the easily extracted ultimate analysis results. ATR-FTIR spectroscopy is a rapid characterization technique and more information could be extracted from it that may be validated by results from well-established ^{13}C NMR and XRD techniques for structural parameters. The impact of the char characteristics; pore size, micropore surface area and carbon crystallite properties, play a role during gasification and this study investigates the characteristics that significantly impact the gasification reactivities as well as co-gasification with coal.

Gasification is one route through which biomass may be converted into value added products (Dudyński et al., 2015). The gasification process may be sub-divided into; pyrolysis zone, combustion zone and the gasification zone (Patra and Sheth, 2015). In South Africa, fixed bed dry bottom (FBDB) gasification is still in use and typically, temperatures in the pyrolysis zone may rise up to 1000°C at relatively low heating rates (10 – 20°C/min) (Skhonde et al., 2009). In the pyrolysis zone, the feedstock is converted into char and char characteristics are dependent on the pyrolysis conditions and the biomass origin. For instance, different woody biomass have slightly similar characteristics and it is expected that for similar characteristics, combustion, pyrolysis and gasification properties would be similar (Kataki and Konwer, 2001; Wannapeera and Worasuwannarak, 2012). A correlation has also been drawn between the aromaticity, elemental composition and carbon fraction analysis with pyrolysis conditions (temperature, time and heating rate) (Guerrero et al., 2005; Kim et al., 2012; Uchimiya et al., 2011). The cost attached to the use of some analytical techniques is expensive and this is a limitation towards comprehensively understanding biomass characteristics. As a result, the use of cheaper alternatives has to be maximised. This advocates for a systemic correlation of characteristics extracted from the characterization of biomass. The char formation process for biomass is scantily investigated, from low temperature pyrolysis to high temperatures, compared to studies reported for coal (Roberts et al., 2015).

In the gasification zone, high reactivities are recorded for biomass. This has been alluded to the composition of the ash, even though lignocellulosic biomass has low ash amount (Suarez-Garcia et al., 2002). Biomass ash is rich in K, Ca; known for their catalytic function, whilst having low amounts of Si and Al reported to hinder the gasification reactivity (Zhang et al., 2010). In addition, the high volatile matter in biomass results in soot formation, the radiation phenomenon and the production of high amounts of tars during conversion for thermochemical applications though pyrolysis and gasification (Ruiz et al., 2013; Tumuluru et al., 2012). Nonetheless, most of the shortcomings of biomass conversion may be resolved by biomass-coal co-gasification which reduces the disadvantages of using the individual feedstock whilst exploiting the advantages of the separate fuels (Taba et al., 2012).

The addition of up to 30% biomass to coal could achieve the integration of biomass in energy production without significant changes in infrastructure (Taba et al., 2012). Biomass has significantly different fuel characteristics than coal and consequently the use of biomass in the current infrastructure will result in less efficient thermochemical conversion of the feedstock to value added products. Since the inorganic elements in biomass play a catalytic role during

gasification, the addition of biomass to coal, in low quantities, provides the coal gasification reaction with a cheap catalyst whilst reducing the consumption of coal in the already available infrastructure. In addition, the use of waste biomass for energy applications mitigates greenhouse gases from the environment in two ways. Biomass left in landfills for longer periods breaks down releasing CO_2 and may release CH_4, NH_3 and H_2S through anaerobic means (Van Loo and Koppejan, 2008 and Sami et al., 2001). It is also documented that biomass co-combustion has reduced SO_2 by up to 75% and NO_x by 15% (Van Loo and Koppejan, 2008). The emission factor of CO_2, SO_2 and NO_x of forest residues is approximately 24, 0.06 and 0.57 g/KWh against 955, 11.8 and 4.3 g/KWh for coal, respectively (Boyle, 2014). As such, assuming at least weighted averages, the emissions during co-gasification should be lower than during coal gasification.

1.2 Aims and objectives

Aim:

This study seeks to investigate the comparative characteristic changes of three biomass samples abundantly available in South Africa as they undergo torrefaction and pyrolysis, correlate the final char characteristics to observed CO_2 char gasification reactivity and co-gasification performance.

This will be achieved by addressing the following specific objectives:

- Investigate and compare the chemical and structural properties of three biomass samples; softwood chips, hardwood chips and sweet sorghum bagasse,
- Follow the characteristics changes on the different biomass samples after torrefaction,
- Evaluate, chemically and structurally, the char formation from torrefied biomass to chars prepared at 1100°C,
- Draw correlations between the different biomass and biomass char characteristics and
- Correlate the char characteristics with the reactivities of biomass CO_2 char gasification and assess the impact of adding up to 30% biomass during co-gasification.

1.3 Scope and outline of Thesis

This thesis is organised into 6 chapters.

This thesis is introduced in Chapter 1. It contains a brief background description, including a motivation, and the aims and objectives of the study.

The literature review is given in Chapter 2. Published investigations in the areas of torrefaction, pyrolysis, gasification and co-gasification are analysed.

Results from the changes in characteristics after the torrefaction of biomass targeting a 30% mass loss will be discussed in Chapter 3. This will include results from ultimate and proximate analysis, fibre analysis, Thermogravimetric analysis (TGA), X-Ray Diffraction (XRD), CO_2 adsorption and solid state ^{13}C Nuclear Magnetic Resonance (NMR) spectroscopy.

The char development will be investigated by mapping the characteristics of chars prepared from torrefied biomass at the following temperatures; 300, 400, 600 and 1100°C and the results and discussion will form Chapter 4.

Chars prepared at 1100°C, both biomass and coal, will be gasified in a small particle TGA and kinetics evaluated. Available kinetic models will be fitted into the experimental data and kinetic parameters investigated. Further, the co-gasification of biomass char and coal char at 1:9, 2:8 and 3:7 ratios will be investigated and the reaction kinetics and kinetic model fitting studied. In the thesis, this will form Chapter 5. Characterization results from Chapter 4 will be used to understand the gasification and co-gasification characteristics of this chapter.

Chapter 6 will outline and discuss conclusions reached from the results of this study. Recommendations drawn from the reached conclusions will be aimed at future works in the area of biomass energy.

References

Aboyade, A.O., Carrier, M., Meyer, E.L., Knoetze, J.H., Görgens, J.F., 2012. Model fitting kinetic analysis and characterisation of the devolatilization of coal blends with corn and sugarcane residues. Thermochim. Acta 530, 95–106.

Aboyade, A. O., Hugo, T. J., Carrier M., Meyer, E. L., Stahl, R., KNoetze, J. H., Gorgens J. F., 2011. Non-isothermal kinetic analysis of the devolatilization of corn cobs and sugarcane bagasses in an inert atmosphere. Thermochimica Acta. 517, 81-89.

Alan, B., 2014. The agricultural sector as a biofuels producer in South Africa. Understanding the Food Energy Water Nexus. WWF-SA, South Africa.

Almeida, G., Brito, J.O., Perré, P., 2010. Alterations in energy properties of eucalyptus wood and bark subjected to torrefaction : The potential of mass loss as a synthetic indicator. Bioresour. Technol. 101, 9778–9784.

Anupam, K., Sharma, A.K., Lal, P.S., Dutta, S., Maity, S., 2016. Preparation, characterization and optimization for upgrading Leucaena leucocephala bark to biochar fuel with high energy yielding. Energy 106, 743–756.

Arregi, A., Lopez, G., Amutio, M., Barbarias, I., Bilbao, J., Olazar, M., 2016. Hydrogen production from biomass by continuous fast pyrolysis and in-line steam reforming. RSC Adv. 6, 25975–25985.

Baranzini, A., Weber, S., Bareit, M., Mathys, N.A., 2013. The causal relationship between energy use and economic growth in the United States. Energy Econ. 36, 464–470.

Boyle, G,. 2012. Renewable Energy: Power for a Sustainable Future. 3rd ed.. Oxford: Oxford University Press and Open University.

Bunt, J.R., Waanders, F.B., 2008. Identification of the reaction zones occurring in a commercial-scale Sasol-Lurgi FBDB gasifier. Fuel 87, 1814–1823.

Dalton, G.J., Lockington, D.A., Baldock, T.E., 2008. Feasibility analysis of stand-alone renewable energy supply options for a large hotel. Renew. Energy 33, 1475–1490.

Damm, O., Triebel, R., 2008. A Synthesis Report on Biomass Energy Consumption and Availability in South Africa A report prepared for ProBEC by by Dr Oliver Damm and Ralph Triebel.

Dudyński, M., van Dyk, J.C., Kwiatkowski, K., Sosnowska, M., 2015. Biomass gasification:

Influence of torrefaction on syngas production and tar formation. Fuel Process. Technol. 131, 203–212.

Field, C.B., Campbell, J.E., Lobell, D.B., 2008. Biomass energy: the scale of the potential resource. Trends Ecol. Evol. 23, 65–72.

Fisher, E.M., Dupont, C., Darvell, L.I., Commandré, J.M., Saddawi, A., Jones, J.M., Grateau, M., Nocquet, T., Salvador, S., 2012. Combustion and gasification characteristics of chars from raw and torrefied biomass. Bioresour. Technol. 119, 157–165.

Gil, M.V., García, R., Pevida, C., Rubiera, F., 2015. Grindability and combustion behavior of coal and torrefied biomass blends. Bioresour. Technol. 191, 205–212.

Guerrero, M., Ruiz, M.P., Alzueta, M.U., Bilbao, R., Millera, A., 2005. Pyrolysis of eucalyptus at different heating rates : studies of char characterization and oxidative reactivity. J. Anal. Appl. Pyrolysis 74, 307–314.

Gunaseelan, V.N., 1997. Anaerobic digestion of biomass for methane production: A review. Biomass and Bioenergy 13, 83–114.

Gupta, R.P., 2005. Coal research in Newcastle — past, present and future 84, 1176–1188.

Herbert, G.M.J., Krishnan, A.U., 2016. Quantifying environmental performance of biomass energy. Renew. Sustain. Energy Rev. 59, 292–308.

Inyang, M., Gao, B., Pullammanappallil, P., Ding, W., Zimmerman, A.R., 2010. Biochar from anaerobically digested sugarcane bagasse. Bioresour. Technol. 101, 8868–8872.

Kataki, R., Konwer, D., 2001. Fuelwood characteristics of some indigenous woody species of north-east India. Biomass and Bioenergy 20, 17–23.

Kim, H.K., Kim, J., Cho, T., Choi, W.J., 2012. Influence of pyrolysis temperature on physicochemical properties of biochar obtained from the fast pyrolysis of pitch pine (*Pinus rigida*). Bioresour. Technol. 118, 158–162.

Langsdorf, S., 2011. EU Energy Policy : From the ECSC to the Energy Roadmap 2050, Green European Foundation.

Liu, S., 2010. Woody biomass : Niche position as a source of sustainable renewable chemicals and energy and kinetics of hot-water extraction/hydrolysis. Biotechnol. Adv. 28, 563–582.

Liu, Z., Qin, L., Pang, F., Jin, M., Li, B., Kang, Y., Dale, B.E., Yuan, Y., 2013. Effects of biomass particle size on steam explosion pretreatment performance for improving the

enzyme digestibility of corn stover. Ind. Crop. Prod. 44, 176–184.

Mafu, L.D., Neomagus, H.W.J.P., Everson, R.C., Carrier, M., Strydom, C.A., Bunt, J.R., 2016. Structural and chemical modifications of typical South African biomasses during torrefaction. Bioresour. Technol. 202, 192–197.

Manoj, B., 2016. A comprehensive analysis of various structural parameters of Indian coals with the aid of advanced analytical tools. Int. J. Coal Sci. Technol. 3, 123–132.

Masnadi, M.S., Grace, J.R., Bi, X.T., Lim, C.J., Ellis, N., 2015. From fossil fuels towards renewables: Inhibitory and catalytic effects on carbon thermochemical conversion during co-gasification of biomass with fossil fuels. Appl. Energy 140, 196–209.

Patra, T.K., Sheth, P.N., 2015. Biomass gasification models for downdraft gasifier: A state-of-the-art review. Renew. Sustain. Energy Rev. 50, 583–593.

Prins, M.J., Ptasinski, K.J., Janssen, F.J.J.G., 2006. More efficient biomass gasification via torrefaction. Energy 31, 3458–3470.

Rehrah, D., Bansode, R.R., Hassan, O., Ahmedna, M., 2015. Physico-chemical characterization of biochars from solid municipal waste for use in soil amendment. J. Anal. Appl. Pyrolysis 118, 42–53.

Roberts, M.J., Everson, R.C., Neomagus, H.W.J.P., Okolo, G.N., Van Niekerk, D., Mathews, J.P., 2015. The characterisation of slow-heated inertinite- and vitrinite-rich coals from the South African coalfields. Fuel 158, 591–601.

Ruiz, J.A., Juarez, M.C., Morales, M.P., Munoz, P., Mendivil, M.A., 2013. Biomass gasification for electricity generation : Review of current technology barriers. Renew. Sustain. Energy Rev. 18, 174–183.

Sami, M., Annamalai, K., Wooldridge, M., 2001. Co-firing of coal and biomass fuel blends. Progress in Energy and Combustion Science. 27, 171-214.

Sasaki, M., 2003. Fractionation of sugarcane bagasse by hydrothermal treatment. Bioresour. Technol. 86, 301–304.

Skhonde, M.P., Matjie, R.H., Bunt, J.R., Strydom, A.C., Schobert, H., 2009. Sulfur Behavior in the Sasol-Lurgi Fixed-Bed Dry-Bottom Gasification Process. Energy & Fuels 23, 229–235.

Suarez-Garcia, F., Martinez- Alonso, A., Fernandez Llorente, M., Tascon, J.M.., 2002. Inorganic matter characterization in vegetable biomass feedstocks. Fuel 81, 1161–1169.

Taba, L.E., Faisal, M., Ashri, W., Wan, M., Chakrabarti, M.H., 2012. The effect of temperature on various parameters in coal , biomass and Co-gasification : A review. Renew. Sustain. Energy Rev. 16, 5584–5596.

Tumuluru, J.S., Hess, J.R., Boardman, R.D., Wright, C.T., Westover, T.L., 2012. Formulation, pretreatment, and densification options to improve biomass specifications for co-firing high percentages with coal. Ind. Biotechnol. 8, 113–133.

Tumuluru, J.S., Sokhansanj, S., Hess, J.R., Wright, C.T., Boardman, R.D., 2011. A review on biomass torrefaction process and product properties for energy applications. Ind. Biotechnol. 7, 384–402.

Uchimiya, M., Wartelle, L.H., Klasson, K.T., Fortier, C.A., Lima, I.M., 2011. Influence of pyrolysis temperature on biochar property and function as a heavy metal sorbent in soil. J. Agric. Food Chem. 59, 2501–2510.

Van der Walt, M.-L., Masangane, P., Balmer, M., Qase, N., 2015. State of Renewable Energy in South Africa.

Van Loo, S. and Koppejan, J., 2008. The Handbook of Biomass Combustion and Co-Firing. Earthscan, London.

Vosloo, A. C., 2013. Bio-energy in Southern Africa? A commodity bussiness perspective. Sasol's public presentation.

Wannapeera, J., Fungtammasan, B., Worasuwannarak, N., 2011. Effects of temperature and holding time during torrefaction on the pyrolysis behaviors of woody biomass. J. Anal. Appl. Pyrolysis 92, 99–105.

Wannapeera, J., Worasuwannarak, N., 2012. Upgrading of woody biomass by torrefaction under pressure. J. Anal. Appl. Pyrolysis 96, 173–180.

Weldemichael, Y., Assefa, G., 2015. Assessing the energy production and GHG (greenhouse gas) emissions mitigation potential of biomass resources for Alberta. J. Clean. Prod. 112, 4257–4264.

Wikberg, H., Maunu, S.L., 2004. Characterisation of thermally modified hard- and softwoods by ^{13}C CPMAS NMR. Carbohydr. Polym. 58, 461–466.

Zhang, J., Yuan, J., Sheng, C., Xu, Y., 2000. Characterization of coals utilized in power stations of China 79, 95–102.

Zhang, Y., Hara, S., Kajitani, S., Ashizawa, M., 2010. Modeling of catalytic gasification kinetics of coal char and carbon. Fuel 89, 152–157.

Chapter 2: Literature review

2.1 Introduction

The importance of understanding structural characteristics of biomass, coal and prepared char samples cannot be overemphasized. This information becomes valuable in understanding gasification and possible co-gasification properties of biomass and coal. This chapter presents a review on the available literature on biomass for energy. It includes thermochemical conversion processes, characterization, gasification and gasification kinetic modelling.

2.2 Biomass for energy

Historically, biomass has been a significant source of energy through traditional conversion during heating, cooking and lighting at household level (Liu, 2010; Malico et al., 2015). There is a renewed interest into biomass which may be viewed as revitalization in the wake of the need for renewable energy to play a significant role in the global energy mix and / or supply. Depending on the available feedstock and its characteristics, biomass has been used in the production of liquid biofuels such as bioethanol, methanol, biomethane, biodiesel as well as for electricity and heating purposes (Basu et al., 2011; Chen and Fu, 2016; Guerrero et al., 2005; Naik et al., 2010). Based on the chemical and structural characteristics, different biomass samples are better suited for different fuel applications (Rosillo-Calle, 2016). Current technologies for both domestic and industrial heating purposes have been using up to 67% residues and wastes and 33% lignocellulosic energy crops, whilst for electricity generation, up to 50% of feedstock can be energy crops and residues and wastes, the rest (Van der Walt et al., 2015).

The interest into biomass for energy purposes has also received renewed attention because of its environmentally friendly characteristics. Even though biomass may emit CO_2 of comparable levels to that of coal, the carbon neutrality sets it apart (Painuly, 2001). The emissions from biomass use are offset by the shorter cycle of the emitted CO_2 compared to that from coal use (Basu et al., 2011). CO_2 emissions during energy generation is currently being addressed technologically by proposing methods of burning coal and capturing and sequestrating CO_2, so that it does not reach the environment in large amounts (Basu et al., 2011; Cannell, 2002; Weldemichael and Assefa, 2015). However, in most cases, this may result in the escalation of generation costs. Recent research has shown that CO_2 emission reductions are more a function of technological progress than a feedstock dependent parameter (Ahmed et al., 2016a). This means that, even though the feedstock plays a role, the technological designs of gasifiers, digesters and

boilers have a significant impact. Renewable energy use also reduces the depletion of fossil fuels.

The use of waste biomass for energy applications mitigates greenhouse gases from the environment in two ways. Biomass left in landfills for longer periods breaks down releasing CO_2 and may release CH_4, NH_3 and H_2S through anaerobic means (Boyle, 2014; Van Loo and Koppejan, 2008 and Sami et al., 2001). It is also documented that biomass co-combustion has reduced SO_2 by up to 75% and NO_x by 15% (Van Loo and Koppejan, 2008). The emission factor of CO_2, SO_2 and NO_x of forest residues is approximately 24, 0.06 and 0.57 g/KWh against 955, 11.8 and 4.3 g/KWh for coal, respectively (Boyle, 2014). As such, assuming at least weighted averages, the emissions during co-gasification should be lower than during coal gasification.

2.3 Thermal conversion processes

Solid fuels, such as biomass and coal, undergo thermal conversion to provide various forms of energy and other products. The three thermochemical processes by which solid fuels are converted are presented in Figure 2.1.

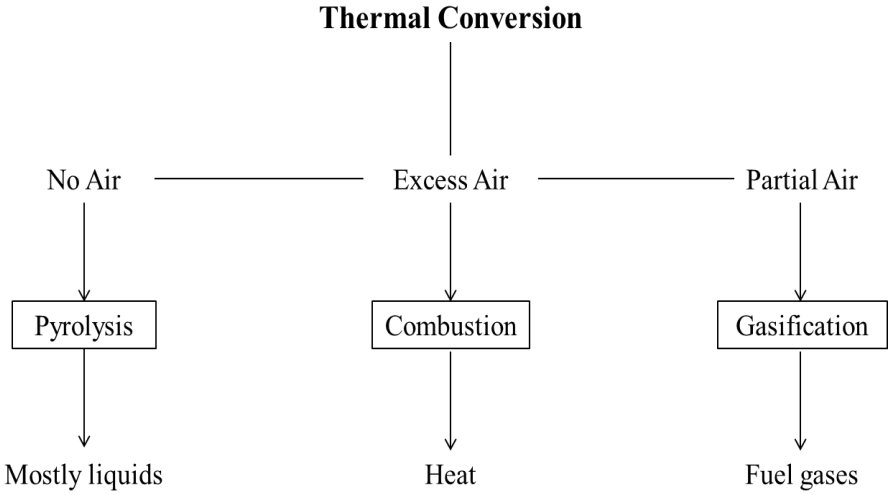

Figure 2-1: Thermal conversion processes

These processes differ in the reactant gas used and consequently, the products obtained and the product distribution depends on the pyrolysis conditions. Energy needs for the world today require the use of all these processes at different levels. As a stand-alone process, biomass pyrolysis has its main products as liquids due to the high tar yields, depending on the pyrolysis conditions (Tumuluru et al., 2012). However, with carefully chosen process parameters, the production of gases and chars may be maximised (Kan et al., 2016). Combustion has been used

for many years in the African rural setting, where woody biomass has been combusted at household levels to provide heat. This use of biomass to provide energy has been evaluated to be mostly inefficient and as such, modernised methods that ensure complete reactions have been developed. These methods also include, but not limited to, gasification, where fuel gases are produced, which can be used for many applications (Liu, 2010; Ruiz et al., 2013).

2.3.1 Torrefaction

The realisation that biomass has a low energy density, is highly hygroscopic and is a smoking fuel, has motivated research into pre-treatment methods (Boateng and Mullen, 2013; Brodeur et al., 2011; Harmsen et al., 2010). Pre-treatment methods seek to improve the fuel properties of fuel feedstock and have a significant influence on the performance chains, more especially on logistics and efficiencies (Uslu, 2008). Torrefaction is one of such pre-treatment methods, and improves the fuel properties of lignocellulosic biomass for thermochemical applications (Bach and Skreiberg, 2016; Chew and Doshi, 2011; Tumuluru et al., 2011; van der Stelt et al., 2011). It is often referred to as a low temperature pyrolysis process, as it is restricted to temperatures between 200 and 300 °C (Bridgeman and Jones, 2008; Chen et al., 2015; Shang et al., 2014). When compared with other pre-treatment processes, such as pelletization and pyrolysis, torrefaction has the highest process efficiency (Uslu, 2008). Traditionally, torrefaction takes place under inert conditions, however oxidising conditions have also been investigated (Broström et al., 2012a; W. Chen et al., 2014; Rousset et al., 2012).

The torrefaction of lignocellulosic biomass results in the change in characteristics and these changes are dependent on the process parameters and biomass origin (Park et al., 2012; Prins et al., 2006a; Tumuluru et al., 2011). Higher torrefaction temperatures and longer torrefaction times have resulted in lower solid yields or higher mass loss (Medic et al., 2012). Deng et al., (2009) compared the torrefaction of rice straw and rape stalk in the temperature range; 200 - 300°C. Rice straw showed more sensitivity towards heat treatment at low temperatures from (59% at 200°C to 36% at 300°C) whilst rape stalk recorded higher mass loss than rice stalk at higher temperatures (from 63% at 200°C to 25% at 300°C) (Deng et al., 2009). These may be linked to the differences in the lignocellulosic fibre components in the different biomass samples. The degradation during torrefaction may also be enhanced by the composition of the carrier gas. Chen et al., (2014) studied the torrefaction of eucalyptus, coconut fibre, oil palm fibre and

cryptomeria japonica by varying the O_2 concentrations from 0 to 20%. The weight loss (evaluated using Equation 2.1) increased from 39% at 0% O_2 to 54% at 20% O_2 for eucalyptus.

Generally, the extent and effect of torrefaction was evaluated by weight loss, changes in ultimate and proximate analyses data. However, the calorific value measurements have been used to ascertain the extent of fuel upgrade by torrefaction. This has been achieved by the quantification of the energy yield (EY) (Equation 2.2) and the mass energy density (MED) (Equation 2.3) (Chen et al., 2014; Poudel et al., 2015). The MED also incorporates the mass of the biomass, where the fuel upgrade is analysed with respect to the mass lost (Kan et al., 2016; Tumuluru et al., 2011). A measure of the MED > 1, indicates an upgrade in the fuel properties of the torrefied fuel (material).

$$MY(wt.\%) = \frac{m_t}{m_i} * 100 \quad (2.1)$$

$$EY = \frac{CV_{torr}}{CV_{raw}} * 100 \quad (2.2)$$

$$MED = \frac{MY}{EY} \quad (2.3)$$

Where $m_{t,i}$ is the mass at the end of the reaction and at the beginning of the reaction, respectively. CV_{torr} and CV_{raw} are the calorific value of the torrefied biomass and raw biomass respectively.

Torrefaction parameters (temperature, carrier gas and time) determine the torrefaction product and its characteristics. A torrefied product with less elemental oxygen than carbon, maintain a mass energy density above 1 (or 100%), improve the friability and hydrophobicity (Stelte et al., 2011; Yang et al., 2014). At around 280°C, low temperature carbonization takes place and the torrefied product loses more elemental carbon and the mass energy density falls below 100% (net energy loss) and the essence of 'fuel upgrade' is compromised. More accurate and optimized torrefaction conditions may be achieved by the use of a full factorial design.

Progress in torrefaction studies has resulted in the use of advanced characterization techniques to investigate physical and chemical changes that may accompany torrefaction (Boateng and Mullen, 2013; Chew and Doshi, 2011; Ibrahim et al., 2013). The loss of elemental H and O is relatively faster compared to elemental C, resulting in less elemental O than C (Chen and Kuo, 2011; H. K. Kim et al., 2012; Y. Kim et al., 2012). This results in a less smoking fuel and with reducing O, an increased calorific value of the solid product (Chew and Doshi, 2011; Crombie, 2013; Tumuluru et al., 2012, 2011; Uslu, 2008). Torrefaction has also been characterised by an

increase in the fixed carbon and a reduction in the volatile matter and moisture content (Bridgeman and Jones, 2008; Chew and Doshi, 2011; Lasode et al., 2014).

The changes in biomass characteristics are as a result of the fibre composition and their characteristic degradation patterns at torrefaction conditions (Cagnon et al., 2009; Chen and Kuo, 2011; Varhegyif and Antal, 1989). Hemicellulose is the most sensitive to torrefaction, followed by cellulose and lignin, as torrefaction temperature increase (Barnette et al., 2012; Gírio et al., 2010; Licursi et al., 2015). The variation of these fibres in biomass results in different structural characteristics, however, the characteristics variability of lignocellulosic biomass is reduced by torrefaction. This may be determined or investigated by the use of Fourier Transforms Infrared (FT-IR) spectroscopy, ^{13}C Nuclear Magnetic Resonance (NMR) spectroscopy to follow characteristic chemical changes (Bilba and Ouensaga, 1996; Elmay et al., 2015; Keiluweit et al., 2010). Structural changes may be studied with assistance from; X-Ray diffraction (XRD), CO_2 adsorption, scanning electron microscopy (SEM) and Thermogravimetry (Lahijani et al., 2013a; Zhao et al., 2013).

For an elaborate analysis of the chemical and structural changes of biomass during torrefaction, complimentary use of chemical and structural characterization is needed. For instance, there has been various studies reporting on the use of ^{13}C NMR spectroscopy for characterization where most discussions are around the functional groups found (or not found) in a biomass sample and how some are eliminated by torrefaction (Melkior et al., 2012; Wikberg and Maunu, 2004). ^{13}C NMR spectroscopy data can be used to estimate accurately fibre components of raw biomass and track the fibre component residues after heat treatment, analysis of torrefaction products and the evaluation of structural parameters where comparisons with other established techniques such as XRD would be useful as validation. Similar approaches have been employed in coal characterization (Baysal et al., 2016; Okolo et al., 2015). This applies to the other characterization techniques as well, where the extraction of aromaticity, development of van Krevelen plots, analysis of the pore structure and the analysis of crystalline parameters may be further studied.

2.3.2 Pyrolysis

Pyrolysis occurs under inert conditions. It is also a process viewed as a pre-treatment for gasification (Uslu, 2008). Pyrolysis occurs in 3 stages; the drying, primary pyrolysis and secondary pyrolysis stage (Brewer et al., 2009; Tripathi et al., 2016). In the drying stage (< 150 °C), moisture is evaporated and light molecular weight hydrocarbons are broken down (Kan et

al., 2016; Wannapeera and Worasuwannarak, 2012). During the primary pyrolysis stage, volatiles are produced as chemical bonds of lignocellulosic components are broken to form gases, condensable species and char (Anca-Couce, 2016; Yaman, 2004; Yang et al., 2006). A final stage, secondary pyrolysis, may take place following, or simultaneously with, the primary pyrolysis stage. Where secondary pyrolysis occurs after primary pyrolysis, the char from the primary pyrolysis may be converted via cracking reactions, and vapours may be polymerized into secondary char (Neves et al., 2011).

The products formed from pyrolysis are dependent on the pyrolysis conditions (Bridgwater, 2011; Carrier et al., 2011a). The char fraction normally contains inorganic material, which is normally <10 wt.% for lignocellulosic biomass. This fraction contains elements that are essential (either as catalysts or inhibitors) during biomass conversion such as K, Na, Si and Al (Tortosa Masiá et al., 2007). The liquid fraction is a complex mixture of water, oxygenated aliphatic and oxygenated phenolic compounds (Li et al., 2014; Suliman et al., 2016). The constitution of these liquids is dependent on the fibre components.

The product distribution of biomass samples is evaluated in terms of wt.% of char (solid or biochar), liquid (light condensable gas or bio-oil) and gases (Buhenne et al.,2013). The product distribution for woody biomass (high lignin);43% solid, 16% gas, 41% liquid whilst for other agricultural wastes (high hemicellulose) may be approximated as follows; 32% solid, 20% gas and 48% liquid normally have the product distribution (Yin et al., 2013; Aysu et al., 2014). This is as a result of the differences in the lignocellulosic composition.

Feedstock with high cellulose amounts usually produces liquids with acids, alcohols, aldehydes, ketones, esters and phenolic compounds (Moser, 2016; S. Zhang et al., 2015). However, feedstock with higher hemicellulose or lignin also have varying distributions of products (Bulushev and Ross, 2011; Efika et al., 2012). The gases produced during biomass conversion also depend on the fibre components since hemicellulose has a higher CO_2 yield, cellulose has a higher CO yield and lignin produces more CH_4 and H_2 during conversion (Yang et al, 2007). Consequently, a biomass feedstock with more lignin is expected to produce more CH_4 and H_2 during conversion than does a sample with less lignin. The same assumptions are true for samples with higher hemicellulose and cellulose, separately.

For the different pyrolysis conditions, and feedstock types, one of the primary observations has been the different in weight loss kinetics (Kan et al., 2016; Velden et al., 2010). This may be noted from the percentage solid yield for different biomass feedstock and different pyrolysis

conditions in Table 2.1. Some studies analysed all product yields, i.e. solid yield, gas yield and liquid yield (Sellin et al., 2016). However, the interest into biomass pyrolysis is far fetching and has progressed over the years. Some researchers have investigated the kinetics with which biomass samples degrade at pyrolysis conditions (Park et al., 2009), the analysis of derived pyrolysis compounds (Kan et al., 2016), the effect of pyrolysis carrier gas (Guerrero et al., 2005) as well as in-depth characterization of the solid pyrolysis product (Huang et al., 2015; Uchimiya et al., 2011).

2.3.2.1 Fast Pyrolysis

In fast pyrolysis the biomass is heated up to a temperature of 850–1250 °C with a heating rate of 10–200 °C for a short span of time varying between 1 and 10 s (Tripathi et al., 2016). Typically, fast pyrolysis produces 60 – 75% of liquid product, 15 – 25% of biochar and 10 – 20% of non-condensable gas products (Uzun et al., 2006). Uzun and co-workers (Uzun et al., 2006) studied the product characteristics from the fast pyrolysis of soybean cake and investigated the effects of particle size, gas flow rate and heating rates on the oil yield and quality. It was observed that the moisture content in the oil slightly increased with increasing heating rate and that the oil yields were improved at higher temperatures (> 450 °C). Other important findings included the negligible effect of particle size on the oil yield and the mass balances between the liquid phase compounds and gas phase products depending on the studied range (Uzun et al., 2006).

However, increasing the particle size (from 0.5 mm to 2.2 mm) increased the biochar yield from 19.4 to 35.6% for olive husk and other increases in biochar yield were observed for corncob and wheat stalk (Tripathi et al., 2016). A different observation was made by Onay and Kockar (2007) on pyrolysing rapeseed up to a temperature of 550 °C with the heating rate 30 °C/min and carrier gas flow rate of 100 cm^3/min. Biochar yield decreased till the particle size increased from 0.425 to 0.85 mm but as the particle size exceeded 0.85 mm the biochar yield was seen to be increased. Fast pyrolysis have also been used for co-pyrolysis of coal and wheat straw and there were no synergistic effects due to the short residence times as well as the high heating rates (Zhu et al., 2008)

Even though pyrolysis has been mostly studied under inert conditions, steam has also been investigated as a sweeping gas, as well as catalytic pyrolysis (Efika et al., 2012; Giudicianni et al., 2013; Uzun and Sarioğlu, 2009). Flash pyrolysis in N_2 results in highly oxygenated bio-oil and increased fractions of phenol compounds (Yaman, 2004), whilst pyrolysis in the range 400 - 500 °C results in highly oxygenated and less viscous, homogenous liquids (Onay, 2007; Yaman,

2004). In as much as fast pyrolysis favours the production of liquid products, some biochar is still produced, which can be used for gasification, waste water treatment and soil amendment (Carrier et al., 2012a; Tripathi et al., 2016).

2.3.2.2 Slow Pyrolysis

At heating rates between 5 – 30 °C/min, pyrolysis is referred to as slow pyrolysis (Carrier et al., 2012c, 2011a; Giudicianni et al., 2013). The feedstock may be held at a constant temperature or slowly heated to a desired final temperature (Mohan et al., 2006). In comparison to fast pyrolysis, slow pyrolysis is characterised by much longer residence times which results in vapours not escaping easily (Mohan et al., 2006). For bench scale investigations, slow pyrolysis has been very important to produce chars for gasification and other applications. There is no clear cut-off between slow and fast pyrolysis when it comes to temperature, as it depends on the targeted application of the products (Baniasadi et al., 2016; Giudicianni et al., 2013; Sellin et al., 2016). Temperatures as high as 1000 °C have been reported for both processes (Ahmed et al., 2016; Baniasadi et al., 2016; Y. Chen et al., 2014; Wannapeera et al., 2011). However, temperatures as high as 1200°C have also been reported (Anupam et al., 2016; Taba et al., 2012). The complicated char formation process forms an important part of biomass research as its comprehensive understanding is still sought.

Char from slow pyrolysis has received significant attention in recent times (Angin and Sensoz, 2014; Rosendahl et al., 2007; Rutherford et al., 2012). Slow pyrolysis char has been used for soil upgrade, electricity production via gasification and combustion, and in water treatment (Angin and Sensoz, 2014; Ding et al., 2016; Inyang et al., 2010; Rutherford et al., 2012). The characteristics of biomass char samples determine how biomass may be utilised. For instance, water retention of biochar has been a characteristic needed in soil amendment (Le Brech et al., 2016; Uchimiya et al., 2011). Not only has the water retention capacity a positive, the high surface area of chars, and alkali and alkali earth metals (AAEMs) composition is useful for soil upgrades for farming (Suliman et al., 2016). For water treatment applications, biomass chars with less metals is preferred (Mafu et al., 2013). Other characteristics of biomass char samples, such as the functional groups, the surface morphology and the microcrystalline structures determine how and where the char samples may be used (Carrier et al., 2012a, 2011a; Rutherford et al., 2012; Suliman et al., 2016).

2.3.3 Gasification

Gasification has been in use for many years as a process that converts solid and liquid fuels into gaseous products (Min et al., 2011; Wang et al., 2015). The end product (sometimes after fuel upgrade) is called syngas (a mixture of CO and H_2) and has been used to supply heat, generate electricity, produce chemicals and liquid fuels for automobiles (Wang et al., 2015). In practice, gasification is broader. It includes drying, pyrolysis, gasification and combustion where all these processes take place in a gasifier, as illustrated in Figure 2.2 (Skhonde et al., 2009).

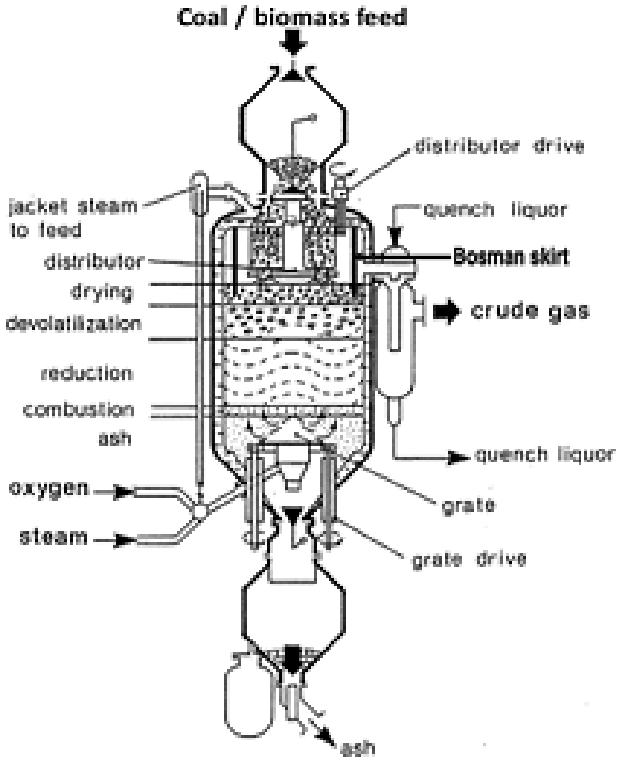

Figure 2-2: Schematic of a fixed bed dry bottom (FBDB) gasifier (Adapted from Bunt et al., (2012))

However, gasification is loosely used to refer to the gasification zone, where the residues from pyrolysis are converted to syngas (Dudyński et al., 2015). The gasification zone is the rate determining step and as a result, has been receiving suitable attention (Everson et al., 2013; Min et al., 2011; Ruiz et al., 2013). In this zone, a reactant gas or gasifier gas is introduced. CO_2, steam, O_2-steam, CO_2-steam, O_2-enriched-CO_2 and O_2-steam-CO_2 have been investigated as the gasifier/reactant gas (Alimuddin et al., 2010). Coal gasification has been a major source of energy in the world for a long time, however efforts to manage its environmental impacts and concerns on its long term availability have resulted in biomass gasification receiving attention in

the recent past (Alimuddin et al., 2010; Howaniec and Smoliński, 2013; Le Brech et al., 2016; Zhang et al., 2016).

2.3.3.1 The gasification process

The gasification process is inclusive of all the reaction zones as highlighted in Figure 2.2. The use of CO_2 as a gasifying agent during the gasification provides a reliable long-term alternative to mitigate the accumulation of CO_2 in the atmosphere. However, H_2O and O_2 has been used for gasification as well (Lahijani et al., 2015 ;Wang et al., 2015). Gasification is normally undertaken either under isothermal or non-isothermal conditions, (Bhatia and Perlmutter, 1980; Wang et al., 2016; Zuo et al., 2015) and the main reactions that take place during CO_2 gasification occur via the reversible oxygen-exchange mechanism presented in Equations 2.4a and b. It has been demonstrated by Turkdogan and Vinters (1969) that desorption reaction (Equation 2.4b) is the rate determining step, which influences the gasification rate by limiting the amount of C(O) formed from the forward reaction in Equation 2.4a. CO_2 is mainly used since it is a good indicator for gasification reactivity although the use of steam is of more practical value, since this is the dominating reaction in industrial gasification. Also CO_2 reactivity is a standard routine used to characterise carbonaceous material in general.

In the gasification zone, the introduction of the gasifier initiates the conversion of the chars produced in the pyrolysis zone into useful products (Butterman and Castaldi, 2007). The rate at which the char is converted has been evaluated using Equations 2.5a and b. Recent studies into gasification have extended the estimation of the gasification rate by calculating the reactivity index (R_s) and average reaction rate, amongst others (Huang et al., 2009). All these determinations have been used to understand the detailed gasification kinetics of different fuels (Jeong et al., 2015; Wang et al., 2015). A thorough understanding of the gasification kinetics is important for reactor design which also influences gasification efficiency (Wang et al., 2015).

$$C_f + CO_2 \leftrightarrow C(O) + CO \quad (2.4a)$$

$$C(O) \rightarrow CO + C_f \quad (2.4b)$$

$$X = \frac{m_0 - m}{m_0 - m_{ash}} \quad (2.5a)$$

$$r = \frac{dX}{dt} \quad (2.5b)$$

Where X is the conversion; m_0, the initial mass; m, is the mass as the reaction progresses; m_{ash}, the final mass at X = 1; and r, the gasification rate.

There have been numerous studies on the gasification of different feedstocks. In addition to the gasification of coal (Everson et al., 2006a; Komarova et al., 2015), many studies have since focussed on other feedstocks, including various biomass samples (Asadullah et al., 2010; Prins et al., 2006b). However, it has been postulated that a combination of coal and biomass, or different feedstocks, could yield positive results where the advantages of the individual fuels would overcome their isolated disadvantages. This resulted in investigations into co-gasification where two different fuels were simultaneously gasified (Jeong et al., 2015; Lahijani et al., 2013b).

2.3.3.2 Biomass gasification

Biomass gasification is an effective way of converting solid biomass into syngas (Fermoso et al., 2009b; Khalil et al., 2009; Mitsuoka et al., 2011). Beech wood, spruce, corn stalk, cedar, wheat stalk, rice lemmar, rice husks, pine bark, pine sawdust, palm empty fruit bunch, almond shells and sugarcane bagasse are amongst the solid biomass samples that have been studied for gasification (Jeong et al., 2015; Kaudal et al., 2016; Lahijani et al., 2013b; Lim et al., 2012; Motghare et al., 2015). There also has been studies into municipal waste as a potential feedstock, and their fuel properties have resulted in some municipalities venturing into converting their waste into energy (Hupponen et al., 2015; Tanigaki et al., 2012; Vassilev et al., 1999). The interest into waste, solid biomass is motivated by the challenges of growing energy crops which would compete for resources with food production.

The conversion of biomass into useful products used in fuel production plays a significant role in reducing fossil fuel dependency and also lowers CO_2, NO_x, and SO_x emissions (Rosillo-Calle, 2016; Taba et al., 2012). However, the difference in the fuel properties of biomass, when compared to coal, has resulted in lower gasification temperatures for biomass than coal. Biomass gasification is characterised by higher reactivities, high tar volumes produced and lower gasification efficiencies (Ahmad et al., 2016; Prins et al., 2006b; Taba et al., 2012; Xue et al., 2014). The gasification efficiencies of biomass samples have been improved by pre-treatment methods, such as torrefaction (Prins et al., 2006b). Biomass utilization drawbacks such as the seasonal availability, high moisture content and lower energy density have been countered by technological advances in reactor design. Efforts to co-utilise with coal have also shown different levels of success, where different coals had different gasification characteristics with different biomass feedstocks (Wei et al., 2011). For biomass gasification, the large volumes of

tar produced are converted into useful gaseous products when biomass is co-gasified with coal, at higher temperatures (Jeong et al., 2015; Pan et al., 2000; Tursun et al., 2016).

Biomass gasification is known for higher reactivities, compared to coal. However, within the biomass classes, there still are significant differences between the gasification characteristics (Kirubakaran et al., 2009). This is as a result of varying feedstock characteristics and by extension the char properties (Bouraouri et al., 2016). For instance, the gasification of wood char has shown slow gasification kinetics compared to the gasification of bagasse which was also not comparable to wood (Erlich et al., 2006; Lahijani et al., 2013b). The pyrolysis conditions have also been reported to have an impact on the gasification reactivities. Chars produced by high heating rates had higher gasification reactivities, compared to chars prepared from slow pyrolysis kinetics (Cetin et al., 2004). This has been attributed to the high surface areas of these chars; however, a correlation between the gasification reactivity and the surface area has not been drawn.

The observation that biomass is highly porous and hence there is an opportunity that the reactant gas may diffuse readily into gasification reaction sites and as a result yield higher gasification reactivities has motivated more research into gasification kinetics (Kirubakaran et al., 2009). Nonetheless, the gasification of feedstock is also governed by other factors, including the carbon lattice, the ash composition and other structural parameters. Even though the ash yield of most biomass samples is relatively low, the amount of Ca and K has been found to influence gasification (Huo et al., 2014). Even though Bouraouri et al (2016) concluded that the ash affected the gasification reactivities at higher conversion, Huo et al., (2014) observed that Ca increased the gasification reactivity at lower conversion whilst K catalysed the gasification reaction at higher conversions. Some biomass families also had significant amounts of Si and Al in the ash and these are associated with reducing the gasification rates (Ding et al., 2014; Zhang et al., 2016). Other parameters such as the aromaticity and crystalline parameters have been found to have an impact on the gasification of coal and recent biomass studies have drawn correlations between the aromaticity, crystalline diameter and alkali index with the gasification reactivity (Everson et al., 2013; Hattingh et al., 2011; Zuo et al., 2015). All these characteristics may not impact on the gasification throughout the conversion range; however, specific parameters may affect the gasification better at specific stages of the gasification. This is another area, in biomass gasification, that still needs further investigation. This would be valuable information that would feed into the supposed influence of biomass on coal gasification during co-gasification.

2.3.3.3 Biomass-coal co-gasification

Through co-gasification, the weaknesses of gasifying the individual fuels may be avoided. In Table 2.1, the gasification and co-gasification properties of individual fuels are presented. Co-gasification is not exclusive to coal and biomass as the co-gasification of tire char with almond shell and empty palm fruit bunch has been reported by Lahijani et al (2013a). Coal-biomass co-gasification is relevant today because, it presents an opportunity to use the available infrastructure for incorporating biomass into the energy matrix, via gasification. A roll-out of biomass gasifiers would be costly, however an addition of biomass to coal, in existing thermal power generators may only need minor modifications (Alimuddin et al., 2010; Lahijani et al., 2013b).

Table 2-1: Properties of biomass, coal and biomass-coal gasification (Irfan et al., 2011; Kirubakaran et al, 2009; Sarkar et al., 2014; Taba et al., 2012)

Properties	**Coal Gasification**	**Biomass Gasification**	**Co-gasification**
Ash	High	Low	Lower
Sulfur	High	Low	Low
Nitrogen	High	Low	Low
Reactivity	High	Low	High
Volatile matter	Low	High	High
Ca+K	Low	High	High
Char porosity	Low	High	High
Energy density	High	Low	High
Availability	Always	Seasonally	Stable
Temperature	High	Low	High

Investigations have reported on the co-gasification of chars from co-pyrolysis as well as blends from chars of different fuels prepared separately (Jeong et al., 2014; Meesri and Moghtaderi, 2002). During co-pyrolysis, the volatiles of each fuel influence equally the char properties and yield of the blends (Li et al., 2015). When gasification is studied through blending of chars of the individual fuels, the biomass char with catalytic properties gets into contact with the coal char.

As gasification progresses, the AAEMs in the biomass char interacts with the coal char, promoting the formation of intercalation compounds reported to increase the C-C bond length (Howaniec and Smoliński, 2013; Jeong et al., 2014; Satyam Naidu et al., 2016). This then improves the gasification rate of the coal and as such, biomass char has been referred to as a cheap catalyst for coal gasification (Kajitani et al., 2010; Lahijani et al., 2013b). Even though the high surface area of biomass chars helps to improve the gasification rate, the ash components seem to play a greater role, as biomass char interaction with coal char materialises. Depending on the biomass sample, co-gasification may be a 2-step process, where initially the biomass char reacts, followed by the coal (Fermoso et al., 2009a; Howaniec and Smoliński, 2013). In the case where the blending of the two fuels resulted in a more homogenous char, the physical effect may have to be overcome to observe a more improved gasification rate (Ding et al., 2014). The physical effect arises when char particles block the 'normal' gasifier gas pathway, consequently blocking some reaction centres hence inhibiting gasification (Ding et al., 2014). The physical effect does not, however, reduce the gasification rate but promotes inhibition in synergy terms.

For co-gasification, synergy and inhibition are a measure of the predictability of the co-gasification rate (Howaniec and Smoliński, 2013). Synergy (or inhibition) is evaluated by weighted averages as given in Equation 2.6. Synergistic effect has been reported when the reactivity of the blends is higher than the predicted reactivity from the individual fuels, through weighted averages (Haykiri-Acma and Yaman, 2007). Equally, when the experimental gasification reactivity is lower than the predicted rate through weighted averages, then inhibition is reported (Ding et al., 2014; Krerkkaiwan et al., 2013). Synergy and/or inhibition is dependent on the biomass origin, coal type and the ratio of each fuel in the blends (Howaniec and Smoliński, 2013; Zhang et al., 2016). The more biomass fraction in the blends, the higher the synergy, and as the biomass is reduced, synergy is reduced to inhibition (Jeong et al., 2015; Y. Zhang et al., 2015; Zhang et al., 2016). Zhang et al (2016) reported synergies only at higher conversion, which was attributed to the catalytic effect of the ash. Many studies have reported on the co-gasification biomass and coal, focussing on biomass to coal ratios such as 20:80, 40:60, 50:50, 60:40 and 80:20. However, to ensure that minor to no modification of available gasifiers, more studies at lower ratios at 30% biomass and below needs more attention.

$$R_{calc} = f_b R_b + f_c R_c \tag{2.6}$$

Where $f_{b,c}$ is the fraction of biomass- and coal-char; and $R_{b,c}$ the reactivity of biomass and coal char, respectively.

2.3.4 Gasification kinetic modelling

The overall gasification process is better described as a two-step process where the first step (rapid devolatisation) produces char that is gasified in the second step (Tanner and Bhattacharya, 2016). Since the second step is the slowest, its kinetic analysis is essential as the step governs the overall reactivity of the gasification process. However, there has been efforts in extraction the kinetic properties of the devolatilisation step for most feedstocks as well (Antal et al., 1998; Broström et al., 2012b; Várhegyi et al., 2002). Even though the gasification process also includes the devolatilisation step, gasification kinetics investigations have mostly involved only the char conversion step. There have been adequate investigations on the effect of the physical char characteristics on gasification; however the conversion of char through gasification is also dependent on heterogeneous reactions that take place during char gasification. These are the char-CO_2 and char-H_2O gasification reactions. The rate at which these reactions take place, is influenced by the physical or chemical properties of the char and the gasification medium (Lasa et al., 2011; Xiao and Yang, 2016). These factors are incorporated in the general equation that describes the rate of conversion of char during gasification (Equation 2.7).

$$\frac{dX}{dt} = k(T, P)f(X) \qquad (2.7)$$

Where f(X) describes the changes in physical or chemical properties of the char as the reaction proceeds, and may be modelled with varying degrees of accuracy and k(T, P) is the intrinsic surface reaction rate. Most gasification reactions satisfy the Arrhenius equation (Lahijani et al., 2013). As a result, the Arrhenius parameters, the activation energy (E_a) and the pre-exponential factor (A), may be extracted from the experimental data. Different feedstocks produce different Arrhenius parameters and these form a significant part of reaction kinetics (Lahijani et al., 2013c; Starink, 1996).

Depending on the nature of interactions between the char, gasification conditions and the gasification progress, three scenarios have been identified in gasification kinetics. These are; the chemical controlled (Regime I), pore diffusion controlled (Regime II) and mass transfer controlled (Regime III) regimes (Everson et al., 2006b; Mani et al., 2011). However, most gasification kinetics have been investigated in a TGA, which excludes the possibility of mass transfer or pore diffusion limitations but the extracted information has been useful in the prediction of upscale gasification and modelling at industrial scale (Anca-Couce, 2016; Hognon et al., 2014). Therefore, gasification kinetics are extracted by experimentally determining the values of dX/dt as conversion progresses and then various gas-solid models (shown in Table 2.3)

are fitted into the experimental data. There are many other models that have been developed to explain the solid-gas reactions during gasification and these include; the Johnson model (Molina and Mondragón, 1998), Dutta and Wen model, Unification theory model and the Adshiri and Furusawa models (Liu et al., 2003; Molina and Mondragón, 1998; Nilsson et al., 2012; Ollero et al., 2003; Puig-Arnavat et al., 2010; Struis et al., 2002). Models that are widely used in the prediction of gasification kinetics are given in Table 2.2.

Table 2-2: Summary of char conversion models (Bhatia and Perlmutter, 1980; Dupont et al., 2011; Wu et al., 2009)

Model	**Equation**
Volumetric model (VM)	$\frac{dX}{dt} = k_{VM}(1 - X)$
Grain model (GM)	$\frac{dX}{dt} = k_{GM}1 - X)^{2/3}$
Random pore model (RPM)	$\frac{dX}{dt} = k_{RPM}\sqrt{1 - \psi \ln(1 - X)}$

2.3.4.1 Volumetric (VM) and grain model (GM)

The VM has been instrumental in the extraction of gasification kinetics as it assumed that a chemical reaction takes place at all points within the particle (Wu et al., 2009; Zuo et al., 2015). It does not consider structural changes of the char particles as gasification proceeds and presumes that the particle size does not change but only the density does (Gao et al., 2016). The VM is reduced to the GM (or the shrinking core model) when it is assumed that the gasification takes place in a sphere from the outside. The GM assumes that the reaction initially takes place at the external surface of the char. it also assumes that the particles are spheres and the reactions begin in the outer sphere, into the particle. As a result, at the intermediary conversion of the solid, there is an unreacted core of char and it is significantly reduced as the reaction proceeds (Lahijani et al., 2015). The surface area reduces non-linearly with increase of the reaction degree (Zoulalian et al., 2015). Both the VM and the GM predict that the reaction rate will decrease with increasing conversion, as a result, they give a poor fit for gasification reactions which

present a maximum in their rate profile (Lahijani et al., 2015). There are many other models which have also been proposed to account for deviations from the standard models presented in Table 2.3. They include adjustments to account for the effect of surface area; char type, pyrolysis temperature and active surface area; and the ratio of initial to instantaneous pore surface area (Dutta et al., 1977; Irfan et al., 2011; Johnson, 1974).

2.3.4.2 Volumetric (VM) and grain model (GM)

The RPM (Equation 2.8) was developed by Bhatia and Perlmutter (1980) for fluid-solid reactions and it allows for non-uniform pore size distribution in the reacting solid. It considers the competing mechanisms of pore growth and overlap in a char particle undergoing conversion (Ochoa et al., 2001). This model represents the behaviour of a system that has a maximum reaction rate and one that does not, where the reaction proceeds through pore development (Wu et al., 2009). Even though the RPM has been the most successful in describing coal gasification (Everson et al., 2008; Wang et al., 2015), it has also been adopted to describe biomass gasification with different levels of success (Ding et al., 2014; Wang et al., 2015). For a system in which the gasification rate increases with conversion, to a maximum within $X < 0.393$, then the RPM can predict the gasification (Ding et al., 2014). This implies that the RPM fails for most biomass char gasification and catalytic gasification (Gupta and Bhatia, 2000; Kajitani et al., 2010; Zhang et al., 2014).

$$\frac{\mathrm{dX}}{\mathrm{dt}} = \mathrm{k}(1-\mathrm{X})\sqrt{1-\psi \mathrm{Ln}(1-\mathrm{X})} \tag{2.8}$$

Where ψ is the RPM structural parameter and X if the fractional carbon conversion of the char. The kinetic parameters are dependent on the char structure and the identity of the gasifier gas (Molina and Mondragón, 1998; Wang et al., 2015). The structural parameter has been extracted in various ways. A regression fit of the data has been used, but Everson et al. (Everson et al., 2008) proposed the use of the reduced time, ($t/t_{0.9}$), given by Equation 2.11. The reduced time is only dependent on the structural parameter and the conversion, as a result, a plot of the conversion against $t/t_{0.9}$ can be used to determine ψ. The structural parameter has been used to predict the gasification mechanism, for instance, a structural parameter < 2 means the reaction proceeds by pore collapse and normally does not exhibit a maximum (Everson et al., 2008).

$$\frac{t}{t_{0.9}} = \frac{\sqrt{1-\psi \ln(1-X)}-1}{\sqrt{1-\psi \ln(1-0.9)}-1} \tag{2.9}$$

Where $t_{0.9}$ is the time for 90% carbon conversion, t is the time, X the conversion and ψ the structural parameter.

The gasification of coal char has been widely predicted by the RPM (Molina and Mondragón, 1998; Ochoa et al., 2001; Zhang et al., 2010) even though the grain model and the homogeneous model has been successfully used to predict the gasification of Brownian coals (Ye et al., 1998). For biomass chars, the RPM has been used to predict the gasification with a correlation coefficient (R^2) of 0.87 (Zuo et al., 2015). Kramb et al., (2016) modelled the effect of catalyst additions to spruce wood gasification and found that acid leached wood gasification produced a better RPM fit, while virgin wood and wood impregnated with Ca and K resulted in a RPM fit with $R^2 < 0.5$.

As RPM and other available models could not fit biomass gasification, Zhang et al. (2010) modified the RPM by incorporating an extra term in Equation 2.9 as given in Equation 2.10. The parameter θ is referred to as a variable function and is related to the catalytic activity of inorganic materials found in the char matrix (Ding et al., 2014; Zhang et al., 2010). It is given by c(1-X) for reactivity maximums occurring at low conversions whilst it is cX for maximum that occur at higher conversion. Typical biomass gasification fits the second pattern (Brown et al., 2000; Kuo et al., 2014). Further studies on the modelling of biomass and catalytic gasification, demonstrated that the value of the empirical constants, c and p are significantly dependent on the catalytic components in the ash (Brown et al., 2000; Kramb et al., 2016). The extent to which a model may be qualified as able to predict the gasification reactivity is measured by the quality of fit (QOF) given by Equation 2.11.

$$\frac{dX}{dt} = k(1-X)\sqrt{1-\psi Ln(1-X)}\,(1+\theta^p) \tag{2.10}$$

$$QOF\ (\%) = 100 * \left[1 - \frac{\sum_1^n \frac{|X_{calc} - X_{exp}|}{X_{exp}}}{N}\right] \tag{2.11}$$

Where θ is variable function, c and p are empirical constants governing the catalytic activity during gasification, N is the number of data points, X_{calc} is the calculated conversion from the model equation and X_{exp} is the experimental conversion.

Table 2-3: Summary of kinetic modelling for selected biomass and coal gasification studies (Ding et al., 2014; Zhang et al., 2010; Jeong et al., 2014; Zuo et al., 2015)

Sample	**Gasification conditions**	**Model**	**Model parameters**				
			ψ (-)	**E_a (kJ/mol)**	**c (-)**	**p (-)**	**R^2 (-)g**
Bituminous coal	Non-isothermal kinetics varying the heating rates (5, 10 and 15 °C/min	VM	-	304.2	-	-	0.986
		GM	-	236.8	-	-	0.983
		RPM	0.91	258.5	-	-	0.996
Chestnut residues		VM	-	258.9	-	-	0.989
		GM	-	197.5	-	-	0.951
		RPM	0.01	258.3	-	-	0.989
Olive stones		VM	-	415.0	-	-	0.694
		GM	-	376.6	-	-	0.800
		RPM	$2.7x10^{05}$	339.0	-	-	0.845
KD	Charring at 900 °C and gasification under CO_2 (800 – 1000 °C). The effect of Ca and K as catalysts was also investigated and modelled.	MRPM	0	-	0	-	-
KD-Ca-2.5			15	-	1.33	5	-
KD-Ca-5			15	-	1.37	4.3	-
AC			0	-	0	-	-
AC-K-1.0			2	-	1.80	4.4	-
AC-K-3.5			2	-	2.29	1.8	-

NB: KD- low rank Indonesian coal char, AC – coal based activated carbon, Ea – Activation Energy, c & p – empirical constants used in the modified random pore model, VM – Volumetric model, RPM – random pore model, MRPM – modified random pore model.

Table 2.3 (contd.): Summary of kinetic modelling for selected biomass and coal gasification studies (Ding et al., 2014; Zhang et al. 2010; Jeong et al., 2014; Zuo et al., 2015)

Sample	**Gasification conditions**		**Model**	**Model parameters**				
				ψ (-)	**E_a (kJ/mol)**	**c (-)**	**p (-)**	**R^2 (-)**
Tire	Charring at 700°C isothermal CO_2-gasification	850	MRPM	0.27	250.3	1.17	1.12	0.966
		900		1.46		1.72	1.03	0.922
		950		4.99		1.21	2.52	0.978
		1000		17.1		0.50	0.34	0.993
AS:Tire (1:1)		850	MRPM	2.6	203.3	0.90	2.84	0.955
		875		20.7		1.24	3.58	0.981
		900		34.7		1.19	2.86	0.984
EFB:tire (1:1)		825	MRPM	3.78	187.6	1.45	3.42	0.945
		850		14.7		1.91	1.45	0.995
		875		39.1		1.64	1.12	0.997
HLC	Charring at 900 °C Steam gasification	800	RPM	1.19	104.7	-	-	0.980
		850		2.18		-	-	0.975
		900		1.44		-	-	0.987
		950		2.59		-	-	0.991

NB: AS – almond shell, EFB – palm empty fruit bunch, HLC – Hulunbeier lignite coal char.

Table 2.3 (contd.): Summary of kinetic modelling for selected biomass and coal gasification studies (Ding et al., 2014; Zhang et al. 2010; Jeong et al., 2014; Zuo et al., 2015)

Sample	**Gasification conditions**	**Model**	**Model parameters**				
			ψ (-)	**E_a (kJ/mol)**	**c (-)**	**p (-)**	**R^2 (-)**
SMC	850	RPM	1.41	173.7			0.994
	900		3.04				0.993
	950		3.59				0.999
	1000		5.00				0.999
JCC	900	RPM	2.76	162.3			0.994
	950		2.87				0.991
	1000		3.50				0.997
	1050		4.60				0.988
CSC	750	MRPM	7.39	204.1	1.80	3.76	0.988
	800		7.72		1.82	2.66	0.998
	850		5.75		1.72	2.47	0.998
	900		2.82		1.80	2.29	0.989
CSC:HLC (1:1)	800	RPM	0.51	116.6			0.975
	850		1.09				0.986
	900		3.69				0.991
	950		7.40				0.968

NB: SMC – Shenmu bituminous coal char, JCC – Jincheng anthracite coal char, CSC – corn stalk char, HLC – Hulunbeier lignite coal char.

Table 2.3 (contd.): Summary of kinetic modelling for selected biomass and coal gasification studies (Ding et al., 2014; Zhang et al. 2010; Jeong et al., 2014; Zuo et al., 2015)

Sample	**Gasification conditions**	**Model**	**Model parameters**				
			ψ (-)	**E_a (kJ/mol)**	**c (-)**	**p (-)**	**R^2 (-)**
CSC:SMC (1:1)	850	RPM	3.23	132.4			0.999
	900		5.92				0.992
	950		6.03				0.979
	1000		8.33				0.994
CSC:JCC (1:1)	900	RPM	0.52	141.9			0.992
	950		2.70				0.989
	1000		4.41				0.992
	1050		3.15				0.995

NB: CSC – corn stalk char, SMC – Shenmu bituminous coal char, JCC – Jingcheng anthracite coal char

Kinetic modelling of biomass – coal co-gasification have been studied by both the RPM and the MRPM (Lahijani et al., 2013b). However, better fits were achieved by the MRPM. The empirical constants have shown a dependence on the temperature, biomass origin and the fraction of biomass in the char blends (Zhang et al., 2016). Some studies have shown that the structural parameter ψ is not dependent on the temperature, however for some co-gasification studies, ψ varied with temperature. Dominant in the kinetic modelling of co-gasification, c and p varied both with changing temperature and catalytic addition of biomass fraction (Jeong et al., 2014). There also have been observations that the activation energy was substantially reduced by the addition of biomass in coal gasification and it reduced linearly with increasing biomass fraction (Ding et al., 2014; Zhang et al. 2010).

2.4 Material Characterization

The area of material characterization has been gradually receiving attention and constantly advancing in technology in recent years. Areas such as nanotechnology, medicinal chemistry and energy has been reporting on highly advanced characterization techniques (Baghel et al., 2007; Erdal et al., 2009; Licursi et al., 2015; Roberts et al., 2015). There has been significant breakthroughs in the characterization of coal (Everson et al., 2013; Papanicolaou et al., 2004). Similar approaches have been adopted for biomass as a possible feedstock for energy applications (Ibrahim et al., 2013; Rosendahl et al., 2007; Tortosa Masiá et al., 2007). Structural and chemical properties have been investigated and used to decide on applications that suits different biomass samples (Angin and Sensoz, 2014; Jeong et al., 2014; Rutherford et al., 2012). For instance, the use of biomass chars for soil upgrades has been informed by the observation that biomass chars are rich in K and have high surface areas (Rehrah et al., 2015).

Even though there has been a growing volume of reports on biomass characterization, the characteristics variability within samples of the same class as well as differences between samples of different classes has been a challenge (Field et al., 2008). The following characterization techniques have been useful in extracting advanced characteristics of biomass and other fuels such as coal; ultimate and proximate analyses, surface area analysis, X-ray methods (XRD and XRF), fibre analysis, Fourier Transforms Infrared (FT-IR) spectroscopy and solid state ^{13}C Nuclear Magnetic Resonance (NMR) spectroscopy (Brewer et al., 2009; Freitas et al., 2001; Melkior et al., 2012; Murillo et al., 2014; Okolo et al., 2015; Zhao et al., 2013).

2.4.1 Ultimate and proximate analysis

Ultimate analysis refers to the determination of elemental carbon, hydrogen, nitrogen, sulfur and oxygen (C, H, N, S and O). C, H, N and S is determined through a combination of ISO-SAB and ASTM standards whilst O is calculated by difference (Okolo et al., 2015). Using the ultimate analysis data, a fuel could be classified by comparing the amount of elemental O compared to elemental C. In the case where a fuel has more elemental O than C, the fuel is classified as a "bad smoking fuel" (Chen et al., 2014; Motghare et al., 2015). Information on the comparative amounts of elemental N and S has been important in predicting the emission of NO_x and SO_x gases into the environment during thermal conversion (Al-Mansour and Zuwala, 2010; Saidur et al., 2011). For instance, a feedstock with high amounts of either N or S can be predicted to emit more NO_x and SO_x than a fuel with less elemental N and S (Al-Mansour and Zuwala, 2010; Amaral et al., 2014). Char formation has been followed by means of ultimate analysis. An increase in elemental C, reduction in elemental O and H, has characterized the pyrolysis process; with increasing pyrolysis temperature (Wannapeera and Worasuwannarak, 2012). This resulted in the evaluation of the ratios H/C and O/C, which could be linked to aromaticity and degree of graphitization (Anupam et al., 2016; Odeh, 2015a). These ratios have been useful in fuel ranking by means of the Van Krevelen diagram. Anthracite coal, a high rank fuel, has the lowest H/C and O/C ratios whilst biomass, with the highest H/C and O/C ratios has been categorised as a low rank fuel (Anupam et al., 2016).

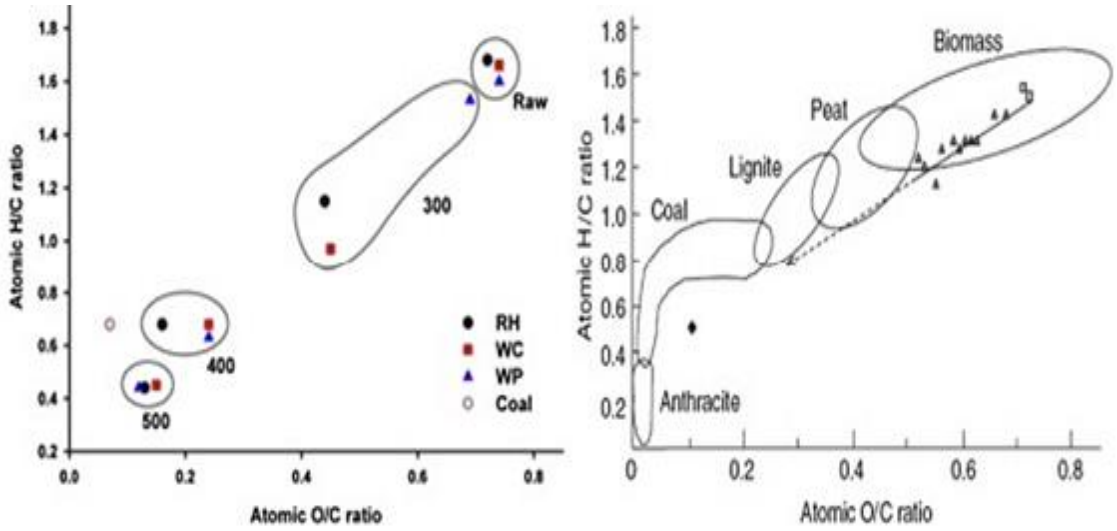

Figure 2-3: Van Krevelen diagram showing the H/C and O/C ratio positions for biomass char samples prepared at different final temperatures compared with those of different coal ranks (Prins et al., 2006b; Park and Jang, 2012)

Figure 2.3 shows how biomass pyrolysed at different final temperatures compare with known different coals in a Van Krevelen ranking. It has also been observed that the fuel rank increased with increasing aromaticity, decreasing H/C and O/C, the maturation of coal and the increase in pyrolysis temperature for raw feedstock (Anupam et al., 2016; McBeath et al., 2011; Murillo et al., 2014).

Proximate analysis is the determination of volatile matter, moisture and fixed carbon contents, as well as the ash yields of fuels (Bridgeman and Jones, 2008; Motghare et al., 2015; Pimenidou and Dupont, 2012; Wannapeera and Worasuwannarak, 2012). The fixed carbon content is determined by difference whilst the other components of proximate analysis are determined using standard procedures (Naik et al., 2010). The hygroscopic nature of biomass has been probed by monitoring the moisture content before and after drying (Chew and Doshi, 2011; Tumuluru et al., 2011). Moisture contents as high as 50 wt.% (as received biomass) have been reported for biomass samples, depending on the basis of the analyses (Tumuluru et al., 2012). However for air-dried basis (wt.%, adb), biomass typically has 10% moisture, approximately 75% volatiles, less than 1% ash and approximately 15% fixed carbon (Bridgwater, 2011; Tumuluru et al., 2011; Vassilev et al., 2010). Another important characteristic of biomass fuels is the calorific value (CV); the amount of energy released from a sample during combustion per unit mass (Friedl et al., 2005). It has been used in torrefaction studies to evaluate the energy yield and mass energy density (Mehrabadi et al., 2016; Shang et al., 2014) as well as for fuel ranking purposes (Roberts et al., 2015). The CV of most lignocellulosic biomass samples is in the range 14–18 MJ/kg and this value increases at torrefaction (20-25 MJ/kg) and after pyrolysis (up to 30 MJ/kg) (Crombie, 2013; Motghare et al., 2015). The change in CV during pre-treatment could be quantified by the analysis of the energy yield and the mass energy density.

2.4.2 Fibre Analysis

Fibres in biomass samples, also referred to as lignocellulosic components, are hemicellulose, cellulose and lignin and are found in lignocellulosic biomass (Carrier et al., 2012b; Park et al., 2013). For some biomass samples, such as sweet sorghum bagasse, another component, the nonstructural carbohydrates, forms a significant fraction of the fibres. Non-structural carbohydrates may also be detected in lesser amounts in woody biomass samples and other class of samples. The quantitative determination of fibre components has been achieved through the ‘food method’ and thermogravimetric analysis (TGA) (Carrier et al., 2011b). Using the TGA

method, characteristic temperature peaks are identified and deconvoluted to quantify the fibre components (Carrier et al., 2011b; Vieira et al., 2007). The characteristic temperature ranges for hemicellulose, cellulose and lignin are 240 – 300 °C, 320 – 400 °C and 220 – 450 °C, respectively (Chen and Kuo, 2011). However, this is only an approximation as adjacent TGA peaks may overlap, more especially lignin and cellulose peaks, hence compromising the accuracy of the quantities of these components. The food industry method involves dissolution in different solvents which may promote inconsistent estimations of the fibres (Maria et al., 2011). The quantification of fibres after heat-treatment remains inconclusive and using the food industry method (Carrier et al., 2011b). Advanced analytical techniques (FTIR and ^{13}C NMR) have been proposed as alternative and accurate methods of determining fibre components. This has been achieved by quantifying characteristic peaks associated with the presence of some fibres. For instance, non-structural carbohydrates have a characteristic ^{13}C NMR peak at 21 ppm whilst at around 150 ppm peaks linked to the presence of lignins have been identified (Cagnon et al., 2009; Santoni et al., 2015; Zhao et al., 2007). However, the use of ^{13}C NMR spectroscopy is costly, whilst the high density of functional groups in biomass coupled with different groups appearing in the same wavelength presents a challenge in engaging FTIR spectroscopy (Rutherford et al., 2012).

The amount of fibre components in biomass samples is dependent on the biomass source. Woody biomass exhibits higher lignin and cellulose contents than herbaceous plants, while bagasse and other grasses have higher hemicellulose contents (Carrier et al., 2012c; Sasaki, 2003; Tumuluru et al., 2011). A good understanding of the fibre analysis data of biomass samples may be used as a quick determinant of the applicability and usability of biomass feedstocks in different applications, possible pre-treatment methods, and may give insights on data resulting from other characterization techniques (Chew and Doshi, 2011; Kuo et al., 2014; Liu et al., 2010; Tumuluru et al., 2012). Biomass samples with higher lignin content are better suited for producing chars and hence for thermochemical applications for char conversion while biomass samples rich in hemicellulose and cellulose may have better yields in the production of various liquid biofuels; such as bioethanol and biodiesel (Pasangulapati et al., 2012; van der Stelt et al., 2011). The typical quantities of lignocellulosic components in plant biomass samples are; hemicellulose (20 – 35%), cellulose (30 – 60%), and lignin (15 – 30%) (Chen and Kuo, 2011).

2.4.3 Infrared (IR) spectroscopy

Infrared (IR) spectroscopy is an absorption technique that functions in the IR region of the electromagnetic spectrum (Bilba and Ouensaga, 1996; Orrego-Ruiz et al., 2011). It uses the different vibrational modes of a molecule after being exposed to radiation. The collection of all the bending and stretching data is used to reconcile the structure of a sample based on the characteristic signals obtained against a certified reference database (Bilba and Ouensaga, 1996; Rodriguez et al., 2016). IR spectroscopy has also been utilised to characterise raw biomass, solid and liquid yields from biomass thermal processing (Santoni et al., 2015). Depending on the data processing method, various modifications to traditional IR have been developed and these include Fourier Transforms Infrared and attenuated total reflectance FT-IR (ATR-FTIR) spectroscopy (Murillo et al., 2014; Uchimiya et al., 2011). Even though analysis may be carried out in the near IR (14000 – 4000 cm^{-1}), mid IR (4000 – 400 cm^{-1}) or the far IR region (400 – 10 cm^{-1}), most biomass analysis for energy applications are undertook in the mid IR region (Li et al., 2011; Orrego-Ruiz et al., 2011; Q. Wang et al., 2016).

The functional groups in biomass may be grouped into aliphatic and aromatic groups (Zhao et al., 2013). However, due to the complex nature of biomass, one functional group may appear at different positions as shown by Gusiatin et al. (2016) for aromatic C=O, which appears at both 1250 and 1591 cm^{-1}. This is a consequence of adjacent groups which affect the vibration frequency of the functional group being analysed. This is also true for functional groups that may either be aromatic or aliphatic; i.e. aliphatic –CH and aromatic –CH appear at different wavenumbers of the FT-IR spectrum (Anca-Couce, 2016; Okolo et al., 2015). The following functional groups have been identified in most lignocellulosic biomass samples; –OH, –CH, CH_2, CH_3, C–O, C=O and COOH (Bian et al., 2015; Elmay et al., 2015; Li et al., 2013; Suliman et al., 2016). Most of the functional groups originate from the lignocellulosic fibres that make up biomass (Varhegyi et al., 1998; Zhao et al., 2013).

During thermochemical conversion of biomass, lignocellulosic fibres degrade and bring about chemical changes to the biochar and these changes have been followed by FT-IR (De Jong et al., 2003). Mainly, the disappearance and narrowing of peaks signalled the removal of functional groups from the samples. The dehydration of biomass during pyrolysis could be followed by monitoring the –OH peak around 3300 cm^{-1} whilst the aromatization of feedstocks as temperatures increased could be concluded from the analysis of the aromatic peaks against the aliphatic peaks (Odeh, 2015b). Quantitatively, the deconvolution of the principal peaks from FT-

IR spectra significantly contributes in the analysis of biomass and comprehensively mapping the char formation process (Okolo et al., 2015). Information extracted from FT-IR analysis data may be complimentary used with other techniques, such as ^{13}C NMR and XRD, to map the chemical composition of biomass (Wikberg and Maunu, 2004; Zhao et al., 2013). However, FT-IR may still be explored to quantify aromaticity (against the use of the complicated NMR and XRD), map the char formation by analyses of the functional group evolution as pyrolysis temperatures are increased and this presents an opportunity to extract more information from this relatively inexpensive technique.

2.4.4 Surface area

Surface area is determined from the adsorption isotherm data of adsorbate gases (N_2 or CO_2) onto the pore surface of the analysed material. Adsorption isotherm models such as Brunauer Emmett and Teller (BET), Langmuir and Dubinin-Radushkevich have been very useful in estimating surface areas (Kaufhold et al., 2010). For better estimation of the surface area, the size of the pores in a porous material determines the adsorbate gas to be used. For either adsorbate gas, degassing conditions and the relative pressure (P/P_0) remain crucial for accurate estimation of the surface areas. The different adsorbate gases require different relative pressures to give better estimates of the surface area; for N_2 as an adsorbate gas, P/P_0 of 0.3 is considered adequate whilst this value is 0.03 for CO_2 (Okolo et al., 2015).

Surface areas of biomass can be related to its other characteristics: such as an increase in surface area with decrease in ash content, and an increase in surface area when biomass undergoes heat treatment (Suliman et al., 2016). High ash yields have been associated with the blockage of pores which results in lower surface areas. It has also been concluded that the fibre composition affects the pore network and the surface area, and its changes during and pyrolysis (Zhang et al., 2008). Investigations on the surface area of biomass and biochar samples have been reported using N_2 and CO_2 as the adsorbate gas. Suliman et al., (2016) compared the characteristics of Douglas fir wood, Douglas fir bark and hybrid poplar wood using both N_2- and CO_2 adsorption. At lower pyrolysis temperature the differences between the surface areas determined from the N_2 adsorption data and those from the CO_2 adsorption results were significant. Similarities were however witnessed for Douglas fir wood pyrolised at 550 and 600 °C and the rest of the biochars having N_2 surface areas less than CO_2 surface areas. Increasing the pores volume in the micropore network, achieved through increasing pyrolysis temperatures, means CO_2, with smaller molecular diameter, accesses these pores easier than N_2 and therefore the use of CO_2

better estimates the surface area. Even though the use of N_2 as an adsorbate for surface area analyses of biomass and biochars may result in inaccurate relations, CO_2 adsorption experiments give more accurate results (Suliman et al., 2016; Zhang et al., 2008).

2.4.5 X-ray analysis

X-ray methods (X-ray diffraction (XRD) and X-ray fluorescence (XRF) spectroscopy) have found applications in fuel characterization where XRD has been used to identify the different crystalline mineral phases in a material. X-ray fluorescence spectroscopy has provided insights in the elemental composition of the solid samples, mostly reporting them in their oxide forms.

2.4.5.1 X-ray diffraction

XRD is a non-destructive analytical technique used to identify mineral phases of a crystalline material (Zhao et al., 2013). X-rays are directed at a sample where they are diffracted to d-spacings which are transformed into a diffractograms. These d-spacings are unique for each mineral as well as for each phase of the mineral in a sample. XRD has found applications in both biomass and coal characterization (Murillo et al., 2014; Okolo et al., 2015; Zhao et al., 2007). Even though biomass samples are mainly non-crystalline, they have a crystalline fraction mainly consisting of cellulose. As such, the fraction of the crystalline peak against the amorphous peak has been used to determine the crystallinity of a sample (Bansal et al., 2010). There was a correlation between the fibre composition of a biomass sample with the crystallinity as determined by XRD where the crystallinity increased with increasing cellulose fraction in the biomass matrix (Murillo et al., 2014). It was also observed that crystallinity increased with increasing pyrolysis temperature (< 300 °C) after which the crystallinity decreased (Sasmal et al., 2012).

A typical biomass XRD diffractogram consists of two peaks, at approximately 16 and 25° 2θ, assigned to the aliphatic phase and graphitic basal planes respectively (Zhao et al., 2013). However, during pyrolysis, the emergence of mineral peaks, which were mainly due to the release of volatiles and increase of mineral matter fraction in the sample, has been observed (Andersen et al., 2013; Lu et al., 2001; Zhao et al., 2013). The calculation of structural parameters from XRD has given valuable information about the carbon structure of biomass (Huang et al., 2009). These are; crystallite height (L_a), crystallite diameter (L_c), inter-planar distance (d_{002}) and average number of crystallites in a stack, N_{ave}. These parameters may be calculated using Equations 2.12 (a)-(d). The crystallite parameters have been linked with fuel rank (Everson et al., 2013). These parameters change as biomass is heated. For instance, with

increasing pyrolysis temperature, L_a has been reported to increase, while d_{002} decreased. Due to the heterogeneity of biomass, more investigations into the biomass microcrystalline structure are needed (Guerrero et al., 2008).

$$L_c = \frac{K_c \lambda}{\beta_{002} \cos\theta_{002}} \quad (2.12a)$$

$$L_a = \frac{K_a \lambda}{\beta_{10} \cos\theta_{10}} \quad (2.12b)$$

$$d_{002} = \frac{\lambda}{2\sin\theta_{002}} \quad (2.12c)$$

$$N_{ave} = \frac{L_c}{d_{002}} + 1 \quad (2.12d)$$

Where, λ, is the wavelength of the incident X-ray; $\theta_{002,10}$ is the peak position of (002) or (10) band (°); $\beta_{002,10}$ is the full width at half maximum (FWHM) of the corresponding peak or band (°); $K_{c,a}$ is a constant depending on X-ray reflection plane (0.89 for the (002) band and 1.84 for the (10) band.

2.4.5.2 X-ray fluorescence (XRF) spectroscopy

XRF spectroscopy is used to quantify the elemental composition of materials. It is a non-destructive technique that measures the fluorescence of emitted rays from a sample that has been exposed to an X-ray source (Andersen et al., 2013). The behaviour of an incident X-ray is exclusive to a specific element and as such XRF is a reliable qualitative and quantitative elemental analysis method, which has found applications in coal and biomass analyses (Niu et al., 2013). XRF data reports metal composition in its oxide form. The elements analysed by XRF have been grouped into major and minor elements. The major elements include Si, Ti, Al, Fe, Mn, Mg, Ca, Na, K, P, Cr and S; while minor elements include As, Ba, Bi, Br, Cd, Ce, Cl, Co, Cs, Cu, Ga, Ge, Hf, Hg, La, Lu, Mo, Nb, Nd, Ni, Pb, Rb, Sb, Sc, Se, Sm, Sn, Sr, Ta, Te, Th, Tl, Zn and Zr (Niu et al., 2013; Robinson et al., 2009; Umamaheswaran and Batra, 2008).

There has been comparisons drawn between the ash contents of different biomass samples as well as comparisons between biomass samples and coal samples using data generated from XRF (Andersen et al., 2013; Roberts et al., 2015). Bagasse, groundnut shell, areca nut shell and cashew nut shell consist mainly of Si, while woody biomass such as beech had less silica and more of K, Ca and Mg (Suarez-Garcia et al., 2002; Vassilev and Vassileva, 2009; Vassilev et al., 2012). The ash composition of fuels has been used to explain the inherent catalysis, or lack of it, during gasification (Suarez-Garcia et al., 2002).

The quantification of the elements K, Al, Si, Ca, Fe, Na, Mg and P in fuel feedstocks has resulted in the quantification of the alkali index (AI) which is also referred to as the catalytic factor (Hattingh et al., 2011). The different definitions of AI are given in equations 2.13 (a-c) (Bouraoui et al., 2016; Hattingh et al., 2011; Niu et al., 2016), however the general definition is given by the ratio of the catalytic elements to the inhibiting elements. For biomass conversion, with significantly lower ash yield, the impact of AI on pyrolysis and gasification may differ from the observations for coal conversion.

$$AI_1 = Ash * \frac{Fe_2O+CaO+MgO+Na_2O+K_2O}{SiO_2+Al_2O_3+P_2O_5} \quad (2.13a)$$

$$AI_2 = Ash * \frac{K_2O}{SiO_2+Al_2O_3+P_2O_5} \quad (2.13b)$$

$$AI_2 = Ash * \frac{K_2O+CaO}{SiO_2+Al_2O_3+P_2O_5} \quad (2.13c)$$

2.4.6 13C Nuclear Magnetic Resonance (NMR) spectroscopy

Solid state ^{13}C NMR has been useful as a chemical analysis tool and has since become an indispensable tool for fuel characterization (Cao et al., 2012). It reveals important chemical properties at molecular level and different sample analysis techniques have resulted in different NMR techniques such as cross polarization (CP) and direct polarization magnetic angle spinning solid state (DPMAS) NMR (Cao et al., 2012; Wikberg and Maunu, 2004). Even though CP-MAS ^{13}C NMR has been the mostly used, DP-MAS ^{13}C NMR provides more reliable condensed aromatic carbon quantification (Cao et al., 2012; McBeath et al., 2011).

In ^{13}C NMR spectroscopy for biomass samples, peaks have been assigned to crystalline or aliphatic cellulose carbons, methoxy groups of lignin and aromatic carbons (Brewer et al., 2009; Wikberg and Maunu, 2004). The quantification of the carbon functionalities present have been used to calculate the aromaticities of raw and carbonised biomass samples including corn, pine, hazelnut and bull manure (McBeath et al., 2014). ^{13}C NMR has also been useful in complementing other characterization techniques such as FTIR and XRD, for both biomass and coal samples (Freitas et al., 2001; Okolo et al., 2015; Roberts et al., 2015). For instance, the quantification of lignocellulosic fibres requires complex dissolution which introduces larger margins of error, but through a careful utilization of ^{13}C NMR, cellulose and lignin may be quantified and followed as biomass undergoes thermal treatment (Melkior et al., 2012; Rutherford et al., 2012).

Characteristic peak intensities have been used to monitor how heat treatment affected the lignocellulosic fibres in the biomass (Melkior et al., 2012). In particular, is the prediction of crystallinity by analysing the crystalline cellulose peak areas against the amorphous peaks areas (McBeath et al., 2014, 2011). Okolo et al (2015b) reported aromaticities of various coals and coal char samples as determined by solid state CPMAS ^{13}C NMR. However, extracting structural parameters from ^{13}C NMR data of biomass and biomass char samples is an area that needs more investigation. The quantification of aromaticity has been successfully estimated by H/C and O/C ratios and the integration of aromatic peaks from CPMAS and DP ^{13}C NMR spectroscopy. In a study by McBeath et al., (2014), the aromaticity increased with increasing charring temperature and these increases were similar for the different biomass samples investigated. For instance, corn and bull manure charred between 400°C and 600°C had the aromaticities increase from 0.86 to 0.96 (Brewer et al., 2009; McBeath et al., 2011).

2.5 Gasification kinetic modelling

From the available literature in the subject area of biomass energy, the following conclusions are made;

- ✓ The use of biomass for energy applications provides a part of the solution for energy supply in the world today. It promises to contribute immensely in the reduction of greenhouse gas emissions and consequently the managing the adverse effects of climate change.
- ✓ It is also evident that, for lignocellulosic biomass, pre-treatment is a necessary step in its thermochemical conversion. Torrefaction has been widely investigated in this area and it has been shown that torrefied biomass material has improved fuel properties and consequently increased gasification efficiency. However, accompanying the upgrade in fuel properties is a change in the chemical and structural characteristics as studied by XRD, ^{13}C NMR, CO_2 adsorption and other advanced techniques.
- ✓ Another area of biomass conversion that has been investigated is biomass pyrolysis. The pyrolysis kinetics, and change in char properties as pyrolysis conditions change were dependent on the biomass type. For instance, characteristics changes for woody biomass, agricultural wastes and municipal wastes revealed different patterns and different kinetic responses to heat treatment. This would then lead to predictions that they would react differently during gasification (both CO_2 and steam). It could be noted, however, that the

characteristics variability were significant and as a result no generalities could be made from the investigated samples.

- ✓ Biomass gasification results in high reactivities. Various evaluations have been made to understand gasification kinetics as well as to draw a linkage between the observed reactivities and the char characteristics. Overall, the observed high gasification reactivities are as a result of the high surface areas of chars, low gasification retardants in the ash as well as the structural parameters that play a role during gasification. The random pore model has failed to predict the kinetics of biomass gasification however; the modified random pore model could predict biomass gasification.
- ✓ A significant number of studies have reported on the addition of biomass to coal in an effort to incorporate biomass in existing boilers to generate electricity. The co-gasification reactivity is dependent on the coal and biomass type, and the gasification conditions. Coal gasification reactivity has been significantly increased by the addition of biomass and this reactivity increased with increasing biomass fraction in the blends. Depending on the amount of biomass in the blends, the biomass-coal co-gasification kinetic modelling fitted the random pore model, however, with increasing biomass fraction, the modified random pore model predicted the gasification.

References

Ahmad, A.A., Zawawi, N.A., Kasim, F.H., Inayat, A., Khasri, A., 2016. Assessing the gasification performance of biomass: A review on biomass gasification process conditions, optimization and economic evaluation. Renew. Sustain. Energy Rev. 53, 1333–1347.

Ahmed, A., Uddin, G.S., Sohag, K., 2016. Biomass energy, technological progress and the environmental Kuznets curve: Evidence from selected European countries. Biomass and Bioenergy 90, 202–208.

Ahmed, M.B., Zhou, J.L., Ngo, H.H., Guo, W., 2016. Insight into biochar properties and its cost analysis. Biomass and Bioenergy 84, 76–86.

Al-Mansour, F., Zuwala, J., 2010. An evaluation of biomass co-firing in Europe. Biomass and Bioenergy 34, 620–629.

Alimuddin, Z., Zainal, B., Lahijani, P., Mohammadi, M., Rahman, A., 2010. Gasification of lignocellulosic biomass in fluidized beds for renewable energy development : A review. Renew. Sustain. Energy Rev. 14, 2852–2862.

Amaral, S.S., De Carvalho Junior, J.A., Costa, M.A.M., Neto, T.G.S., Dellani, R., Leite, L.H.S., 2014. Comparative study for hardwood and softwood forest biomass: Chemical characterization, combustion phases and gas and particulate matter emissions. Bioresour. Technol. 164, 55–63.

Anca-Couce, A., 2016. Reaction mechanisms and multi-scale modelling of lignocellulosic biomass pyrolysis. Prog. Energy Combust. Sci. 53, 41–79.

Andersen, L.K., Morgan, T.J., Boulamanti, A.K., Alvarez, P., Vassilev, S. V., Baxter, D., 2013. Quantitative X-ray fluorescence analysis of biomass: Objective evaluation of a typical commercial multi-element method on a WD-XRF spectrometer. Energy and Fuels 27, 7439–7454.

Angin, D., Sensoz, S., 2014. Effect of pyrolysis temperature on chemical and surface properties of biochar of rapeseed (*Brassica napus L.*). Int. J. Phytoremediation 16, 684–693.

Antal, M.J., Varhegyi, G., Jakab, E., 1998. Cellulose Pyrolysis Kinetics : Revisited. Ind. Eng. Chem. Res. 37, 1267–1275.

Anupam, K., Sharma, A.K., Lal, P.S., Dutta, S., Maity, S., 2016. Preparation, characterization and optimization for upgrading *Leucaena leucocephala* bark to biochar fuel with high

energy yielding. Energy 106, 743–756.

Asadullah, M., Zhang, S., Min, Z., Yimsiri, P., Li, C.-Z., 2010. Effects of biomass char structure on its gasification reactivity. Bioresour. Technol. 101, 7935–43.

Bach, Q.V., Skreiberg, O., 2016. Upgrading biomass fuels via wet torrefaction: A review and comparison with dry torrefaction. Renew. Sustain. Energy Rev. 54, 665–677.

Baghel, A., Boopathi, M., Singh, B., Pandey, P., Mahato, T.H., Gutch, P.K., Sekhar, K., 2007. Synthesis and characterization of metal ion imprinted nano-porous polymer for the selective recognition of copper. Biomass Bioelectron. 22, 3326–3334.

Baniasadi, M., Tugnoli, A., Conti, R., Torri, C., Fabbri, D., Cozzani, V., 2016. Waste to energy valorization of poultry litter by slow pyrolysis. Renew. Energy 90, 458–468.

Bansal, P., Hall, M., Realff, M.J., Lee, J.H., Bommarius, A.S., 2010. Multivariate statistical analysis of X-ray data from cellulose : A new method to determine degree of crystallinity and predict hydrolysis rates. Bioresour. Technol. 101, 4461–4471.

Barnette, A.L., Lee, C., Bradley, L.C., Schreiner, E.P., Bum, Y., Shin, H., Cosgrove, D.J., Park, S., Kim, S.H., 2012. Quantification of crystalline cellulose in lignocellulosic biomass using sum frequency generation (SFG) vibration spectroscopy and comparison with other analytical methods. Carbohydr. Polym. 89, 802–809.

Basu, P., Butler, J., Leon, M.A., 2011. Biomass co-firing options on the emission reduction and electricity generation costs in coal-fired power plants. Renew. Energy 36, 282–288.

Baysal, M., Yürüm, A., Yıldız, B., Yürüm, Y., 2016. Structure of some western Anatolia coals investigated by FTIR, Raman, ^{13}C solid state NMR spectroscopy and X-ray diffraction. Int. J. Coal Geol. 163, 166–176.

Bhatia, S.K., Perlmutter, D.D., 1980. A random pore model for fluid-solid reactions: I. Isothermal, kinetic control. AIChE J. 26, 379–386.

Bian, R., Ma, B., Zhu, X., Wang, W., Li, L., Joseph, S., Liu, X., Pan, G., 2015. Pyrolysis of crop residues in a mobile bench-scale pyrolyser: Product characterization and environmental performance. J. Anal. Appl. Pyrolysis 119, 52–59.

Bilba, K., Ouensaga, A., 1996. Fourier transform infrared spectroscopic study of thermal degradation of sugar cane bagasse. J. Anal. Appl. Pyrolysis 38, 61-73.

Boateng, A.A., Mullen, C.A., 2013. Fast pyrolysis of biomass thermally pretreated by

torrefaction. J. Anal. Appl. Pyrolysis 100, 95–102.

Bouraoui, Z., Dupont, C., Jeguirim, M., Limousy, L., Gadiou, R., 2016. CO_2 gasification of woody biomass chars: The influence of K and Si on char reactivity. Comptes Rendus Chim. 19, 457–465.

Brewer, C.E., Schmidgt-Rohr, K., Satrio, J.A., Brown, R.., 2009. Characterization of biochar from fast pyrolysis and gasification systems. Environ. Prog. Sustain. energy 28, 404–409.

Bridgeman, T.G., Jones, J.M., 2008. Torrefaction of reed canary grass , wheat straw and willow to enhance solid fuel qualities and combustion properties. Fuel 87, 844–856.

Bridgwater, A.V., Meier, D., Radlein, D., 1999. An overview of fast pyrolysis of biomass. Org. Geochem. 30, 1479–1493.

Bridgwater, A. V, 2011. Review of fast pyrolysis of biomass and product upgrading. Biomass and Bioenergy 38, 68–94.

Brodeur, G., Yau, E., Badal, K., Collier, J., Ramachandran, K.B., Ramakrishnan, S., 2011. Chemical and Physicochemical Pretreatment of Lignocellulosic Biomass : A Review. Enzyme Res. 2011, 1-17.

Broström, M., Nordin, A., Pommer, L., Branca, C., Blasi, C. Di, 2012. Influence of torrefaction on the devolatilization and oxidation kinetics of wood. J. Anal. Appl. Pyrolysis 96, 100–109.

Brown, R.C., Liu, Q., Norton, G., 2000. Catalytic effects observed during the co-gasification of coal and switchgrass. Biomass and Bioenergy 18, 499–506.

Bulushev, D.A., Ross, J.R.H., 2011. Catalysis for conversion of biomass to fuels via pyrolysis and gasification : A review. Catal. Today 171, 1–13.

Butterman, H.C., Castaldi, M.J., 2007. Influence of CO_2 Injection on biomass gasification. Ind. Eng. Chem. Res. 46, 8875–8886.

Cagnon, B., Py, X., Guillot, A., Stoeckli, F., Chambat, G., 2009. Contributions of hemicellulose, cellulose and lignin to the mass and the porous properties of chars and steam activated carbons from various lignocellulosic precursors. Bioresour. Technol. 100, 292–298.

Cannell, M.G.R., 2002. Carbon sequestration and biomass energy offset: Theoretical, potential and achievable capacities globally, in Europe and the UK. Biomass and Bioenergy 24, 97–116.

Cao, X., Pignatello, J.J., Li, Y., Lattao, C., Chappell, M.A., Chen, N., Miller, L.F., Mao, J., 2012. Characterization of wood chars produced at different temperatures using advanced solid-state ^{13}C NMR spectroscopic techniques. Energy and Fuels 26, 5983–5991.

Carrier, M., Hardie, A.G., Uras, Ü., Görgens, J., Hansie, J., 2012a. Production of char from vacuum pyrolysis of South-African sugar cane bagasse and its characterization as activated carbon and biochar. J. Anal. Appl. Pyrolysis 96, 24–32.

Carrier, M., Hugo, T., Gorgens, J., Knoetze, H., 2011a. Comparison of slow and vacuum pyrolysis of sugar cane bagasse. J. Anal. Appl. Pyrolysis 90, 18–26.

Carrier, M., Loppinet-serani, A., Absalon, C., Aymonier, C., Mench, M., 2012b. Degradation pathways of holocellulose , lignin and α -cellulose from *Pteris vittata* fronds in sub- and super critical conditions. Biomass and Bioenergy 43, 65–71.

Carrier, M., Loppinet-serani, A., Denux, D., Lasnier, J., Ham-Pichavant, F., Cansell, F., Aymonier, C., 2011b. Thermogravimetric analysis as a new method to determine the lignocellulosic composition of biomass. Biomass and Bioenergy 5, 1–10.

Carrier, M., Neomagus, H.W., Görgens, J., Knoetze, J.H., 2012c. Influence of chemical pretreatment on the internal structure and reactivity of pyrolysis chars produced from sugar cane bagasse. Energy and Fuels 26, 4497–4506.

Cetin, E., Moghtaderi, B., Gupta, R., Wall, T.., 2004. Influence of pyrolysis conditions on the structure and gasification reactivity of biomass chars. Fuel 83, 2139–2150.

Chen, H., Fu, X., 2016. Industrial technologies for bioethanol production from lignocellulosic biomass. Renew. Sustain. Energy Rev. 57, 468–478.

Chen, W., Kuo, P., 2011. Torrefaction and co-torrefaction characterization of hemicellulose , cellulose and lignin as well as torrefaction of some basic constituents in biomass. Energy 36, 803–811.

Chen, W., Lu, K., Lee, W., Liu, S., Lin, T., 2014. Non-oxidative and oxidative torrefaction characterization and SEM observations of fibrous and ligneous biomass. Appl. Energy 114, 104–113.

Chen, W., Peng, J., Bi, X.T., 2015. A state-of-the-art review of biomass torrefaction , densification and applications. Renew. Sustain. Energy Rev. 44, 847–866.

Chen, Y., Yang, H., Yang, Q., Hao, H., Zhu, B., Chen, H., 2014. Torrefaction of agriculture

straws and its application on biomass pyrolysis poly-generation. Bioresour. Technol. 156, 70–77.

Chew, J.J., Doshi, V., 2011. Recent advances in biomass pretreatment – Torrefaction fundamentals and technology. Renew. Sustain. Energy Rev. 15, 4212–4222.

Crombie, K.N., 2013. Torrefaction/biochar production by microwave and conventional slow pyrolysis – comparison of energy properties 2, 144–152.

De Jong, W., Pirone, A., Wójtowicz, M.A., 2003. Pyrolysis of *Miscanthus Giganteus* and wood pellets: TG-FTIR analysis and reaction kinetics. Fuel 82, 1139–1147.

Ding, L., Zhang, Y., Wang, Z., Huang, J., Fang, Y., 2014. Interaction and its induced inhibiting or synergistic effects during co-gasification of coal char and biomass char. Bioresour. Technol. 173C, 11–20.

Ding, Z., Wan, Y., Hu, X., Wang, S., Zimmerman, A.R., Gao, B., 2016. Sorption of lead and methylene blue onto hickory biochars from different pyrolysis temperatures: Importance of physicochemical properties. J. Ind. Eng. Chem. 37, 261–267.

Dudyński, M., van Dyk, J.C., Kwiatkowski, K., Sosnowska, M., 2015. Biomass gasification: Influence of torrefaction on syngas production and tar formation. Fuel Process. Technol. 131, 203–212.

Dupont, C., Nocquet, T., Da Costa, J.A., Verne-Tournon, C., 2011. Kinetic modelling of steam gasification of various woody biomass chars: influence of inorganic elements. Bioresour. Technol. 102, 9743–8.

Dutta, S., Wen, C.Y., Belt, R.J., 1977. Reactivity of coal and char. 1. In carbon dioxide atmosphere, Ind. Eng. Chem. Process Des. Dev. 16 (1977). Ind. Eng. Chem. Process Des. Dev. 16, 20–30.

Efika, C.E., Wu, C., Williams, P.T., 2012. Syngas production from pyrolysis – catalytic steam reforming of waste biomass in a continuous screw kiln reactor. J. Anal. Appl. Pyrolysis 95, 87–94.

Elmay, Y., Brech, Y. Le, Delmotte, L., Dufour, A., Brosse, N., Gadiou, R., 2015. Characterization of Miscanthus pyrolysis by DRIFTs, UV Raman spectroscopy and mass spectrometry. J. Anal. Appl. Pyrolysis 113, 402–411.

Erdal, U., Denkbas, E.B., Öztürk, E., Tuncel, S.A., Kabasakal, O.S., 2009. Preparation and

characterization of polyethyleneglycolmethacrylate (PEGMA) - co -vinylimidazole (VI) microspheres to use in heavy metal removal. J. Hazard. Mater. 162, 1073–1080.

Erlich, C., Bjornbom, E., Bolado, D., Giner, M., Fransson, T., 2006. Pyrolysis and gasification of pellets from sugar cane bagasse and wood. Fuel 85, 1535–1540.

Everson, R.C., Neomagus, H.W.J.P., Kaitano, R., Falcon, R., Vivien, M., 2008. Properties of high ash coal-char particles derived from inertinite-rich coal : II. Gasification kinetics with carbon dioxide. Fuel 87, 3403–3408.

Everson, R.C., Neomagus, H.W.J.P., Kasaini, H., Njapha, D., 2006a. Reaction kinetics of pulverized coal-chars derived from inertinite-rich coal discards: Gasification with carbon dioxide and steam. Fuel 85, 1076–1082.

Everson, R.C., Neomagus, H.W.J.P., Kasaini, H., Njapha, D., 2006b. Reaction kinetics of pulverized coal-chars derived from inertinite-rich coal discards: Characterisation and combustion. Fuel 85, 1067–1075.

Everson, R.C., Okolo, G.N., Neomagus, H.W.J.P., Santos, J., 2013. X-ray diffraction parameters and reaction rate modeling for gasification and combustion of chars derived from inertinite-rich coals. Fuel 109, 148–156.

Fermoso, J., Arias, B., Plaza, M.G., Pevida, C., Rubiera, F., Pis, J.J., García-peña, F., Casero, P., 2009a. High-pressure co-gasification of coal with biomass and petroleum coke. Fuel Process. Technol. 90, 926–932.

Fermoso, J., Stevanov, C., Moghtaderi, B., Arias, B., Pevida, C., Plaza, M.G., Rubiera, F., Pis, J.J., 2009b. High-pressure gasification reactivity of biomass chars produced at different temperatures. J. Anal. Appl. Pyrolysis 85, 287–293.

Field, C.B., Campbell, J.E., Lobell, D.B., 2008. Biomass energy: the scale of the potential resource. Trends Ecol. Evol. 23, 65–72.

Freitas, J.C.C., Bonagamba, T.J., Emmerich, F.G., 2001. Investigation of biomass- and polymer-based carbon materials using ^{13}C high-resolution solid-state NMR. Carbon. 39, 535–545.

Friedl, A., Padouvas, E., Rotter, H., Varmuza, K., 2005. Prediction of heating values of biomass fuel from elemental composition. Anal. Chim. Acta 544, 191–198.

Gao, X., Zhang, Y., Li, B., Yu, X., 2016. Model development for biomass gasification in an entrained flow gasifier using intrinsic reaction rate submodel. Energy Convers. Manag.

108, 120–131.

Gírio, F.M., Fonseca, C., Carvalheiro, F., Duarte, L.C., Marques, S., 2010. Hemicelluloses for fuel ethanol : A review. Bioresour. Technol. 101, 4775–4800.

Giudicianni, P., Cardone, G., Ragucci, R., 2013. Cellulose , hemicellulose and lignin slow steam pyrolysis : Thermal decomposition of biomass components mixtures. J. Anal. Appl. Pyrolysis 100, 213–222.

Guerrero, M., Ruiz, M.P., Alzueta, M.U., Bilbao, R., Millera, A., 2005. Pyrolysis of eucalyptus at different heating rates : studies of char characterization and oxidative reactivity. J. Anal. Appl. Pyrolysis 74, 307–314.

Guerrero, M., Ruiz, M.P., Millera, Á., Alzueta, M.U., Bilbao, R., 2008. Characterization of biomass chars formed under different devolatilization conditions : differences between rice husk and eucalyptus. Energy & Fuels 22, 1275–1284.

Gupta, J.S., Bhatia, S.K., 2000. A modified discrete random pore model allowing for different initial surface reactivity. Carbon 38, 47–58.

Gusiatin, Z.M., Kurkowski, R., Brym, S., Wiśniewski, D., 2016. Properties of biochars from conventional and alternative feedstocks and their suitability for metal immobilization in industrial soil. Environ. Sci. Pollut. Res. 23, 21249–21261.

Harmsen, P., Huijgen, W., Bermudez, L., Bakker, R., 2010. Literature review of physical and chemical pretreatment processes for lignocellulosic biomass (Report 1184).

Hattingh, B.B., Everson, R.C., Neomagus, H.W.J.P., Bunt, J.R., 2011. Assessing the catalytic effect of coal ash constituents on the CO_2 gasification rate of high ash, South African coal. Fuel Process. Technol. 92, 2048–2054.

Haykiri-Acma, H., Yaman, S., 2007. Synergy in devolatilization characteristics of lignite and hazelnut shell during co-pyrolysis. Fuel 86, 373–380.

Hognon, C., Dupont, C., Grateau, M., Delrue, F., 2014. Comparison of steam gasification reactivity of algal and lignocellulosic biomass: influence of inorganic elements. Bioresour. Technol. 164, 347–53.

Howaniec, N., Smoliński, A., 2013. Steam co-gasification of coal and biomass - Synergy in reactivity of fuel blends chars. Int. J. Hydrogen Energy 38, 16152–16160.

Huang, L., Chen, Y., Liu, G., Li, S., Liu, Y., Gao, X., 2015. Non-isothermal pyrolysis

characteristics of giant reed (*Arundo donax L.*) using thermogravimetric analysis. Energy 87, 31–40.

Huang, Y., Yin, X., Wu, C., Wang, C., Xie, J., Zhou, Z., Ma, L., Li, H., 2009. Effects of metal catalysts on CO_2 gasification reactivity of biomass char. Biotechnol. Adv. 27, 568–72.

Huo, W., Zhou, Z., Chen, X., Dai, Z., Yu, G., 2014. Study on CO_2 gasification reactivity and physical characteristics of biomass, petroleum coke and coal chars. Bioresour. Technol. 159, 143–9.

Hupponen, M., Grönman, K., Horttanainen, M., 2015. How should greenhouse gas emissions be taken into account in the decision making of municipal solid waste management procurements ? A case study of the South Karelia region , Finland. Waste Manag. 42, 196–207.

Ibrahim, R.H.H., Darvell, L.I., Jones, J.M., Williams, A., 2013. Physicochemical characterisation of torrefied biomass. J. Anal. Appl. Pyrolysis 103, 21–30.

Inyang, M., Gao, B., Pullammanappallil, P., Ding, W., Zimmerman, A.R., 2010. Biochar from anaerobically digested sugarcane bagasse. Bioresour. Technol. 101, 8868–8872.

Irfan, M.F., Usman, M.R., Kusakabe, K., 2011. Coal gasification in CO_2 atmosphere and its kinetics since 1948 : A brief review. Energy 36, 12–40.

Jeong, H.J., Hwang, I.S., Hwang, J., 2015. Co-gasification of bituminous coal – pine sawdust blended char with H_2O at temperatures of 750 – 850 °C. Fuel 156, 26–29.

Jeong, H.J., Park, S.S., Hwang, J., 2014. Co-gasification of coal – biomass blended char with CO_2 at temperatures of 900 – 1100 °C. Fuel 116, 465–470.

Johnson, J.L., 1974. Kinetics of bituminous coal char gasification with gases containing steam and hydrogen, in: L.G. Massey (Ed.). Coal Gasification, Am. Chem. Soc. 145–178.

Kajitani, S., Zhang, Y., Umemoto, S., Ashizawa, M., Hara, S., 2010. Co-gasification reactivity of coal and woody biomass in high-temperature. Energy & Fuels 24, 145–151.

Kan, T., Strezov, V., Evans, T.J., 2016. Lignocellulosic biomass pyrolysis: A review of product properties and effects of pyrolysis parameters. Renew. Sustain. Energy Rev. 57, 126–1140.

Kaudal, B.B., Chen, D., Madhavan, D.B., Downie, A., Weatherley, A., 2016. An examination of physical and chemical properties of urban biochar for use as growing media substrate. Biomass and Bioenergy 84, 49–58.

Kaufhold, S., Dohrmann, R., Klinkenberg, M., Siegesmund, S., Ufer, K., 2010. N_2 -BET specific surface area of bentonites. J. Colloid Interface Sci. 349, 275–282.

Keiluweit, M., Nico, P.S., Johnson, M.G., Kleber, M., 2010. Dynamic molecular structure of plant biomass-derived black carbon (biochar). Environ. Sci. Technol. 44, 1247–53.

Khalil, R., Ja, S., Grønli, M.G., Hustad, J., 2009. CO_2 Gasification of Biomass Chars : A Kinetic Study 94–100.

Kim, H.K., Kim, J., Cho, T., Choi, W.J., 2012. Influence of pyrolysis temperature on physicochemical properties of biochar obtained from the fast pyrolysis of pitch pine (*Pinus rigida*). Bioresour. Technol. 118, 158–162.

Kim, Y., Lee, S., Lee, H., Lee, J., 2012. Physical and chemical characteristics of products from the torrefaction of yellow poplar (*Liriodendron tulipifera*). Bioresour. Technol. 116, 120–125.

Kirubakaran, V., Sivaramakrishnan, V., Nalini, R., Sekar, T., Premalatha, M., Subramanian, P., 2009. A review on gasification of biomass. Renew. Sustain. Energy Rev. 13, 179–186.

Komarova, E., Guhl, S., Meyer, B., 2015. Brown coal char CO_2-gasification kinetics with respect to the char structure. Part I: Char structure development. Fuel 152, 38–47.

Kramb, J., Demartini, N., Perander, M., Moilanen, A., Konttinen, J., 2016. Modeling of the catalytic effects of potassium and calcium on spruce wood gasification in CO_2. Fuel Process. Technol. 148, 50–59.

Krerkkaiwan, S., Fushimi, C., Tsutsumi, A., Kuchonthara, P., 2013. Synergetic effect during co-pyrolysis/gasification of biomass and sub-bituminous coal. Fuel Process. Technol. 115, 11–18.

Kuo, P.-C., Wu, W., Chen, W.-H., 2014. Gasification performances of raw and torrefied biomass in a downdraft. Fuel 117, 1231–1241.

Lahijani, P., Zainal, Z.A., Mohamed, A.R., Mohammadi, M., 2013a. Ash of palm empty fruit bunch as a natural catalyst for promoting the CO_2 gasification reactivity of biomass char. Bioresour. Technol. 132, 351–355.

Lahijani, P., Zainal, Z.A., Mohamed, A.R., Mohammadi, M., 2013b. Co-gasification of tire and biomass for enhancement of tire-char reactivity in CO_2 gasification process. Bioresour. Technol. 138, 124–130.

Lahijani, P., Zainal, Z.A., Mohamed, A.R., Mohammadi, M., 2013c. CO_2 gasification reactivity of biomass char: catalytic influence of alkali, alkaline earth and transition metal salts. Bioresour. Technol. 144, 288–95.

Lahijani, P., Zainal, Z.A., Mohammadi, M., Mohamed, A.R., 2015. Conversion of the greenhouse gas CO2 to the fuel gas CO via the Boudouard reaction: A review. Renew. Sustain. Energy Rev. 41, 615–632.

Lasa, H. De, Salaices, E., Mazumder, J., Lucky, R., 2011. Catalytic steam gasification of biomass : Catalysts , Thermodynamics and Kinetics 5404–5433.

Lasode, O.A., Balogun, A.O., Mcdonald, A.G., 2014. Torrefaction of some Nigerian lignocellulosic resources and decomposition kinetics. J. Anal. Appl. Pyrolysis 109, 47–55.

Le Brech, Y., Raya, J., Delmotte, L., Brosse, N., Gadiou, R., Dufour, A., 2016. Characterization of biomass char formation investigated by advanced solid state NMR. Carbon 108, 165–177.

Li, G., Huang, L., Hse, C., Qin, T., 2011. Chemical compositions , infrared spectroscopy , and X-ray diffractometry study on brown-rotted woods. Carbohydr. Polym. 85, 560–564.

Li, S., Chen, X., Liu, A., Wang, L., Yu, G., 2015. Co-pyrolysis characteristic of biomass and bituminous coal. Bioresour. Technol. 179, 414–420.

Li, S., Chen, X., Liu, A., Wang, L., Yu, G., 2014. Study on co-pyrolysis characteristics of rice straw and Shenfu bituminous coal blends in a fixed bed reactor. Bioresour. Technol. 155, 252–257.

Li, X., Shen, Q., Zhang, D., Mei, X., Ran, W., Xu, Y., Yu, G., 2013. Functional Groups Determine Biochar Properties (pH and EC) as Studied by Two-Dimensional 13C NMR Correlation Spectroscopy. PLoS One 8.

Licursi, D., Antonetti, C., Bernardini, J., Cinelli, P., Coltelli, M.B., Lazzeri, A., Martinelli, M., Galletti, A.M.R., 2015. Characterization of the Arundo Donax L. solid residue from hydrothermal conversion: Comparison with technical lignins and application perspectives. Ind. Crops Prod. 76, 1008–1024.

Lim, J.S., Manan, Z.A., Rafidah, S., Alwi, W., Hashim, H., 2012. A review on utilisation of biomass from rice industry as a source of renewable energy. Renew. Sustain. Energy Rev. 16, 3084–3094.

Liu, H., Luo, C., Kaneko, M., Kato, S., 2003. Unification of gasification kinetics of char in CO_2 at elevated temperatures with a Modified Random Pore Model. Energy and Fuels 17, 961–970.

Liu, S., 2010. Woody biomass : Niche position as a source of sustainable renewable chemicals and energy and kinetics of hot-water extraction/hydrolysis. Biotechnol. Adv. 28, 563–582.

Liu, Z., Zhang, F., Wu, J., 2010. Characterization and application of chars produced from pinewood pyrolysis and hydrothermal treatment. Fuel 89, 510–514.

Lu, L., Sahajwalla, V., Kong, C., Harris, D., 2001. Quantitative X-ray diffraction analysis and its application to various coals. Carbon 39, 1821–1833.

Mafu, L.D., Msagati, T.A.M., Mamba, B.B., 2013. Adsorption studies for the simultaneous removal of arsenic and selenium using naturally prepared adsorbent materials. Int. J. Environ. Sci. Technol. 11, 1723–1732.

Malico, I., Carrajola, J., Gomes, C.P., Lima, J.C., 2015. Biomass residues for energy production and habitat preservation. Case study in a montado area in Southwestern Europe. J. Clean. Prod. 112, 3676–3683.

Mani, T., Mahinpey, N., Murugan, P., 2011. Reaction kinetics and mass transfer studies of biomass char gasification with CO_2. Chem. Eng. Sci. 66, 36–41.

Maria, A., Galletti, R., Antonetti, C., 2011. Biomass pre-treatment: Seperation of cellulose, hemicellulose and lignin. Existing tehcnologies and perspectives, Eurobioref.

McBeath, A. V, Smernik, R.J., Krull, E.S., Lehmann, J., 2014. The influence of feedstock and production temperature on biochar carbon chemistry : A solid-state ^{13}C NMR study. Biomass and Bioenergy 60, 121–129.

McBeath, A. V, Smernik, R.J., Schneider, M.P.W., Schmidt, M.W.I., Plant, E.L., 2011. Determination of the aromaticity and the degree of aromatic condensation of a thermosequence of wood charcoal using NMR. Org. Geochem. 42, 1194–1202.

Medic, D., Darr, M., Shah, A., Potter, B., Zimmerman, J., 2012. Effects of torrefaction process parameters on biomass feedstock upgrading. Fuel 91, 147–154.

Meesri, C., Moghtaderi, B., 2002. Lack of synergetic e ects in the pyrolytic characteristics of woody biomass/coal blends under low and high heating rate regimes. Biomass and Bioenergy 23, 55–66.

Mehrabadi, A., Farid, M.M., Craggs, R., 2016. Variation of biomass energy yield in wastewater treatment high rate algal ponds. Algal Res. 15, 143–151.

Melkior, T., Jacob, S., Gerbaud, G., Hediger, S., Pape, L. Le, Bonnefois, L., Bardet, M., 2012. NMR analysis of the transformation of wood constituents by torrefaction. Fuel 92, 271–280.

Min, F., Zhang, M., Zhang, Y., Cao, Y., Pan, W.-P., 2011. An experimental investigation into the gasification reactivity and structure of agricultural waste chars. J. Anal. Appl. Pyrolysis 92, 250–257.

Mitsuoka, K., Hayashi, S., Amano, H., Kayahara, K., Sasaoaka, E., Uddin, M.A., 2011. Gasification of woody biomass char with CO_2: The catalytic effects of K and Ca species on char gasification reactivity. Fuel Process. Technol. 92, 26–31.

Mohan, D., Pittman, C.U., Steele, P.H., 2006. Pyrolysis of wood/biomass for bio-oil: A critical review. Energy and Fuels 20, 848–889.

Molina, A., Mondragón, F., 1998. Reactivity of coal gasification with steam and CO_2. Fuel 77, 1831–1839.

Moser, B.R., 2016. Fuel property enhancement of biodiesel fuels from common and alternative feedstocks via complementary blending. Renew. Energy 85, 819–825.

Motghare, K.A., Rathod, A.P., Wasewar, K.L., Labhsetwar, N.K., 2015. Comparative study of different waste biomass for energy application. Waste Manag. 47, 40–45.

Murillo, J.D., Ware, E.A., Biernacki, J.J., 2014. Characterization of milling effects on the physical and chemical nature of herbaceous biomass with comparison of fast pyrolysis product distributions using Py-GC/MS. J. Anal. Appl. Pyrolysis 108, 234–247.

Naik, S., Goud, V. V, Rout, P.K., Jacobson, K., Dalai, A.K., 2010. Characterization of Canadian biomass for alternative renewable biofuel. Renew. Energy 35, 1624–1631.

Neves, D., Thunman, H., Matos, A., Tarelho, L., Gómez-barea, A., 2011. Characterization and prediction of biomass pyrolysis products. Prog. Energy Combust. Sci. 37, 611–630.

Nilsson, S., Gómez-barea, A., Fuentes-cano, D., Ollero, P., 2012. Gasification of biomass and waste in a staged fluidized bed gasifier : Modeling and comparison with one-stage units. Fuel 97, 730–740.

Niu, Y., Du, W., Tan, H., Xu, W., Liu, Y., Xiong, Y., Hui, S., 2013. Further study on biomass

ash characteristics at elevated ashing temperatures: the evolution of K, Cl, S and the ash fusion characteristics. Bioresour. Technol. 129, 642–5.

Niu, Y., Tan, H., Hui, S., 2016. Ash-related issues during biomass combustion: Alkali-induced slagging, silicate melt-induced slagging (ash fusion), agglomeration, corrosion, ash utilization, and related countermeasures. Prog. Energy Combust. Sci. 52, 1–61.

Ochoa, J., Cassanello, M.C., Bonelli, P.R., Cukierman, A.L., 2001. CO_2 gasification of Argentinean coal chars: A kinetic characterization. Fuel Process. Technol. 74, 161–176.

Odeh, A.O., 2015a. Comparative study of the aromaticity of the coal structure during the char formation process under both conventional and advanced analytical techniques. Energy and Fuels 29, 2676–2684.

Odeh, A.O., 2015b. Oualitative and quantitative ATR-FTIR analysis and its application to coal char of different ranks. J. Fuel Chem. Technol. 43, 129–137.

Okolo, G.N., Neomagus, H.W.J.P., Everson, R.C., Roberts, M.J., Bunt, J.R., Sakurovs, R., Mathews, J.P., 2015. Chemical–structural properties of South African bituminous coals: Insights from wide angle XRD–carbon fraction analysis, ATR–FTIR, solid state ^{13}C NMR, and HRTEM techniques. Fuel 158, 779–792.

Ollero, P., Serrera, A., Arjona, R., Alcantarilla, S., 2003. The CO_2 gasification kinetics of olive residue. Biomass and Bioenergy 24, 151–161.

Onay, O., 2007. Influence of pyrolysis temperature and heating rate on the production of bio-oil and char from safflower seed by pyrolysis , using a well-swept fixed-bed reactor. Fuel Process. Technol. 88, 523–531.

Orrego-Ruiz, J.A., Cabanzo, R., Mejía-Ospino, E., 2011. Study of Colombian coals using photoacoustic Fourier transform infrared spectroscopy. Int. J. Coal Geol. 85, 307–310.

Painuly, J.P., 2001. Barriers to renewable energy penetration: A framework for analysis. Renew. Energy 24, 73–89.

Pan, Y.G., Velo, E., Roca, X., Manya, J.J., Puigjaner, L., 2000. Fluidized-bed co-gasification of residual biomass/poor coal blends for fuel gas production. Fuel 79, 1317–1326.

Papanicolaou, C., Kotis, T., Foscolos, A., Goodarzi, F., 2004. Coals of Greece : a review of properties , uses and future perspectives 58, 147–169.

Park, J., Meng, J., Lim, K.H., Rojas, O.J., Park, S., 2013. Transformation of lignocellulosic

biomass during torrefaction. J. Anal. Appl. Pyrolysis 100, 199–206.

Park, S., Jang, C., Baek, K., Yang, J., 2012. Torrefaction and low-temperature carbonization of woody biomass : Evaluation of fuel characteristics of the products. Energy 45, 676–685.

Park, Y., Kim, J., Kim, S., Park, Y., 2009. Pyrolysis characteristics and kinetics of oak trees using thermogravimetric analyzer and micro-tubing reactor 100, 400–405.

Pasangulapati, V., Ramachandriya, K.D., Kumar, A., Wilkins, M.R., Jones, C.L., Huhnke, R.L., 2012. Effects of cellulose, hemicellulose and lignin on thermochemical conversion characteristics of the selected biomass. Bioresour. Technol. 114, 663–669.

Patra, T.K., Sheth, P.N., 2015. Biomass gasification models for downdraft gasifier: A state-of-the-art review. Renew. Sustain. Energy Rev. 50, 583–593.

Pimenidou, P., Dupont, V., 2012. Characterisation of palm empty fruit bunch (PEFB) and pinewood bio-oils and kinetics of their thermal degradation. Bioresour. Technol. 109, 198–205.

Poudel, J., Ohm, T., Cheon, S., 2015. A study on torrefaction of food waste. Fuel 140, 275–281.

Prins, M.J., Ptasinski, K.J., Janssen, F.J.J.G., 2006a. Torrefaction of wood Part 2 . Analysis of products. J. Anal. Appl. Pyrolysis 77, 35–40.

Prins, M.J., Ptasinski, K.J., Janssen, F.J.J.G., 2006b. More efficient biomass gasification via torrefaction. Energy 31, 3458–3470.

Puig-Arnavat, M., Bruno, J.C., Coronas, A., 2010. Review and analysis of biomass gasification models. Renew. Sustain. Energy Rev. 14, 2841–2851.

Rehrah, D., Bansode, R.R., Hassan, O., Ahmedna, M., 2015. Physico-chemical characterization of biochars from solid municipal waste for use in soil amendment. J. Anal. Appl. Pyrolysis 118, 42–53.

Roberts, M.J., Everson, R.C., Neomagus, H.W.J.P., Okolo, G.N., Van Niekerk, D., Mathews, J.P., 2015. The characterisation of slow-heated inertinite- and vitrinite-rich coals from the South African coalfields. Fuel 158, 591–601.

Robinson, J.M., Barrett, S.R., Nhoy, K., Pandey, R.K., Phillips, J., Ramirez, O.M., Rodriguez, R.I., 2009. Energy Dispersive X-ray Fluorescence Analysis of Sulfur in Biomass. Energy and fuels 23, 2235–2241.

Rodriguez, F.J., Schlenger, P., Garcia-Valverde, M., 2016. Monitoring changes in the structure

and properties of humic substances following ozonation using UV-Vis, FTIR and ^{1}H NMR techniques. Sci. Total Environ. 541, 623–637.

Rosendahl, L.A., Yin, C., Kær, S.K., Friborg, K., Overgaard, P., 2007. Physical characterization of biomass fuels prepared for suspension firing in utility boilers for CFD modelling. Biomass and Bioenergy 31, 318–325.

Rosillo-Calle, F., 2016. A review of biomass energy- shortcomings and concerns. J. Chem. Technol. Biotechnol. 1933–1945.

Rousset, P., Macedo, L., Commandré, J., Moreira, A., 2012. Biomass torrefaction under different oxygen concentrations and its effect on the composition of the solid by-product. J. Anal. Appl. Pyrolysis 96, 86–91.

Ruiz, J.A., Juarez, M.C., Morales, M.P., Munoz, P., Mendivil, M.A., 2013. Biomass gasification for electricity generation : Review of current technology barriers. Renew. Sustain. Energy Rev. 18, 174–183.

Rutherford, D.W., Wershaw, R.L., Rostad, C.E., Kelly, C.N., 2012. Effect of formation conditions on biochars : Compositional and structural properties of cellulose , lignin , and pine biochars. Biomass and Bioenergy 46, 693–701.

Saidur, R., Abdelaziz, E.A., Demirbas, A., Hossain, M.S., Mekhilef, S., 2011. A review on biomass as a fuel for boilers. Renew. Sustain. Energy Rev. 15, 2262–2289.

Santoni, I., Callone, E., Sandak, A., Sandak, J., Dirè, S., 2015. Solid state NMR and IR characterization of wood polymer structure in relation to tree provenance. Carbohydr. Polym. 117, 710–721.

Sarkar, M., Kumar, A., Tumuluru, J.S., Patil, K.N., Bellmer, D.D., 2014. Gasification performance of switchgrass pretreated with torrefaction and densification. Appl. Energy 127, 194–201.

Sasaki, M., 2003. Fractionation of sugarcane bagasse by hydrothermal treatment. Bioresour. Technol. 86, 301–304.

Satyam Naidu, V., Aghalayam, P., Jayanti, S., 2016. Synergetic and inhibition effects in carbon dioxide gasification of blends of coals and biomass fuels of Indian origin. Bioresour. Technol. 209, 157–165.

Sellin, N., Krohl, D.R., Marangoni, C., Souza, O., 2016. Oxidative fast pyrolysis of banana

leaves in fluidized bed reactor. Renew. Energy 96, 56–64.

Shang, L., Ahrenfeldt, J., Holm, J.K., Bach, L.S., Stelte, W., Henriksen, U.B., 2014. Kinetic model for torrefaction of wood chips in a pilot-scale continuous reactor. J. Anal. Appl. Pyrolysis 108, 109–116.

Skhonde, M.P., Matjie, R.H., Bunt, J.R., Strydom, A.C., Schobert, H., 2009. Sulfur Behavior in the Sasol-Lurgi Fixed-Bed Dry-Bottom Gasification Process. Energy & Fuels 23, 229–235.

Starink, M.J., 1996. A new method for derivation of activation energies from experiments performed at constant heating rate. Thermochim. Acta 288, 97–104.

Struis, R.P.W.J., Scala, C. Von, Stucki, S., Prins, R., 2002. Gasiÿcation reactivity of charcoal with CO 2 . Part I : Conversion and structural phenomena 57, 3581–3592.

Suarez-Garcia, F., Martinez- Alonso, A., Fernandez Llorente, M., Tascon, J.M.., 2002. Inorganic matter characterization in vegetable biomass feedstocks. Fuel 81, 1161–1169.

Suliman, W., Harsh, J.B., Abu-Lail, N.I., Fortuna, A.M., Dallmeyer, I., Garcia-Perez, M., 2016. Influence of feedstock source and pyrolysis temperature on biochar bulk and surface properties. Biomass and Bioenergy 84, 37–48.

Taba, L.E., Faisal, M., Ashri, W., Wan, M., Chakrabarti, M.H., 2012. The effect of temperature on various parameters in coal , biomass and Co-gasification : A review. Renew. Sustain. Energy Rev. 16, 5584–5596.

Tanigaki, N., Manako, K., Osada, M., 2012. Co-gasification of municipal solid waste and material recovery in a large-scale gasification and melting system. Waste Manag. 32, 667–675.

Tanner, J., Bhattacharya, S., 2016. Kinetics of CO_2 and steam gasification of Victorian brown coal chars. Chem. Eng. J. 285, 331–340.

Tortosa Masiá, A.A., Buhre, B.J.P., Gupta, R.P., Wall, T.F., 2007. Characterising ash of biomass and waste. Fuel Process. Technol. 88, 1071–1081.

Tripathi, M., Sahu, J.N., Ganesan, P., 2016. Effect of process parameters on production of biochar from biomass waste through pyrolysis: A review. Renew. Sustain. Energy Rev. 55, 467–481.

Tumuluru, J.S., Hess, J.R., Boardman, R.D., Wright, C.T., Westover, T.L., 2012. Formulation, pretreatment, and densification options to improve biomass specifications for co-firing

high percentages with coal. Ind. Biotechnol. 8, 113–133.

Tumuluru, J.S., Sokhansanj, S., Hess, J.R., Wright, C.T., Boardman, R.D., 2011. A review on biomass torrefaction process and product properties for energy applications. Ind. Biotechnol. 7, 384–402.

Turkdogan, E.T., Vinters, J. V, 1969. Kinetics of Oxidation of graphite and charcoal in CO_2. Carbon 78, 115-126.

Tursun, Y., Xu, S., Wang, C., Xiao, Y., Wang, G., 2016. Steam co-gasification of biomass and coal in decoupled reactors. Fuel Process. Technol. 141, 61–67.

Uchimiya, M., Wartelle, L.H., Klasson, K.T., Fortier, C.A., Lima, I.M., 2011. Influence of pyrolysis temperature on biochar property and function as a heavy metal sorbent in soil. J. Agric. Food Chem. 59, 2501–2510.

Umamaheswaran, K., Batra, V.S., 2008. Physico-chemical characterisation of Indian biomass ashes. Fuel 87, 628–638.

Uslu, A., 2008. Pre-treatment technologies , and their effect on international bioenergy supply chain logistics . Techno-economic evaluation of torrefaction , fast pyrolysis and pelletisation. Energy 33, 1206–1223.

Uzun, B.B., Putun, A.E., Ersan, P., 2006. Fast pyrolysis of soybean cake : Product yields and compositions. Bioresour. Technol. 97, 569–576.

Uzun, B.B., Sarioğlu, N., 2009. Rapid and catalytic pyrolysis of corn stalks. Fuel Process. Technol. 90, 705–716.

van der Stelt, M.J.C., Gerhauser, H., Kiel, J.H.A., Ptasinski, K.J., 2011. Biomass upgrading by torrefaction for the production of biofuels : A review. Biomass and Bioenergy 35, 3748–3762.

Van der Walt, M.-L., Masangane, P., Balmer, M., Qase, N., 2015. State of Renewable Energy in South Africa.

Várhegyi, G., Szabó, P., Antal, M.J., 2002. Kinetics of charcoal devolatilization. Energy and Fuels 16, 724–731.

Varhegyi, G., Szabo, P., Till, F., Antal, M.J., Dai, X., 1998. TG, TG-MS, and FTIR characterization of high-yield biomass charcoals. Energy and fuels 969–974.

Varhegyif, G., Antal, M.J., 1989. Kinetics of the thermal decomposition of cellulose ,

hemicellulose, and sugar cane bagasse 329–335.

Vassilev, S. V., Baxter, D., Andersen, L.K., Vassileva, C.G., 2010. An overview of the chemical composition of biomass. Fuel 89, 913–933.

Vassilev, S. V., Vassileva, C.G., 2009. A new approach for the combined chemical and mineral classification of the inorganic matter in coal. 1. Chemical and mineral classification systems. Fuel 88, 235–245.

Vassilev, S. V, Baxter, D., Andersen, L.K., Vassileva, C.G., Morgan, T.J., 2012. An overview of the organic and inorganic phase composition of biomass. Fuel 94, 1–33.

Vassilev, S. V, Braekman-danheux, C., Laurent, P., 1999. Characterization of refuse-derived char from municipal solid waste 1. Phase-mineral and chemical composition. Fuel Process. Technol. 59, 95–134.

Velden, M. Van De, Baeyens, J., Brems, A., Janssens, B., Dewil, R., 2010. Fundamentals , kinetics and endothermicity of the biomass pyrolysis reaction. Renew. Energy 35, 232–242.

Vieira, E., Jackson, G., Rocha, D.M., 2007. Optimization of acid hydrolysis from the hemicellulosic fraction of Eucalyptus grandis residue using response surface methodology 98, 422–428.

Wang, C., Peng, J., Li, H., Bi, X.T., Legros, R., Lim, C.J., 2013. Oxidative torrefaction of biomass residues and densification of torrefied sawdust to pellets. Bioresour. Technol. 127, 318–325.

Wang, F., Zeng, X., Wang, Y., Su, H., Yu, J., Xu, G., 2016. Non-isothermal coal char gasification with CO2 in a micro fluidized bed reaction analyzer and a thermogravimetric analyzer. Fuel 164, 403–409.

Wang, G., Zhang, J., Hou, X., Shao, J., Geng, W., 2015. Study on CO_2 gasification properties and kinetics of biomass chars and anthracite char. Bioresour. Technol. 177, 66–73.

Wang, Q., Ye, J., Yang, H., Liu, Q., 2016. Chemical composition and structural characteristics of oil shales and their kerogens using Fourier Transform Infrared (FTIR) spectroscopy and Solid-State ^{13}C Nuclear Magnetic Resonance (NMR). Energy & Fuels 30, 6271–6280.

Wang, Y.-L., Zhu, S.-H., Gao, M.-Q., Yang, Z.-R., Yan, L.-J., Bai, Y.-H., Li, F., 2015. A study of char gasification in H_2O and CO_2 mixtures: Role of inherent minerals in the coal. Fuel

Process. Technol. 141, 9–15.

Wannapeera, J., Fungtammasan, B., Worasuwannarak, N., 2011. Effects of temperature and holding time during torrefaction on the pyrolysis behaviors of woody biomass. J. Anal. Appl. Pyrolysis 92, 99–105.

Wannapeera, J., Worasuwannarak, N., 2012. Upgrading of woody biomass by torrefaction under pressure. J. Anal. Appl. Pyrolysis 96, 173–180.

Wei, L., Pordesimo, L.O., Haryanto, A., Wooten, J., 2011. Co-gasification of hardwood chips and crude glycerol in a pilot scale downdraft gasifier. Bioresour. Technol. 102, 6266–6272.

Weldemichael, Y., Assefa, G., 2015. Assessing the energy production and GHG (greenhouse gas) emissions mitigation potential of biomass resources for Alberta. J. Clean. Prod. 112, 4257–4264.

Wikberg, H., Maunu, S.L., 2004. Characterisation of thermally modified hard- and softwoods by ^{13}C CPMAS NMR. Carbohydr. Polym. 58, 461–466.

Wu, Y., Wu, S., Gao, J., 2009. A Study on the applicability of kinetic models for Shenfu coal char gasification with CO_2 at elevated temperatures. Energies 2, 545–555.

Xiao, R., Yang, W., 2016. Kinetics characteristics of straw semi-char gasification with carbon dioxide. Bioresour. Technol. 207, 180–187.

Xue, G., Kwapinska, M., Kwapinski, W., Czajka, K.M., Kennedy, J., Leahy, J.J., 2014. Impact of torrefaction on properties of *Miscanthus×giganteus* relevant to gasification. Fuel 121, 189–197.

Yaman, S., 2004. Pyrolysis of biomass to produce fuels and chemical feedstocks. Energy Convers. Manag. 45, 651–671.

Yang, H., Yan, R., Chen, H., Zheng, C., Lee, D.H., Uni, V., V, N.D., March, R. V, Re, V., Recei, M., September, V., 2006. In-Depth investigation of biomass pyrolysis based on three major components : hemicellulose, cellulose and lignin. Energy and Fuels 388–393.

Ye, D.P., Agnew, J.B., Zhang, D.K., 1998. Gasification of a South Australian low-rank coal with carbon dioxide and steam: kinetics and reactivity studies. Fuel 77, 1209–1219.

Zandersons, J., Gravitis, J., Kokorevics, A., Zhurinsh, A., Bikovens, O., 1999. Studies of the Brazilian sugarcane bagasse carbonisation process and products properties. Biomass and Bioenergy 17, 209–219.

Zhang, F., Ma, H., Chen, J., Li, G., Zhang, Y., Chen, J., 2008. Preparation and gas storage of high surface area microporous carbon derived from biomass source cornstalks. Bioresour. Technol. 99, 4803–4808.

Zhang, J., Wang, G., Shao, J., Zuo, H., 2014. A modified random pore model for the kinetics of char gasification. Bioresources 9, 3497–3507.

Zhang, S., Dong, Q., Zhang, L., Xiong, Y., Liu, X., Zhu, S., 2015. Effects of water washing and torrefaction pretreatments on rice husk pyrolysis by microwave heating. Bioresour. Technol. 193, 442–8.

Zhang, Y., Fan, D., Zheng, Y., 2015. Comparative study on combined co-pyrolysis/gasification of walnut shell and bituminous coal by conventional and congruent-mass thermogravimetric analysis (TGA) methods. Bioresour. Technol. 199, 2013–2016.

Zhang, Y., Hara, S., Kajitani, S., Ashizawa, M., 2010. Modeling of catalytic gasification kinetics of coal char and carbon. Fuel 89, 152–157.

Zhang, Y., Zheng, Y., Yang, M., Song, Y., 2016. Effect of fuel origin on synergy during co-gasification of biomass and coal in CO_2. Bioresour. Technol. 200, 789–794.

Zhao, H., Kwak, J.H., Zhang, Z.C., Brown, H.M., Arey, B.W., Holladay, J.E., 2007. Studying cellulose fiber structure by SEM, XRD, NMR and acid hydrolysis. Carbohydr. Polym. 68, 235–241.

Zhao, X., Chen, J., Chen, F., Wang, X., Zhu, Q., Ao, Q., 2013. Surface characterization of corn stalk superfine powder studied by FTIR and XRD. Colloids Surfaces B Biointerfaces 104, 207–212.

Zoulalian, A., Bounaceur, R., Dufour, A., 2015. Kinetic modelling of char gasification by accounting for the evolution of the reactive surface area. Chem. Eng. Sci. 138, 281–290.

Zuo, H., Geng, W., Zhang, J., Wang, G., 2015. Comparison of kinetic models for isothermal CO_2 gasification of coal char-biomass char blended char. Int. J. Miner. Metall. Mater. 22, 363–370.

Chapter 3: Structural and chemical modifications of typical South African biomass samples during torrefaction

Findings reported in this chapter are published as: Mafu, L.D., Neomagus, H.W.J.P., Everson, R.C., Carrier, M., Strydom, C.A. and Bunt, J.R., 2016. Structural and chemical modifications of typical South African biomasses during torrefaction. *Bioresource Technology*. 202, 192–197. http://dx.doi.org/10.1016/j.biortech.2015.12.007.

Abstract

Torrefaction experiments were carried out for three typical South African biomass samples (softwood chips, hardwood chips and sweet sorghum bagasse) to a weight loss of 30 wt.%. During torrefaction, moisture, non-structural carbohydrates and hemicelluloses contents were reduced, resulting in a structurally modified torrefaction product. There was a reduction in the average crystalline diameter (L_a) (XRD), an increase in the aromatic fraction and a reduction in aliphatics (substituted and unsubstituted) (CPMAS ^{13}C NMR). The decrease in the aliphatic components of the lignocellulosic material under the torrefaction conditions also resulted in a slight ordering of the carbon lattice. The degradation of hemicelluloses and non-structural carbohydrates increased the inclusive surface area of sweet sorghum bagasse, while it did not change significantly for the woody biomass samples.

***Keywords**: Biomass, Torrefaction, CP-MAS ^{13}C NMR, XRD.*

3.1 Introduction

Biomass utilization, either as a precursor for electricity generation or biofuel production, has received a lot of attention in the last decade in the wake of increasing calls for renewable energy utilisation. Waste biomass is of great interest as it avoids the competition between energy and food crops, which may assist with food security in the world (Aboyade et al., 2013). South Africa, amongst other African countries, produces large amounts of waste biomass from the paper industry, sugar industry as well as municipal wastes (Damm and Triebel, 2008). These biomass samples include wood chips (softwood and hardwood), sugarcane bagasse, sweet sorghum bagasse, dried corn cobs and corn stover (Aboyade et al., 2013; Damm and Triebel, 2008), having a large lignocellulosic content, offering potential in thermochemical applications.

Pre-treatment methods are often used to beneficiate biomass, e.g. to ensure a reduction in oxygen, moisture and smoking propensity of the generated fuel (Yang et al., 2014). A number of pre-treatment methods have been studied to provide this highly sought 'new biomass' and the specific application seems to determine the preferred pre-treatment method (Tumuluru et al., 2011). Often referred to as mild pyrolysis, torrefaction is most suited for thermochemical applications and is reported to upgrade biomass by producing a more hydrophobic fuel with an increased fixed carbon content and reduced elemental oxygen (Chen et al., 2015; Tumuluru et al., 2011; Wannapeera and Worasuwannarak, 2012; Yang et al., 2014). Torrefaction does not only reduce bulk and oxygenated discharges but torrefied biomass also has a higher energy yield and mass energy density than raw biomass resulting from the degradation of mostly hemicelluloses and to a lesser extent cellulose and lignin (Kim et al., 2012; van der Stelt et al., 2011).

The chemical and structural characteristics of biomass are mainly dependent on the fibre composition i.e. the amount of hemicellulose, cellulose and lignin. These vary for each biomass family. For instance, woody biomass records highest lignin amounts whilst it is reported that bagasse (sugarcane or sweet sorghum) has high hemicelluloses and non-structural carbohydrates (Carrier et al., 2013; Wannapeera and Worasuwannarak, 2012). The amounts of each of the fibre components contribute to process products in any application, for instance: higher lignin biomass samples are suitable for thermochemical applications for their higher char yield after pyrolysis (Wang et al., 2008; Wannapeera and Worasuwannarak, 2012). In the case of thermochemical applications, char properties are frequently investigated, mostly to explain observed pyrolysis or gasification kinetics (Cao et al., 2014; Guerrero et al., 2008).

Recent research on the characteristics of torrefied biomass focused on the change in elemental compositions, C/O and H/O ratio, fibre composition, thermal stability, hydrophobicity and grindability (Phanphanich and Mani, 2011; Tumuluru et al., 2011; Wannapeera and Worasuwannarak, 2012). There is only limited reporting on structural changes by torrefaction as investigated by solid state ^{13}C Nuclear magnetic resonance (NMR) spectroscopy, wide angle X-ray diffraction carbon fraction analysis (WA-XRD-CFA) as well as explanations of surface area changes in relation to the lignocellulosic compositional alterations by torrefaction. A detailed evaluation of these structural changes could be beneficial to understanding the torrefied material's reactivity towards pyrolysis, combustion and/or gasification (van der Stelt et al., 2011; Xue et al., 2014).

Biomass characterization using WA-XRD-CFA and CP-MAS ^{13}C NMR (cross polarization Magnetic Angle Spinning (CPMAS) ^{13}C NMR has been receiving much attention in the past years. The effect of comminution on raw biomass samples has been investigated using powder WA-XRD-CFA (Murillo et al., 2014; Zhao et al., 2013), and char comparisons (Guerrero et al., 2008) were also established whilst crystallinity and mineralogy changes during pyrolysis are reported elsewhere (Cao et al., 2014; Guerrero et al., 2008). Crystallinity may also be quantified by CPMAS ^{13}C NMR, as shown by Focher et al., (2001), for differently sourced celluloses. Even though raw biomass structure is complicated to understand, CPMAS ^{13}C NMR has been reported and peak positions were assigned to the main groups found. Degradation of lignocellulosic components either by torrefaction or pyrolysis have also been tracked by CPMAS ^{13}C NMR experiments (Freitas et al., 2001; Melkior et al., 2012; Park et al., 2013; Wikberg and Maunu, 2004). Park et al., (2013) reported insightful findings on the transformation of biomass by heat treatment structures using both CPMAS and DPMAS ^{13}C NMR (direct polarization ^{13}C solid state Nuclear Magnetic Resistance spectroscopy) and noted the superiority of DPMAS in quantifying non-protonated carbons. Ben and Ragauskas (2012), elaborated on how torrefaction affects raw pine carbohydrate composition and also conclusions on how heat disrupts the binding between the macro-components together using CPMAS ^{13}C NMR. However, lattice parameters and carbon type changes due to torrefaction as determined by WA-XRD-CFA and CPMAS ^{13}C NMR, respectively, have yet not received considerable attention.

In coal characterization, parameters from WA-XRD-CFA, HR-TEM (high resolution transmission electron microscopy) and CPMAS ^{13}C NMR provided insight in the structural arrangement of the material in relation to gasification kinetics (Okolo et al., 2015; Roberts et al., 2015a). A similar approach to raw and torrefied biomass is currently lacking and forms part of

the motivation of this paper. The overall purpose is to establish the properties of the torrefied biomass to be used for evaluation of gasification kinetics. The effect of torrefaction on the structural and chemical characteristics of three biomass samples abundantly available in South Africa; sweet sorghum bagasse (SB), softwood chips (SW) and hardwood chips (HW) is studied

3.2 Materials and methods

3.2.1 Materials

SW and HW were supplied by the South African Pulp and Paper Industries Limited (Pretoria, Republic of South Africa) and SB was obtained from the Agricultural Research Council (ARC), Potchefstroom (Republic of South Africa). All samples were air-dried for a week, ground to ~ 5 mm using a hammer mill (TRF-70) and milled to < 500 μm using a ball mill. Nitrogen (purity ≥ 99.999 %) and carbon dioxide (purity ≥ 99.998 %) were supplied by Africa Oxygen Limited (Afrox).

3.2.2 Torrefaction

Torrefaction experiments were performed in a thermogravimetric analyser (SDTQ 600). Approximately 10 mg of sample was heated at 10°C/min from 30 to 260°C, in 100 ml/min N_2. The samples were kept at 260°C until a loss of 30 wt.% of the air dried material was obtained. This mass loss was obtained after 110, 100 and 20 minutes heating at the maximum temperature for SW, HW and SB respectively. These conditions were then used for bulk torrefaction which was carried out in a tube furnace from Elite Thermal Systems Limited (Model TSH12/75/610), where 15 g of biomass was torrefied. The furnace was initially flushed with N_2 which was then stabilised at 100 mL/min. The 30% weight loss was achieved in the furnace (within acceptable statistical analysis) even with increasing the sample mass and reaction vessel. In this communication, RSW, RHW and RSB denote raw SW, raw HW and SB respectively, whilst TSW, THW and TSB refer to torrefied SW, HW and SB, respectively.

3.2.3 Characterization of biomass samples

3.2.3.1 Ultimate and proximate analysis

Elemental carbon, hydrogen, oxygen and nitrogen contents were determined on a CE 440 elemental analyser using the ASTM D 5373 method, for both the raw and torrefied material, and the oxygen content was calculated by difference. Proximate analysis was performed using a U-Therm TGA. Standard methods of analyses used are shown in Table 4.1, while the fixed carbon

content was determined by difference. Calorific value measurements were performed using an oxygen bomb calorimeter (IKA 500).

3.2.3.2 Compositional analysis

Adopting the 'food industry' method (Carrier et al., 2011), acid detergent lignin (ADL), acid detergent fibre (ADF), neutral detergent fibre (NDF) and non-structural carbohydrates were determined at ARC-Analytical services, Republic of South Africa. Equations 3.1 and 3.2 were used to determine the hemicellulose and cellulose fractions of the samples. It should be noted that the ADL value was assumed to be the total lignin mass percentage in the samples (Phanphanich and Mani, 2011).

$$Hemicelluloses\ (wt.\%) = NDF - ADF \quad (3.1)$$

$$Cellulose\ (wt.\%) = ADF - ADL \quad (3.2)$$

3.2.3.3 Thermal behaviour

The thermal behaviour of both the raw and torrefied biomass samples was analysed by running pyrolysis experiments in a thermogravimetric analyser (SDTQ 600), using approximately 15 mg of sample, and ramping the temperature from 30°C to 500°C under N_2 (100 mL/min) at 10°C/min.

3.2.3.4 CO2 gas adsorption

CO_2 surface area and porosity properties were determined using a Micrometrics ASAP 2020 surface area and porosity analyser. Approximately 0.2 g of each sample was degassed under vacuum at 75 °C for 48 hours prior to CO_2 adsorption. The analysis was conducted in an ice-water bath at 0 °C in the relative pressure range: $0 < P/P_0 \leq 0.032$; where P is the analysis pressure and P_0 is the saturation vapour pressure of adsorbate gas. Adsorption data were automatically acquired by the ASAP 2020 v4.01 software. The Dubinin-Radushkevich (D-R), Brunauer–Emmet –Teller (BET) and Horvath–Kawazoe (H-K) methods were used to obtain the surface area, maximum pore volume, and median pore width of the samples (Downie et al., 2009)

3.2.3.5 X-ray diffraction

WA-XRD-CFA experiments were conducted at the laboratory of XRD Analytical and Consulting cc, Pretoria, as reported elsewhere (Everson et al., 2013; Roberts et al., 2015b). The resulting spectrum was then corrected for background scattering. Assuming a crystallite layered

in the form ABABAB, as for coal (Everson et al., 2013; Okolo et al., 2015; Roberts et al., 2015b), the (002) band representing the packing of aromatic layers and (10) reflection signifying the 2-dimensional lattices of aromatic rings, were used to determine crystallographic parameters. The interlayer spacing (d_{002}), crystallite height (L_c) and average crystallite size (L_a) were determined, from which the number of crystallites in a stack (N_{ave}) was deduced as reported elsewhere (Everson et al., 2013; Okolo et al., 2015; Roberts et al., 2015a).

3.2.3.6 Solid state ^{13}C NMR spectroscopy

CPMAS ^{13}C NMR experiments were carried out at the Central Analytical Facility of Stellenbosch University (Republic of South Africa) following a method by Melkior et al. (2012), which is a combination of cross polarization and magnetic angle spinning techniques (CPMAS ^{13}C NMR). Chemical shift values were calibrated using a glycine carbonyl signal known to be at 176.3 ppm. The peak at 104.7 ppm was used to normalize the spectra and assigned to C-1, which is known not to change at heat treatments below 270 °C (Focher et al., 2001; Freitas et al., 2001; Melkior et al., 2012). Peak assignments were achieved by reference to published research conducted on biomass, and comparisons between the raw and torrefied biomass were used to determine the effect of heat treatment on the three biomass samples (Focher et al., 2001; Freitas et al., 2001; Melkior et al., 2012). The relative distribution percentage for each functional group was determined after integration of the spectral regions using MestReNova (Version 10) software. Functional groups were assigned as follows: carboxylics (219-190 ppm), phenolics (190-163 ppm), aromatics (162-97 ppm), substituted aliphatics (97-50 ppm) and aliphatics (50-0 ppm) (Cao et al., 2012).

3.3 Results and discussion

3.3.1 Chemical analysis

3.3.1.1 Ultimate, proximate and calorific analysis

In Table 3.1, the ultimate and proximate analyses results for raw and torrefied biomass are presented. After torrefaction, a decrease in moisture content and volatiles and an increase in fixed carbon content were observed. The ultimate analysis shows an increase in elemental carbon, and a decrease in elemental oxygen and hydrogen, and hence a decrease in H/C and O/C ratio for the torrefied material. The calorific value of the torrefied material increased compared to the raw biomass. These general trends and absolute values obtained for the calorific value and proximate and ultimate analysis compare well with other findings (Chen et al., 2015; Tumuluru et al., 2011).

Table 3-1: Proximate and ultimate results for raw and torrefied biomass

Proximate Analysis (wt.% adb)[#]	**Standard**	**RSW**	**TSW**	**RHW**	**THW**	**RSB**	**TSB**
Inherent Moisture	SANS 5925	6.8	3.9	7.6	3.7	7.4	3.6
Ash	ISO 1171	0.39	0.61	0.44	0.60	4.3	6.0
Volatiles	ISO 562	79.5	74.8	78.3	74.5	73.3	67.3
Fixed Carbon	By difference	13.3	20.9	13.7	21.2	15.0	23.1
Gross Calorific Value (MJ/kg)	ISO 1928	18.0	22.3	18.0	22.4	17.3	23.0
Ultimate Analysis (wt.% daf)[*]							
Carbon	ASTM D5373	47.7	55.1	46.4	55.4	43.5	53.4
Hydrogen	ASTM D5373	5.7	5.6	5.5	5.4	5.6	5.0
Nitrogen	ASTM D5373	0.96	0.13	0.10	0.01	0.28	0.32
Total Sulfur	ASTM D 4239	0.16	nd [+]	0.01	nd	0.13	nd
Oxygen	By difference	45.5	39.2	48.0	39.2	50.5	40.9
H/C		1.42	1.21	1.41	1.16	1.53	1.11
O/C		0.72	0.53	0.78	0.53	0.87	0.57

[#]adb – air-dried basis, [*]daf – dry ash-free basis, [+]nd – not detectable

3.3.1.2 Compositional analysis

The distribution of the fibre composition is shown in Table 3.2, and is in accordance with the origin of the raw biomass samples ranging from gramineae to gymnosperms and angiosperms. SB samples exhibited the lowest lignin content, 5.24 wt%, followed by the HW, 16.0 wt%, and the SW, 23.5 wt%, which correspond to the range reported in literature, i.e. 6-25 wt% for plant materials, 18-50 wt% for HW, and 25-40 wt% for SW (Kim et al., 2012; van der Stelte et al., 2011). The amount of lignin in woody biomass did not change significantly after torrefaction, however this was not the case for SB, whose lignin content significantly increased from 5.24 to 16.0 g/g air dried raw biomass (Table 3.2). These results confirmed that lignin compounds are thermally more resistant than carbohydrate components (van der Stelt et al., 2011; Yang et al., 2007). An increase of the lignin in SB (by over 150%) has been previously observed by Park et al. (2013), who concluded that the increase could be a consequence of a rearrangement of the sample matrix into compounds or bonding structures, which are resistant to acid hydrolysis, especially non-structural carbohydrates. The authors also suggest that the torrefaction heat result

in the formation of linkages, within the matrix, that are acid resistant, and hence classified 'newly formed' compounds as lignin (Park et al., 2013; van der Stelt et al., 2011).

Table 3-2: Fibre analysis for raw (wt.%) and torrefied biomass (g/g air dried raw biomass)

	Hemicellulose	**Cellulose**	**Lignin**	**Non.Str[a]**	**Ash**	**Moisture**
RSW	13.8	47.4	23.5	3.1	0.39	6.82
TSW	2.65	36.6	23.2	0.90	0.40	2.35
RHW	11.4	56.9	16.0	3.01	0.44	7.60
THW	1.20	46.7	15.7	1.50	0.40	2.60
RSB	24.4	29.8	5.24	19.8	3.95	7.41
TSB	4.80	19.9	16.0	1.90	4.20	2.50

[a]Non-Str – Non-structural carbohydrates

For the carbohydrates fraction, the hemicelluloses amount was higher in the SB, 24.4 wt%, than in SW, 13.8 wt%, and HW, 11.4 wt%., whereas an opposite trend was observed for cellulose (Table 3.2). During torrefaction, approximately 80% of the hemicelluloses were degraded, whilst there was a slight decrease in the cellulose content. This observation agrees with previous findings showing that hemicelluloses are the most sensitive of the cell-wall components towards temperature (Tumuluru et al., 2011; Velden et al., 2010). Charring of the non-structural carbohydrates under torrefaction may result in an increase in the number of carbon-carbon linkages due to an increase in carbon content and the departure of oxygen and hydrogen during the dehydration stage (Table 3.2).

3.3.1.3 Solid state 13C NMR experiments

From the CP-MAS ^{13}C NMR spectra (Figure 3.1) all the biomass samples showed the following resonance characteristics; the presence of aliphatic carbon side chain groups, structural carbohydrates, carbonyls are represented by the regions between 0-50 ppm, 60-96 ppm and 185 – 220 ppm, respectively. The frequency region between 21 and 172 ppm usually corresponds to hemicelluloses, largely dominated by the resonance of sugar rings (Focher et al., 2001; Park et al., 2013; Santoni et al., 2015). In the aliphatics region, the intense peak at 21 ppm, attributed to the acetyl methyl group of hemicelluloses (Melkior et al., 2012), was significantly reduced after the torrefaction treatment. This observation agrees with the decrease of the hemicellulosic fraction, and earlier conclusions that, at low temperatures, (torrefaction temperature ranges) hemicelluloses are significantly affected (Chen et al., 2015; Wikberg and Maunu, 2004).

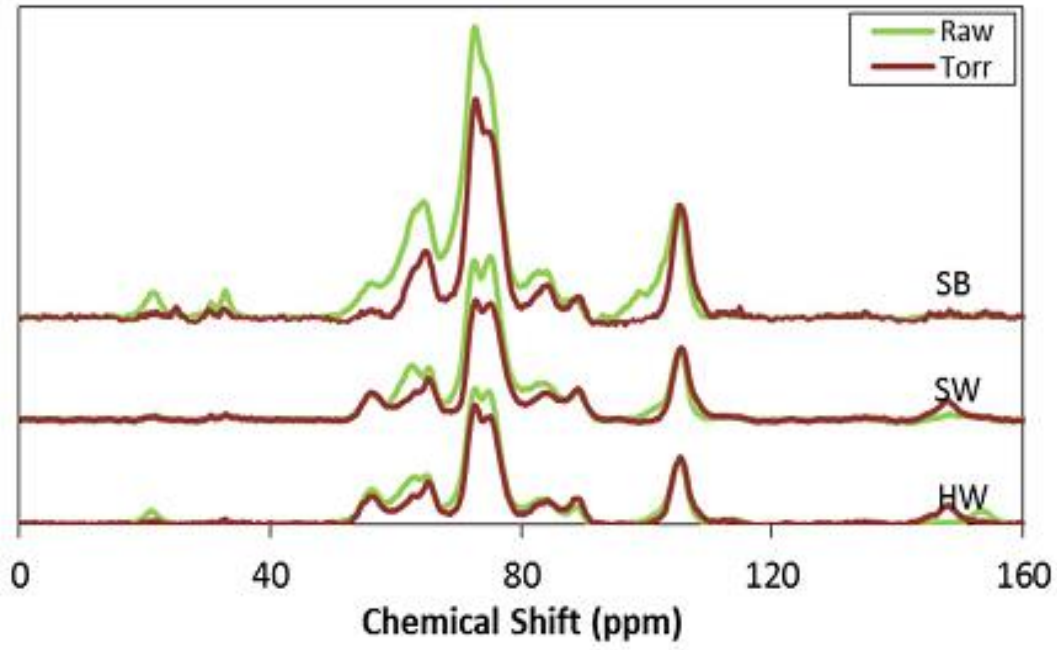

Figure 3-1: CPMAS ^{13}C Solid state NMR spectra for raw and torrefied biomass samples (SB-Sweet sorghum bagasse, SW-Soft wood chips and HW- hardwood chips)

The intensity of the peak at 56 ppm, which is usually assigned to carbons of cellulose sugar rings and methoxy groups in lignocellulosic fibres lignins, decreased in the order HW > SW > SB, and is in agreement with the cellulose content (56.9, 47.4 and 29.8 for HW, SW and SB respectively). In the case of SB, this peak (56 ppm) disappeared after torrefaction, whereas its intensity was only decreased for woody biomass; thus indicating the unstable thermal nature of celluloses derived from grassy biomass and the degradation of methoxy groups in the sample. Finally, and still appearing in this aliphatic region, a unique peak at 32 ppm may be associated with carbons of non-structural carbohydrates, and it was found to be significant for the raw SB compared to the raw woody materials. This observation was in agreement with the large amounts of non-structural carbohydrates of up to 20 wt.% for the raw SB (Table 3.2) that were degraded under torrefaction conditions.

There was a significant overlap between carbon resonances of celluloses and hemicelluloses, and to a little extent with lignin carbons. This was shown by the overlapping of peaks between 61 to 65 ppm linked to the presence of C-6 or ordered and disordered cellulose and lignins (Melkior et al., 2012). The same trend was observed between 70 and 75 ppm, and these are linked with the presence of C-2, 3, 5 as well as α – carbons of lignins. This region is slightly diminished after torrefaction owing to the slight reduction of celluloses. In this region there is also an interference

of carbons aligned to non-structural carbohydrates, hence the higher intensity of these peaks for SB compared to HW and SW.

It was also concluded, from the spectra, that the disordered fractions of all lignocellulosic fibres were mostly affected by torrefaction, while the ordered fraction remains similar. This may be supported by the relative peak areas, between raw and torrefied biomass, at 83 and 89 ppm, which are assigned to disordered as well as C-β in lignin and ordered C-4 of cellulose, respectively. Only the 83 ppm peak is reduced after torrefaction. A shoulder peak at 100 ppm is assigned to C-1 of hemicellulose, and is almost totally removed by torrefaction. Further, the presence of guaiacyl-, syringyl- and etherified lignins, is confirmed by the peaks between 106 – 152 ppm. There were no changes observed for the peak around 110 ppm after torrefaction, in line with the insignificant change in lignin fraction after torrefaction. For SB, there was no evidence of lignin increase by CPMAS ^{13}C NMR, which further supports the conclusion that, rather than an increase in lignin after torrefaction, there is instead an increase in acid detergent linkages brought about by the torrefaction conditions (Park et al., 2013).

Table 3-3: Quantification of carbon fractions from CPMAS ^{13}C NMR spectra

Carbon fraction	**RSW**	**TSW**	**RHW**	**THW**	**RSB**	**TSB**
Carboxylic	0.03	0.21	0.24	0.24	0.04	0.00
Phenolic	0.13	0.18	0.28	0.17	0.04	0.00
Aromatic	12.5	20.3	16.1	21.2	14.96	18.6
Substituted aliphatic	87.1	79.0	81.5	78.2	80.9	81.0
Unsubstituted Aliphatic	0.18	0.36	1.94	0.26	4.15	0.44

Generally, the carbon structure of biomass is a combination of mainly substituted and non-substituted aliphatics, aromatics and to a lesser extent carboxylic and phenolic carbons. The regions; carboxylics (219-190 ppm), phenolics (190-163 ppm), aromatics (162-97 ppm), substituted aliphatics (97-50 ppm) and aliphatics (50-0 ppm) were intergrated to relatively quantify the different carbons and results are presented in Table 3.3. The decreasing order of the amounts of substituted aliphatic carbons in the raw samples was found to be RSW>RHW>RSB and the next mostly abundant carbon grouping, the aromatics, decreased substantially in the

order RHW>RSB>RSW. After torrefaction, there was an overall reduction in the amounts of substituted aliphatic carbons for woody materials, which was not observed for SB. For all types of biomass, an increase in the aromatic fraction (THW>TSW>TSB) was observed. These results reveal the partial transformation of the substituted aliphatic carbons for HW and SW, and unsubstituted aliphatics for SB into aromatic carbons and pyrolysis products.

3.3.2 Physical characteristics

3.3.2.1 Thermal analysis

From differential thermogravimetry (DTG) (Figure 3.2) RSW and RHW had 3 prominent peaks, whilst RSB had a single peak at 200°C in addition to the peaks observed for woody biomass samples. The first peak below 100°C was a result of dehydration, whilst hemicellulose and cellulose were degraded in the region 220 - 300°C and 280 – 380°C respectively (Aboyade et al., 2013; Bridgwater, 2011; Chen et al., 2014). At 200°C, non-structural carbohydrates are degraded and only RSB had plentiful of this component to yield a visible DTG peak. These observations were also reported elsewhere (Carrier et al. 2011; Wannapeera & Worasuwannarak 2012;), and agreed with the compositional analysis (Table 3.2).

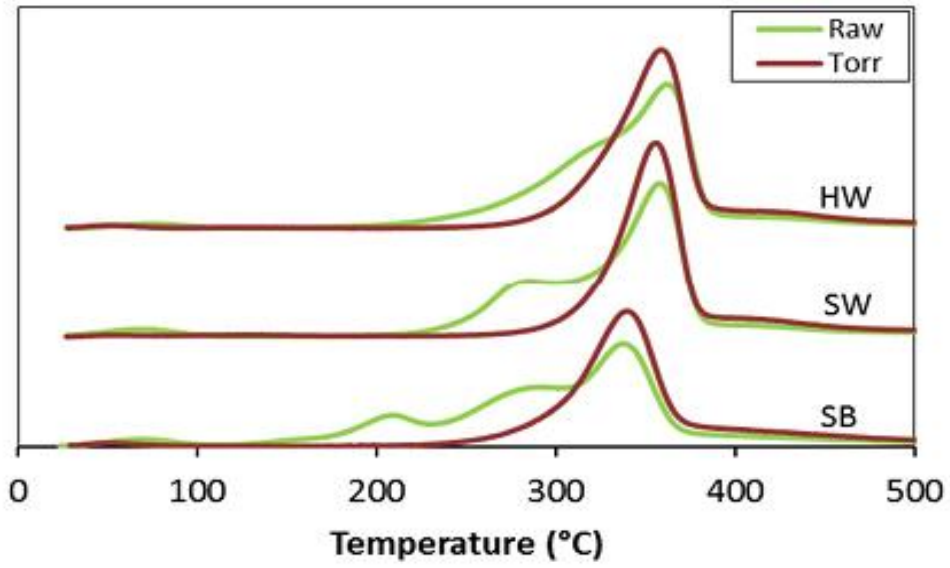

Figure 3-2: DTG analysis curves for raw and torrefied biomass samples collected under N_2 (SB- sweet sorghum bagasse, SW – Softwood chips, HW – hardwood chips)

After torrefaction, the dehydration peak (≈100°C) was reduced for all biomass samples and the non-structural carbohydrate peak for SB was also diminished, which increases the hydrophobicity of the torrefied material. DTG also showed that torrefaction had a bigger impact on the degradation of hemicelluloses as shown by the decreasing height of the 220-300°C DTG peak. The slight reduction in cellulose content after torrefaction was not as obvious from thermogravimetry; however there was an overall narrowing of the designated peak, resulting in reduction in peak area. The overlap between hemicellulose and cellulose degradation peaks was a consequence of the interactions between the fibres and possibly the presence of inorganic metal cations present in minerals that catalyse the degradation reactions (Collard et al., 2012). The determination of lignin content by thermogravimetry is complicated, as lignin degrades over a broader temperature range (220-500°C) and is always superimposed on the degradation areas of hemicelluloses and cellulose (Carrier et al., 2011; Chen et al., 2014).

3.3.2.2 X-ray diffraction

The X-ray diffractograms (Figure 3.3) showed an intense *(002)* peak at 2θ = 26.1° for RSW and RHW, whereas for RSB, this peak shifted to 25.4°. The wide *(002)* peak and is attributed to the stacking of graphitic basal planes and the aliphatic side chains attached to the edges of crystallites (Guerrero et al., 2008; McBeath et al., 2011). According to Guerrero et al. (2008), a deviation of this peak from the original 2θ = 25° is associated with the structure being highly disordered. This implies that the orderliness in RHW and RSW is of the same degree, but considerably different to that of RSB. Furthermore, the different intensities between grassy and woody materials infer structural differences in graphitic planes and carbon arrangements (Guerrero et al., 2008). The *(10)* peak was observed at 2θ ~ 40°, resembling a graphite-like atomic order within a single plane, and for HW and SW, this peak had a higher intensity than for SB. This was a consequence of the differing mineral matter composition between bagasse and wood wastes and the fibre contents (Rutherford et al., 2012). All three raw biomass samples exhibited a very sharp peak at 51.2°, which is attributed to the presence of small amounts of silicate compounds (Guerrero et al., 2008).

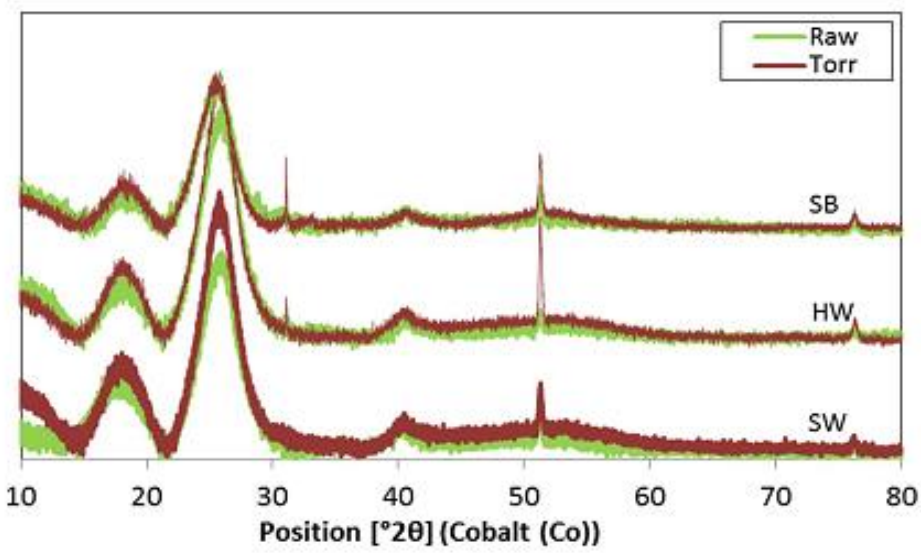

Figure 3-3: Comparison of the XRD diffractograms obtained for raw and torrefied biomass (SB- sweet sorghum bagasse, SW- softwood chips, HW- hardwood chips)

There were small, yet significant differences between raw and torrefied data and this was a consequence of the mild torrefaction conditions. There was an overall shift of the *(002)* band from 2θ = 26.1° to 25.7° for both TSW and THW, while the shift for TSB was from 25.5° to 24.6°. This indicates a variation in the extent of disorder in the samples. It can be concluded, from the shifting of the *(002)* band, that torrefaction results in orderliness of crystallites in biomass. There was an insignificant change in the intensity of the *(10)* band positioned at 2θ = 40° after torrefaction, which was identical for all the torrefied samples. Another perceptible change was the emergence of a very sharp peak at 2θ = 31°, due to the presence of calcite, the most stable polymorph of calcium carbonate, in THW and TSB. Also the significant increase in the intensity of the peak at 51° indicates an increased visibility of silica. The increase in peak intensity of these two mineral peaks was due to the loss of moisture and volatile matter in the lignocellulosic material.

Lattice parameters, calculated from X-Ray diffractograms as outlined by Everson et al. (2013) are presented in Table 3.4. There was only a small difference in the values of interlayer spacing, $d_{002,}$ between raw and torrefied woody materials, but a significant change was found between RSB and TSB, indicating that torrefaction affected the spacing between two planes in bagasse rather than for the woody biomass. While there was no substantial change in the crystallite height, L_c, for both raw and torrefied samples; the average crystallite diameter, L_a, varied significantly. The L_a of the raw biomass samples decreased in the order: RSB > RSW > RHW, and this has the same trend as the hemicellulose amounts (RSB > RSW > RHW). This implies

that the branching in hemicelluloses is directly proportional to the crystallite size. Raw softwood and hardwood had almost the same average number of aromatic layers per carbon crystallite (N_{ave}), which was higher than that of RSB. After torrefaction, slight deviations were observed with respect to the N_{ave} of the samples, decreasing in the case of TSW, and increasing for both THW and TSB. With the degradation of non-structural carbohydrates and hemicelluloses, breakage and formation of some bonds in the residual solid, bond lengths may be reduced and the carbon lattice may contract in the direction of shrinking bond lengths. It is evident from this analysis that, after torrefaction, the carbon crystallite structure was reduced more in the *x*-direction (L_a) than in the *y*-direction (d_{002}, L_c).

Table 3-4: Lattice parameters from XRD analysis

	(002)	**(10)**	**Interlayer spacing (d_{002} (Å))**	**Crystallite Height (L_c (Å))**	**Crystallite size (L_a (Å))**	**No. of crystallites in a stack (N_{ave} (-))**
RSW	26.1	40.2	4.01	28.4	100.4	8.08
TSW	25.7	40.3	4.02	27.5	71.8	7.84
RHW	26.1	40.7	3.99	29.3	91.4	8.33
THW	25.7	40.4	3.98	30.2	64.8	8.59
RSB	25.5	40.4	4.07	27.5	118.2	7.76
TSB	24.6	40.9	4.05	28.3	69.4	7.99

3.3.2.3 CO_2 gas adsorption

The physical-structural properties of both raw and torrefied biomass samples are presented in Table 3.5. RSW recorded the highest BET surface area, followed by RHW and RSB. On analysis of the micropores, RHW had the highest surface area followed by RSW and RSB. The mean pore width for all samples was 3.7 Å < d < 4.0 Å, in the microporous range; where *d* is the average pore diameter. RHW and RSW showed more pore volume than RSB, which may be attributed to the high non-structural carbohydrates content of SB (Downie et al., 2009).

Table 3-5: Porous properties of biomass samples from CO_2 gas adsorption

		RSW	TSW	RHW	THW	RSB	TSB
BET Isotherm	**Surface area (m^2/g)**	77	68	62	60	15	47
D-R Isotherm	**Micropore surface area (m^2/g)**	84	84	91	86	42	92
	Monolayer capacity (cm^3/g)	18	18	20	19	10	20
Horvath-Kawazoe	**Maximum pore volume (cm^3/g)**	0.014	0.016	0.015	0.018	0.006	0.020
	Median pore width (Å)	3.9	3.7	3.7	3.7	4.1	3.7

After torrefaction, SB displayed an increase in BET surface area, D-R micropore surface area, monolayer capacity and maximum pore volume after torrefaction. Whilst there was a reduction of the median pore width after torrefaction, from 4.1 Å to 3.7 Å, in SB, the pore volume increased slightly which resulted in an increase in micropore surface area. For the woody biomass, HW and SW, there was no significant change in BET surface area, micropore surface area, the monolayer capacity, maximum pore volume and the median pore width. This observation may be explained by the difference in the lignin content in these samples. The relative small growth of the surface area may be attributed to the high lignin content; lignin has been shown to soften and melt into pores hence reducing the surface area by means of a reduction of the accessible pore volume (Xue et al., 2014). Coalescence of pores, which also known to reduce the surface area of pre-treated biomass material (Guerrero et al., 2008) seems not be dominant since the pore width does not change significantly during torrefaction.

3.4 Conclusion

Softwood chips and hardwood chips showed comparable structural and chemical characteristics, which were dissimilar to sweet sorghum bagasse. At the torrefaction conditions adopted, hemicelluloses, non-structural carbohydrates and approximately 10% of cellulose were degraded. Torrefaction further doubled the micropore surface area for sweet sorghum bagasse, whilst for softwood chips and hardwood chips the change was insignificant and these changes are linked to the fibre composition. Torrefaction increased the aromaticity of biomass, whilst the overall aliphatic component is reduced. Finally, the crystallite diameter (L_a) is reduced by torrefaction and this change adds to the already documented changes brought about by torrefaction.

References

Aboyade, A.O., Görgens, J.F., Carrier, M., Meyer, E.L., Knoetze, J.H., 2013. Thermogravimetric study of the pyrolysis characteristics and kinetics of coal blends with corn and sugarcane residues. Fuel Process. Technol. 106, 310–320.

Ben, H., Ragauskas, A.J., 2012. Torrefaction of Loblolly pine. Green Chem. 14, 72–76.

Bridgwater, A. V, 2011. Review of fast pyrolysis of biomass and product upgrading. Biomass and Bioenergy 38, 68–94.

Cao, X., Pignatello, J.J., Li, Y., Lattao, C., Chappell, M.A., Chen, N., Miller, L.F., Mao, J., 2012. Characterization of Wood Chars Produced at Different Temperatures Using Advanced Solid-State ^{13}C NMR Spectroscopic Techniques. Energy and Fuels 26, 5983–5991.

Cao, X., Zhong, L., Peng, X., Sun, S., Li, S., Liu, S., Sun, R., 2014. Comparative study of the pyrolysis of lignocellulose and its major components : Characterization and overall distribution of their biochars and volatiles. Bioresour. Technol. 155, 21–27.

Carrier, M., Joubert, J., Danje, S., Hugo, T., Görgens, J., Knoetze, J.H., 2013. Impact of the lignocellulosic material on fast pyrolysis yields and product quality. Bioresour. Technol. 150, 129–138.

Carrier, M., Loppinet-Serani, A., Denux, D., Lasnier, J.-M., Ham-Pichavant, F., Cansell, F., Aymonier, C., 2011. Thermogravimetric analysis as a new method to determine the lignocellulosic composition of biomass. Biomass and Bioenergy 35, 298–307.

Chen, T., Wu, J., Zhang, J., Wu, J., Sun, L., 2014. Gasification kinetic analysis of the three pseudocomponents of biomass-cellulose, semicellulose and lignin. Bioresour. Technol. 153, 223–9.

Chen, W., Peng, J., Bi, X.T., 2015. A state-of-the-art review of biomass torrefaction , densi fi cation and applications. Renew. Sustain. Energy Rev. 44, 847–866.

Damm, O., Triebel, R., 2008. A Synthesis Report on Biomass Energy Consumption and Availability in South Africa A report prepared for ProBEC by by Dr Oliver Damm and Ralph Triebel.

Downie, A., Crosky, A., Munroe, P., 2009. Physical Properties of Biochar, in: Lehmann, J., Joseph, S. (Eds.), Biochar for Environmental Management. Erthscan, United Kingdom, pp. 13–29.

Everson, R.C., Okolo, G.N., Neomagus, H.W.J.P., Santos, J., 2013. X-ray diffraction parameters and reaction rate modeling for gasification and combustion of chars derived from inertinite-rich coals. Fuel 109, 148–156.

Focher, B., Palma, M.T., Canetti, M., Torri, G., Cosentino, C., 2001. Structural differences between non-wood plant celluloses : evidence from solid state NMR , vibrational spectroscopy and X-ray diffractometry. Ind. Crop. Prod. 13, 193–208.

Freitas, J.C.C., Bonagamba, T.J., Emmerich, F.G., 2001. Investigation of biomass- and polymer-based carbon materials using ^{13}C high-resolution solid-state NMR. Carbon. 39, 535–545.

Guerrero, M., Ruiz, M.P., Millera, Á., Alzueta, M.U., Bilbao, R., 2008. Characterization of Biomass Chars Formed under Different Devolatilization Conditions : Differences between Rice Husk and Eucalyptus. Energy & Fuels 22, 1275–1284.

Kim, Y., Lee, S., Lee, H., Lee, J., 2012. Physical and chemical characteristics of products from the torrefaction of yellow poplar (*Liriodendron tulipifera*). Bioresour. Technol. 116, 120–125.

Melkior, T., Jacob, S., Gerbaud, G., Hediger, S., Pape, L. Le, Bonnefois, L., Bardet, M., 2012. NMR analysis of the transformation of wood constituents by torrefaction. Fuel 92, 271–280.

Murillo, J.D., Ware, E.A., Biernacki, J.J., 2014. Characterization of milling effects on the physical and chemical nature of herbaceous biomass with comparison of fast pyrolysis product distributions using Py-GC/MS. J. Anal. Appl. Pyrolysis 108, 234–247.

Okolo, G.N., Neomagus, H.W.J.P., Everson, R.C., Roberts, M.J., Bunt, J.R., Sakurovs, R., Mathews, J.P., 2015. Chemical–structural properties of South African bituminous coals: Insights from wide angle XRD–carbon fraction analysis, ATR–FTIR, solid state ^{13}C NMR, and HRTEM techniques. Fuel 158, 779–792.

Park, J., Meng, J., Lim, K.H., Rojas, O.J., Park, S., 2013. Transformation of lignocellulosic biomass during torrefaction. J. Anal. Appl. Pyrolysis 100, 199–206.

Phanphanich, M., Mani, S., 2011. Impact of torrefaction on the grindability and fuel characteristics of forest biomass. Bioresour. Technol. 102, 1246–1253.

Roberts, M.J., Everson, R.C., Neomagus, H.W.J.P., Niekerk, D. Van, Mathews, J.P., Branken, D.J., 2015. Influence of maceral composition on the structure , properties and behaviour of

chars derived from South African coals. Fuel 142, 9–20.

Roberts, M.J., Everson, R.C., Neomagus, H.W.J.P., Okolo, G.N., Van Niekerk, D., Mathews, J.P., 2015. The characterisation of slow-heated inertinite- and vitrinite-rich coals from the South African coalfields. Fuel 158, 591–601.

Rutherford, D., Wershaw, R., Rostad, C., Kelly, C. 2012. Effect of formation conditions on biochars: Compositional and structural properties of cellulose, lignin and pine biochars. Biomass and Bioenergy 46, 693-701.

Santoni, I., Callone, E., Sandak, A., Sandak, J., Dirè, S., 2015. Solid state NMR and IR characterization of wood polymer structure in relation to tree provenance. Carbohydr. Polym. 117, 710–721.

Stelte, W., Clemons, C., Holm, J.K., Sanadi, A.R., Ahrenfeldt, J., Shang, L., Henriksen, U.B., 2011. Pelletizing properties of torrefied spruce. Biomass and Bioenergy 35, 4690–4698.

Tumuluru, J.S., Sokhansanj, S., Hess, J.R., Wright, C.T., Boardman, R.D., 2011. A review on biomass torrefaction process and product properties for energy applications. Ind. Biotechnol. 7, 384–402.

van der Stelt, M.J.C., Gerhauser, H., Kiel, J.H.A., Ptasinski, K.J., 2011. Biomass upgrading by torrefaction for the production of biofuels : A review. Biomass and Bioenergy 35, 3748–3762.

Velden, M. Van De, Baeyens, J., Brems, A., Janssens, B., Dewil, R., 2010. Fundamentals , kinetics and endothermicity of the biomass pyrolysis reaction. Renew. Energy 35, 232–242.

Wang, G., Li, B., Chen, H., 2008. TG study on pyrolysis of biomass and its three components under syngas. Fuel 87, 552–558.

Wannapeera, J., Worasuwannarak, N., 2012. Upgrading of woody biomass by torrefaction under pressure. J. Anal. Appl. Pyrolysis 96, 173–180.

Wikberg, H., Maunu, S.L., 2004. Characterisation of thermally modified hard- and softwoods by ^{13}C CPMAS NMR. Carbohydr. Polym. 58, 461–466.

Xue, G., Kwapinska, M., Horvat, A, Kwapinski, W., Rabou, L.P.L.M., Dooley, S., Czajka, K.M., Leahy, J.J., 2014. Gasification of torrefied Miscanthus × giganteus in an air-blown bubbling fluidized bed gasifier. Bioresour. Technol. 159, 397–403.

Yang, H., Yan, R., Chen, H., Lee, D.H., Zheng, C., 2007. Characteristics of hemicellulose , cellulose and lignin pyrolysis. Fuel 86, 1781–1788.

Yang, Z., Sarkar, M., Kumar, A., Shankar, J., Huhnke, R.L., 2014. Effects of torrefaction and densification on switchgrass pyrolysis products. Bioresour. Technol. 174, 266–273.

Zhao, X., Chen, J., Chen, F., Wang, X., Zhu, Q., Ao, Q., 2013. Surface characterization of corn stalk superfine powder studied by FTIR and XRD. Colloids Surfaces B Biointerfaces 104, 207–212.

Supplementary information

S3 Effect of torrefaction on the fuel properties

The torrefaction of biomass samples resulted in the improvement of its fuel properties. These results of the solid yields, energy yields, and mass energy density of the torrefied biomass samples are given in Table S3.1.

Table S 3-1: Fuel properties of torrefied biomass

	Solid Yield (wt.%)	Energy Yield (%)	Mass Energy Density (wt.%.MJ/Kg)
SW	70.1	86.6	1.24
HW	69.9	87.0	1.24
SB	70.2	92.8	1.33

Chapter 4 Chemical and structural characterization of char development during lignocellulosic biomass pyrolysis

Findings reported in this chapter are published as: Mafu, L.D., Neomagus, H.W.J.P., Everson, R.C., Strydom, C.A., Carrier, M., Okolo, G.N., Bunt, J.R. **2017**. Chemical and structural characterization of char development during lignocellulosic biomass pyrolysis. *Bioresource Technology*. **243**, 941–948. http://dx.doi.org/10.1016/j.biortech.2017.07.017.

Abstract

The chemical and structural changes of three lignocellulosic biomass samples during pyrolysis were investigated using both conventional and advanced characterization techniques. The use of ATR-FTIR as a characterization tool is extended by the proposal of a method to determine aromaticity, the calculation of both CH_2/CH_3 ratio and the degree of aromatic ring condensation ($(R/C)_u$). With increasing temperature, the H/C and O/C ratios, X_A and CH_2/CH_3 ratio decreased, while $(R/C)_u$ and aromaticity increased. The micropore network developed with increasing temperature, until the coalescence of pores at 1100 °C, which can be linked to increasing carbon densification, extent of aromatization and/or graphitization of the biomass chars. WA-XRD-CFA measurements indicated the gradual formation of nearly parallel basic structural units with increasing carbonization temperature. The char development can be considered to occur in two steps: elimination of aliphatic compounds at low temperatures, and hydrogen abstraction and aromatic ring condensation at high temperatures.

***Key Words**: Aromaticity, ATR-FTIR, biochar, CPMAS ^{13}C NMR, pyrolysis*

4.1 Introduction

Interest in the use of biomass for energy generation has grown considerably in recent years, since it is considered to be a more sustainable alternative to fossil fuels (Mao et al., 2015; Pimenidou and Dupont, 2012). One process of ensuring the efficient use of biomass in energy production is pyrolysis, where fast pyrolysis is often preferred for liquid products and low heating rates are used for the production of chars (Fisher et al., 2012). The biomass origin and the pyrolysis conditions such as heating rate, pyrolysis temperature and gas environment shape the chemical and structural characteristics of the formed chars (Rutherford et al., 2012; Wei et al., 2011). The transformation of a broad range of plant biomass sources resulted in the production of carbonaceous material displaying properties suitable for various applications such as soil amendment, gasification and co-gasification with coal (Angin and Sensoz, 2014; Kaudal et al., 2016). In addition to variable lignocellulosic composition, the presence of inorganic compounds results in peculiar reactivity of plant biomass during pyrolysis, gasification and combustion. For example, feedstocks with a high mineral matter content may be preferred for co-gasification applications due to a favourable catalytic effect of the specific minerals (Huang et al., 2009). On the other hand, low ash feedstocks may be directly transformed into liquids that should result in more stable biofuels (Antonio et al., 2014).

The intended application of pyrolytic chars is dependent on their structural and chemical characteristics, which is in turn reliant on the pyrolysis conditions. For instance, chars produced at higher temperatures have shown higher fixed carbon and elemental carbon, lower volatile matter, lower elemental oxygen and hydrogen contents (Uzun et al., 2006; Zhang et al., 2016). A number of advanced techniques has been developed and used to provide more information on the changes in characteristics induced by pyrolysis (Rutherford et al., 2012; Suliman et al., 2016). Wide angle X-ray diffraction – carbon fraction analysis (WA-XRD-CFA) has been useful in identifying the phases of biomass and has been extended to evaluating the microcrystalline parameters (Huang et al., 2009). This has been done by the determination of the interlayer spacing (d_{002}), crystalline height (L_c), crystalline diameter (L_a) and the average number of aromatic layers per carbon crystallite (N_{ave}) using the Bragg's and Scherrer's equation (Okolo et al., 2015). The transformation of the surface functionalities, or functional groups, as biomass undergoes heat treatment, has been studied by Fourier Transforms infrared (FTIR) spectroscopy. Major findings include the elimination of aliphatic groups at lower temperatures and as heating temperatures were increased, the aromatic functional groups lost their infrared activity resulting in a spectrum with no FTIR peaks (Rutherford et al., 2012; Suliman et al., 2016). Cui et al.

(2016) used FTIR to extract coal structural parameters which included the fraction of aromatic and aliphatic fractions. It was concluded that the CH_2/CH_3 ratio increased with coal rank, pyrolysis temperature and pyrolysis time. Most findings from FTIR have been complemented by results from cross polarization magnetic angle spinning nuclear magnetic resonance (CPMAS ^{13}C NMR) spectroscopy and surface area measurements (McBeath et al., 2011; Suliman et al., 2016).

In addition, the characterization techniques have revealed important details in the process of char formation, which depends on the pyrolysis conditions and biomass characteristics. The lignocellulosic fibre composition has been reported to be the basis of observed chemical and structural changes during low temperature pyrolysis (Mafu et al., 2016; Wannapeera and Worasuwannarak, 2012). At temperatures above 500 °C, the vast majority of fibres have been found to be consumed through decomposition.

When considering processing conditions in a typical fixed bed dry bottom (FBDB) gasifier, the pyrolysis zone may rise up to temperatures above 1000 °C, while the heating rate is relatively low (10 – 20 ℃/min) (Skhonde et al., 2009) and as such, the understanding of slow pyrolysis char formation even up to higher temperatures is justified. The characteristics of chars produced from the pyrolysis zone affect the gasification kinetics during biomass gasification or co-gasification with coal (Kajitani et al., 2010; Y. Zhang et al., 2016). It has been reported that the aromaticity, for instance, is a function of charring temperature (Everson et al., 2013), which increases with increasing pyrolysis temperature, while the gasification reactivity of the formed char has been shown to decrease with increasing aromaticity. However, as aromatization progresses, other chemical transformations that affect the crystallinity, the surface area and the microcrystalline structure are simultaneously taking place. The progress of char formation in slow pyrolysis, together with correlations between the various char characteristics have not yet received significant attention, and forms the motivation of this study.

The chemical and structural characterization of biomass, similar to coal, provides insight in the thermal behaviour, such as the gasification reactivity. As such, this work reports on the slow pyrolysis char development in the region of torrefaction to gasification temperatures. The effect of temperature on three different biomass samples that are widely available in South Africa is discussed, and outcomes include: the determination of aromaticity (f_{aF}), degree of aromatic ring condensation ($(R/C)_u$), and aliphatic CH_2/CH_3 ratios from ATR-FTIR spectroscopy data; fraction of amorphous carbon (X_A) and Van Krevelen plots of the samples. From the reported results, the

char development is then explained using both chemical and structural characteristics by relating aromaticity to other char characteristics, which has been an area that is inadequately explored in biomass studies.

4.2 Materials and methods

4.2.1 Materials

Three abundantly available biomass sources in South Africa were procured. Softwood (SW) and hardwood (HW) chips were supplied by South African Pulp and Paper Industries Limited (SAPPI), whereas sweet sorghum bagasse (SB) was obtained from the Agricultural Research Council (ARC) in Potchefstroom. Approximately 10 kg of each sample was obtained and air-dried overnight. Successively, the sample size was representatively reduced by applying a standardised cone and quartering method (DD CEN/TS 14780:2005) three times. The obtained sample was ground to < 300 µm and was further used for characterisation and conversion experiments. From the bulk samples, about 15 g of the air-dried and ground biomass samples were heated at 10 °C/min using a N_2 gas flow rate of 100 ml/min from room temperature to 260 °C in a tube furnace from Elite Thermal Systems Limited (Model TSH12/75/610) to achieve a 30% mass loss. The changes in characteristics after torrefaction are reported in a previous study (Mafu et al., 2016). Chars for this study were prepared from the torrefied biomass, in the same furnace by heating at 10 °C/min to final temperatures of 300, 400, 600 and 1100 °C and left isothermal for 60 minutes. The series of pyrolytic chars were referred to by the plant biomass that they were produced from, and the highest temperature of the pyrolysis treatment (e.g. softwood char prepared at 300 °C is referred to as SW 300).

4.2.2 Characterization

Ultimate analysis was carried out by means of the standard ASTM D 5373 method for elemental C, H and N, whilst the elemental S and O mass percentages were determined by the ASTM D 4239 method and by difference, respectively. The volatile matter and mineral matter contents were obtained using the ISO 562:2010 and ISO 1171:2010 methods respectively, whilst the fixed carbon content was calculated by difference. Both analyses were carried out by the Council of Geosciences, Pretoria, South Africa. Infrared spectra were recorded using a Perkin–Elmer Paragon 1000 PC Fourier Transforms Infrared (FTIR) spectrometer with an attenuated total reflectance (ATR) accessory between 400 and 4000 cm^{-1} with 4 cm^{-1} resolution, where 32 scans were averaged for one sample run. CPMAS ^{13}C NMR experiments were carried out at the Central Analytical Facility of Stellenbosch University following the method by Melkior et al.

(2012), which involves a combination of cross polarization and magnetic angle spinning techniques. A Quanta FEG 250 Environmental Scanning electron microscope (ESEM) under an acceleration voltage of 30 kV was used to capture the surface morphology of biomass char samples. Ground and air-dried samples were coated with carbon using a sputter-coater to improve conductivity while avoiding sample charging before SEM analysis (Trubetskaya et al., 2016) at the Laboratory of Electron Microscopy (LEM) of the North-West University. WA-XRD-CFA was conducted at the North-West University following a method outlined in Mafu et al. (2016). Surface area measurements were obtained from a Micrometrics ASAP 2020 surface area and porosity analyser. Samples were degassed under vacuum, at 75 °C for 48 h and analysis conducted at 0 °C at a relative pressure range: $0 < P/P_0 \leq 0.032$: where P is the analysis pressure and P_0 is the saturation vapour pressure of CO_2. The Dubinin-Radushkevich (D-R) and Horvath-Kawazoe (H-K) models were used to obtain the micropore surface area, maximum pore volume and median pore width (Okolo et al., 2015).

From ATR-FTIR spectroscopy, the sum of aromatic functional groups and the sum of aliphatic functional groups, derived by Gaussian curve deconvolution, were used to calculate the aromaticity. The aromaticity ($f_{a,F}$), defined as the fraction of aromatic groups from the sum of aliphatic and aromatic groups in the sample is given by Equation 4.1. The aromaticity values from this proposed method were compared to those determined from CPMAS ^{13}C NMR ($f_{a,N}$). The $f_{a,F}$ was then used to calculate the degree of aromatic ring condensation (Equation 4.2) which was found to be proportional to the total aromaticity ($f_{a,F}$ in this case) and the fraction of aromatic hydrogen (H_{ar}) to aromatic carbon (C_{ar}) by Cui et al., (2016). The asymmetric stretching of CH_3 and CH_2 groups have been used as an indication of the degree of cyclization, where a higher value of CH_2/CH_3 revealed longer aliphatic chains or a higher degree of cyclization (Cui et al., 2016). The value of CH_2/CH_3 was determined using Equation 4.3 where A_{2925} and A_{2955} represent the area under the deconvoluted curves of ATR-FTIR peaks at 2925 and 2955 cm^{-1}, respectively. The fraction of amorphous carbon, X_A, was determined by the Gaussian curve deconvolution of the amorphous and crystalline phases of the 002 band of the XRD spectra (Figure 4.1). The area under the curve at position 16° and 25° after deconvolution were assigned to the amount of amorphous carbon (S_A) and crystalline carbon (S_C), respectively. X_A was calculated using Equation 4.4 (Okolo et al., 2015). Using the empirical Bragg's and Scherrer's equations, the crystallite height (L_c), crystallite diameter (L_a), interlayer spacing (d_{002}) and average number of aromatic layers per carbon crystallite (N_{ave}) were calculated (Everson et al., 2013; Okolo et al., 2015).

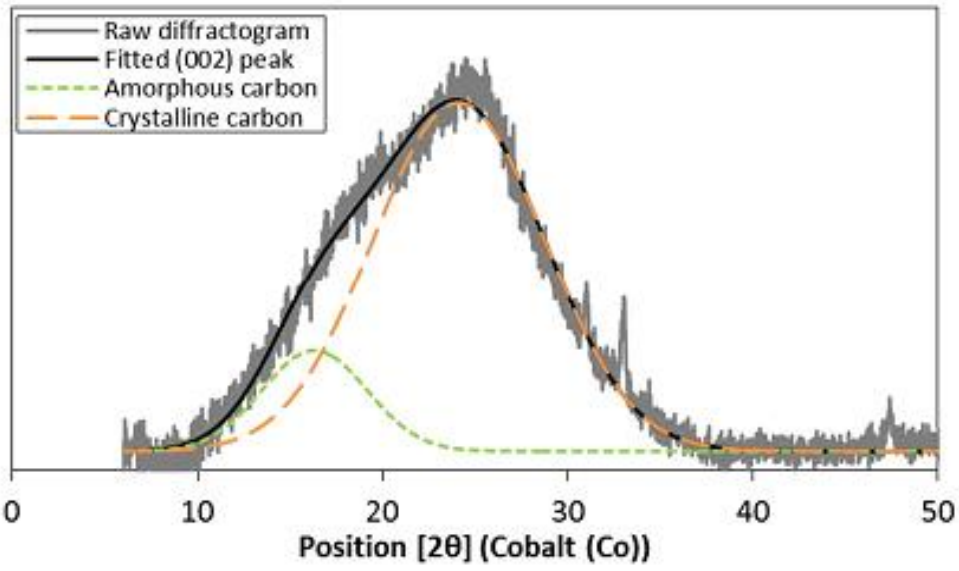

Figure 4-1: Determination of XA by Gaussian curve deconvolution of the (002) band for SB char prepared at 300°C

$$f_{aF} = \frac{\sum C_{ar}}{\sum C_{ar+al}} \tag{4.1}$$

$$\left(\frac{R}{C}\right)_u = 1 - \frac{1}{2}\left(f_a + \frac{H_{ar}}{C_{ar}}\right) \tag{4.2}$$

$$\frac{CH_2}{CH_3} = \frac{A_{2925/cm}}{A_{2955/cm}} \tag{4.3}$$

$$X_A = \frac{S_A}{S_A + S_C} \tag{4.4}$$

4.3 Results and discussion

4.3.1 Chemical characteristics

Table 4.1 presents the chemical characteristics of the pyrolytic chars. Char development progressed with increasing temperature through the evolution of volatiles, which resulted in increased fixed carbon and mineral matter contents.

Table 4-1: Proximate and ultimate analyses results for torrefied biomass and chars prepared at different temperatures

Sample		Proximate Analysis (wt.%, mfb)				Ultimate Analysis (wt.%, daf)						
		VM[1]	FC[2]	Ash	CV[3] (MJ/kg)	C	H	N	S	O	H/C	O/C
SW	**Torr**	76.5	22.9	0.6	22.3	55.1	5.6	0.13	0.09	39.1	1.2	0.5
	300 °C	63.8	35.5	0.7	23.2	65.2	5.2	nd[4]	0.07	29.7	1.0	0.3
	400 °C	30.7	68.5	0.8	28.8	78.9	4.3	nd	0.06	16.7	0.7	0.2
	600 °C	9.9	89.2	1.0	33.1	95.7	2.9	0.08	0.07	1.2	0.4	0.01
	1100 °C	1.3	97.4	1.2	32.3	99.2	0.6	0.02	0.07	0.06	0.1	0.01
HW	**Torr**	77.3	22.1	0.6	22.4	55.4	5.4	0.01	0.03	39.2	1.2	0.5
	300 °C	64.2	35.3	0.6	23.2	61.2	5.1	nd	0.05	33.7	1.1	0.4
	400 °C	30.4	68.9	0.7	28.1	77.2	3.9	nd	0.04	18.8	0.6	0.2
	600 °C	10.1	89.2	0.8	33.7	93.4	3.0	nd	0.05	3.6	0.4	0.03
	1100 °C	1.2	97.5	1.2	32.1	99.2	0.7	0.03	0.04	0.03	0.1	0.01
SB	**Torr**	69.8	23.7	6.5	23.0	53.4	5.5	0.32	0.15	41.1	1.1	0.6
	300 °C	48.1	45.0	6.8	24.5	69.2	5.0	nd	0.16	25.1	1.0	0.3
	400 °C	26.2	66.1	7.6	26.6	77.9	4.3	0.11	0.15	17.6	0.7	0.2
	600 °C	5.8	82.0	12.2	30.1	92.2	3.1	0.36	0.19	4.2	0.4	0.03
	1100 °C	3.2	83.9	12.5	26.6	97.1	1.3	0.39	0.18	1.0	0.2	0.03

[1]VM - volatile matter, [2]FC - fixed carbon and [3]CV - calorific value, [4]nd - not detected, mfb – moisture free basis, daf- dry ash-free basis

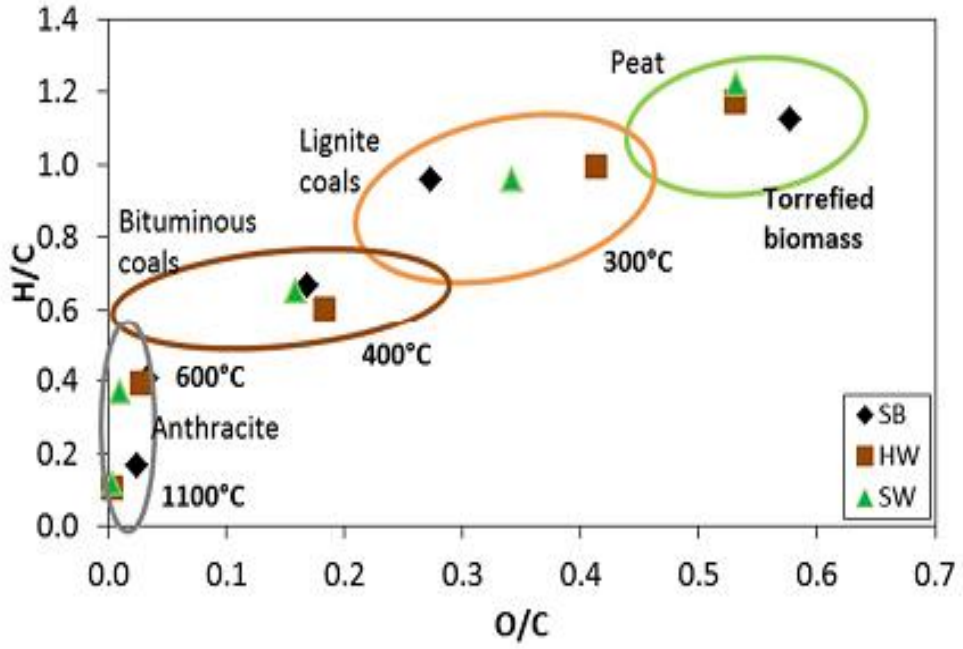

Figure 4-2: The comparison of the coalification process with biomass char formation

The differences in proximate analyses for the chars prepared at 600 and 1100 °C were significant and reported to be mainly driven by secondary reactions (Anca-Couce, 2016). The calorific value (CV) increased with increasing pyrolysis temperature, but decreased at 1100 °C for all biomass samples. The increase in CV at lower temperatures is attributed to the reduction in elemental O and H, and increasing carbon content (carbon densification) in the solid matrix. However, the graphitization of the solid mass at high temperatures accounts for the reduction in CV for the 1100 °C chars, as observed for coal (Suggate and Dickinson, 2004). Increasing pyrolysis temperature resulted in the increase in elemental carbon, whilst elemental oxygen and hydrogen decreased appreciably. Noteworthy were the larger changes in ultimate analysis results from torrefied biomass to chars prepared at 600 °C as a result of the degradation of lignocellulosic fibres (Yang et al., 2006). Beyond 600 °C, changes were a result of bond reordering and hydrogen abstraction as shown by further decreases in elemental H and O (Trubetskaya et al., 2016a). The amounts of N and S were very low; as such no trends could be drawn. The changes in C, H and O amounts resulted in the reduction of the H/C and O/C ratios linked to an increase in aromaticity (Anupam et al., 2016). The decrease of H/C and O/C ratios as shown in the Van Krevelen plot (Figure 4.2) with temperature was comparable to the coalification process with torrefied biomass' ratios similar to those of peat and chars prepared at 1100 °C to anthracite coals (Anupam et al., 2016; Suggate and Dickinson, 2004).

ATR-FTIR spectra for chars prepared at 1100 °C could not be collected due to line broadening and absence of vibrating and stretching functional groups at high temperatures (Roberts et al., 2015; Rutherford et al., 2012). Torrefied biomass displayed characteristic vibrations corresponding to the presence of aliphatic groups (3200-3500, 2800-3000 and 900-1150 cm^{-1}) and aromatic groups (700-900, 1150-1650 cm^{-1}) (Huang et al., 2015; Zhao et al., 2013) which can be attributed to the presence of the residues of lignocellulosic fibres (Anca-Couce, 2016; Pimenidou and Dupont, 2012). The ATR-FTIR spectra of the torrefied and pyrolysed biomass samples up to 600 °C are presented in Figures S4.1 – S4.3 of the supplementary information.

The deconvoluted area under the aromatic ATR-FTIR peaks could not be related to the amounts of lignin at torrefaction conditions (Mafu et al., 2016), but from both aliphatic and aromatic peaks, the aromaticity of the materials could be determined. SB had the lowest aromaticity of the torrefied biomass samples, due to the lower lignin contents in the parent biomass, compared to SW and HW (Mafu et al., 2016). Aromaticity increased with increasing pyrolysis temperature (Table 4.2) as alluded to previously by other researchers (Asadullah et al., 2010; McBeath et al., 2011). The observed increase in aromaticity had two contributing factors: (1) the elimination of aliphatic groups taking place more rapidly than the loss of aromatics and (2) the condensation of aromatic rings as observed by the increase in $(R/C)_u$ with increasing pyrolysis temperature (Table 4.2). The parameter, CH_2/CH_3 ratio, was determined and the results are presented in Table 4.2. For torrefied biomass samples, the CH_2/CH_3 ratio was around 50 and decreased with increasing temperature to approximately 1 for chars prepared at 600 °C. This could be a consequence of progressing cyclization of the aliphatics, as well as the shorter $–CH_2$ aliphatic chains being easily broken compared to the longer $–CH_3$ aliphatic chains (Cui et al., 2016). Functionalities containing elemental H and O gradually decreased at pyrolysis temperatures up to 300 °C as a result of dehydration, decarboxylation and deacetylation of the lignocellulosic fibres (Rutherford et al., 2012; Deng et al., 2009). Subsequent elimination of aliphatic functionalities, H- and O- containing functional groups up to 600 °C were as a result of the breaking of bonds between monomer units (depolymerisation), rearrangement reactions that result in a more stable structure and the recombination of volatiles to form chars (repolymerisation) (Yang et al., 2013; Collard et al., 2012).

Table 4-2: Chemical parameters for torrefied biomass and chars

Sample		Chemical Characteristics			
		$f_{a,N}$	$f_{a,F}$	$(R/C)_u$	CH_2/CH_3 ratio
SW	**Torr**	0.21	0.26	0.12	52.1
	300 °C	0.34	0.37	0.19	39.5
	400 °C	0.71	0.74	0.30	3.2
	600 °C	0.94	0.93	0.48	1.9
	1100 °C	-	-	-	-
HW	**Torr**	0.22	0.24	0.13	50.3
	300 °C	0.32	0.30	0.20	48.1
	400 °C	0.68	0.62	0.31	5.2
	600 °C	0.92	0.92	0.46	1.0
	1100 °C	-	-	-	-
SB	**Torr**	0.18	0.23	0.10	53.8
	300 °C	0.31	0.47	0.16	43.1
	400 °C	0.63	0.63	0.34	2.9
	600 °C	0.90	0.96	0.41	1.6
	1100 °C	-	-	-	-

From CPMAS ^{13}C NMR spectroscopy, the presence of acetyl, methoxyl, amorphous and crystalline carbons of cellulose and aromatic groups of lignin in all biomass samples could be confirmed by the presence of peaks at characteristic positions (Freitas et al., 2001; Mafu et al., 2016). For chars prepared at 300 °C, peaks related to hemicelluloses and amorphous carbons of cellulose and lignin, gradually decreased as a result of the degradation of the lignocellulosic fibres. Peaks at 35, 68, 62, 65, 73, 84, 105, 112 and 149 ppm (supplementary information) were visible for chars at 300 °C and related to the carbons of the crystalline cellulose and lignin (Bardet et al., 2007; Melkior et al., 2012). Shoulder peaks at 62-65 ppm and 72-74 ppm were as a result of residual amorphous carbons (Mafu et al., 2016). At 400 °C, the peak areas of characteristic cellulose and lignin peaks reduced, as a result of the reduction of their carbon functionalities (Rutherford et al., 2012). Chars prepared at 600 °C had mainly aromatic carbon functionalities with fractions of amorphous C=C and C-H left in the chars. The differences between woody biomass and SB were more significant for chars prepared at 300 °C, and

converged to almost the same ^{13}C chemical structure at 600 °C, which was also observed by McBeath et al., (2011) for different lignocellulosic biomass samples. These findings suggests that char development may be broadly defined as a two-step process, where the first step (< 600 °C) is accompanied by lignocellulosic fibre degradation linked to the net loss of the aliphatic fraction of biomass. The second step (> 600 °C) may be assigned to the reorganisation of bonds that resulted in the conjugation of aromatic bonds, hence increasing further, the aromaticity of chars. The aromaticity as determined through both ATR-FTIR and NMR were comparable as presented in Table 4.2.

4.3.2 Structural characteristics

Due to the insignificant changes as pyrolysis temperatures were increased to 1100 °C, only torrefied, 300 and 1100 °C char micrographs are presented and discussed. The surface for all torrefied biomass was smooth, possibly from the melting of lignin and cellulose (Mafu et al., 2016). A slight broadening of the water conducting pores was also observed for all biomass samples with increasing pyrolysis temperature (Liu et al., 2010; Trubetskaya et al., 2016a). With increasing temperature, the matrix did not change but rather became brittle (Cetin et al., 2004), that is, the escape of volatiles left a rigid, hollow biomass matrix (Trubetskaya et al., 2016a). The SEM micrographs of the torrefied biomass and chars prepared at 300 and 1100 °C are presented in Figure S4.4 of the Supplementary Information.

The diffractograms showed two broad and distinct peaks at the 2θ positions 16 and 25° assigned to amorphous and graphitic basal planes, respectively. Most of the crystalline carbon in biomass is in general ascribed to the presence of cellulose, whilst the other lignocellulosic fibres contribute to the amorphous carbon content (Barnette et al., 2012; Murillo et al., 2014). The intensities of both peaks were lesser for SB than HW and SW (presented in Chapter 4), which was a direct consequence of the higher amount of mineral matter and lower content in original lignocellulosic fibres in SB than HW and SW (Mafu et al., 2016). As the pyrolysis temperature increased, the amorphous carbon peak (16°) progressively disappeared, in line with the degradation of hemicelluloses and other amorphous fractions of biomass. The crystalline phase narrowed as the temperature increased from 300 to 600 °C, following the degradation of celluloses at these conditions (Tumuluru et al., 2011; Yang et al., 2007). Chars prepared at 1100 °C showed increased peak intensity at 27° which may be a result of the recrystallization of some of the carbon material in the matrix (Azargohar et al., 2014). Increasing pyrolysis temperature promoted structural orderliness within the residual solid matrix as illustrated by the shift of the

(002) band towards higher angle (2θ) regions (25 – 28°). The emergence of sharp peaks at 52 and 60° reflected the increasing share of minerals such as oxides and carbonates of Si, Mg and Ca (Trubetskaya et al., 2016b; Wen et al., 2014). The WA-XRD-CFA diffractograms of the torrefied biomass samples and their subsequent chars are presented in Figures S4.5 – S4.7 of the Supplementary information.

CO_2 adsorption results showed an increase in the micropore surface area with increasing pyrolysis temperature up to 600 °C (Table 4.3). This occurred through the development of micropores, with increasing micropore volume as volatiles were increasingly driven off, facilitated by carbon densification in the bulk biomass char. At 1100 °C, both micropore surface area and micropore volumes decreased for SW and SB. This was ascribed to pore coalescence at higher temperatures (Angin and Sensoz, 2014; Mukome et al., 2013).

Table 4-3: Structural characteristics of torrefied biomass and subsequent chars

Sample ID		CO_2 adsorption		WA-XRD-CFA					
		S.A (m^2/g)	**M.P.V (cm^3/g)**	**M.P.W (Å)**	**d_{002} (Å)**	**L_c (Å)**	**L_a (Å)**	**N_{ave} (-)**	**X_a (-)**
SW	**Torr**	83	0.017	3.7	4.0	27	72.0	7.8	0.34
	300 °C	107	0.022	3.6	4.1	19	74	5.6	0.42
	400 °C	236	0.055	3.8	3.9	10	86	3.7	0.21
	600 °C	427	0.092	3.9	3.8	10	125	3.6	0.08
	1100 °C	386	0.083	4.4	3.7	9	139	3.5	-
HW	**Torr**	86	0.018	3.7	4.0	30	65	8.5	0.35
	300 °C	103	0.022	3.6	4.0	17	67	5.2	0.41
	400 °C	255	0.059	3.7	3.9	12	85	4.0	0.18
	600 °C	442	0.094	3.8	3.8	10	115	3.7	0.07
	1100 °C	461	0.097	4.0	3.8	9	130	3.5	-
SB	**Torr**	92	0.02	3.7	4.1	28	69	8.0	0.34
	300 °C	121	0.026	3.6	4.2	17	71	5.0	0.15
	400 °C	198	0.049	3.5	4.0	13	89	4.3	0.06
	600 °C	341	0.073	3.6	3.9	12	135	4.0	-
	1100 °C	316	0.072	3.9	3.8	10	151	3.6	-

Pyrolytic chars prepared from HW at 1100 °C were an exception as they demonstrated an increase in the surface area and pore volume (Table 4.3). This could be a consequence of the accumulation of pores in the higher micropore range without a disruption of the lower micropore range, which was not the case for SB and SW. The lower pore volumes, and consequently surface areas of SB compared those of the woody biomass samples may be as a result of the higher ash values which may hinder pore development and/or block the access of pores by CO_2 (Tumuluru et al., 2011). There were no significant changes in the average pore diameter as the pyrolysis temperature increased. They ranged from 3.5-4.1 Å for all biomass samples suggesting that pore development happened through the formation of channels with deeper pores (Mafu et al., 2016).

The structural lattice parameters and fraction of amorphous carbon, X_A, are presented in Table 4.3. The different torrefied biomass samples showed approximately the same amounts (fractions) of amorphous carbon. The determined X_A was reported as being representative of the amorphous sections of the fibres, which were not degraded during heat treatment (Mafu et al., 2016). Pyrolytic chars of SB were more sensitive to heat owing to the limited shielding by the lower lignin contents in SB compared to HW and SW. At 600 °C, X_A could not be determined by means of WA-XRD-CFA for SB char, while this was observed only at 1100 °C for HW and SW chars. As the pyrolysis temperature increased, d_{002}, L_c and N_{ave} decreased significantly, whilst L_a was considerably increased. The reduction in d_{002} resulted in the decrease of L_c producing a more packed microcrystallite lattice. Thus, the carbon crystallites of the biomass chars were significantly stretched in the y-direction resulting in flat layered carbon sheets. The average number of crystallites in a stack was reduced as d_{002} and L_c decreased. These lattice parameter changes may indicate changes of the micropore network. From 600 °C, the structural parameters of woody biomass became more similar to each other and increasingly different from that of the bagasse sample (e.g. the micropore volume, the micropore surface area and the trends in the aliphatic fraction - X_A).

The extracted characteristics of biomass and subsequent chars were correlated with their H/C ratios as presented in Figure 4.3 (a – c). Inverse linear correlations were observed between the H/C ratios and the aromaticity (Figure 4.3(a)), and the degree of aromatic ring condensation, $(R/C)_u$, of the chars as shown in Figure 4.3(b). This implies that both the aromaticity and $(R/C)_u$ can be predicted from the empirical H/C ratios, following the correlation equations shown in Table 4.4, with correlation coefficients > 0.98. Conversely, the CH_2/CH_3 ratio was found to increase with increasing H/C ratio (equivalent to decreasing aromaticity) as presented in Figure

4.3(c) with a power law fitting. It has been demonstrated that the CH_2/CH_3 ratios of the chars can be estimated from the H/C ratios of the studied samples from the correlation equations given in Table 4.4. Thus, with increasing pyrolysis temperature, char development proceeds by the elimination of aliphatic groups while aromaticity increases, complemented by the progression of aromatic ring condensation, $(R/C)_u$, with the concomitant hydrogen abstraction. These processes, coupled with increasing carbon densification of the biomass chars, also impacted the pore structure evolution and development. For example, the micropore surface area as shown in Figure 4.3(d) and the micropore volume (Table 4.3) increased with increasing with increasing pyrolysis temperature up to 600 °C. This may be linked to the elimination of aliphatic chains and the escape of volatiles leaving behind pores as the pyrolysis temperature increased. However, pore coalescence was observed for char samples of SW and SB at 1100 °C, similar to reported findings for coal (Roberts et al., 2015). From these established correlations, it is evident that the charring process is a combination of aliphatics elimination and the aromatic ring condensation which results in the gradual increase in aromaticity with increasing temperature.

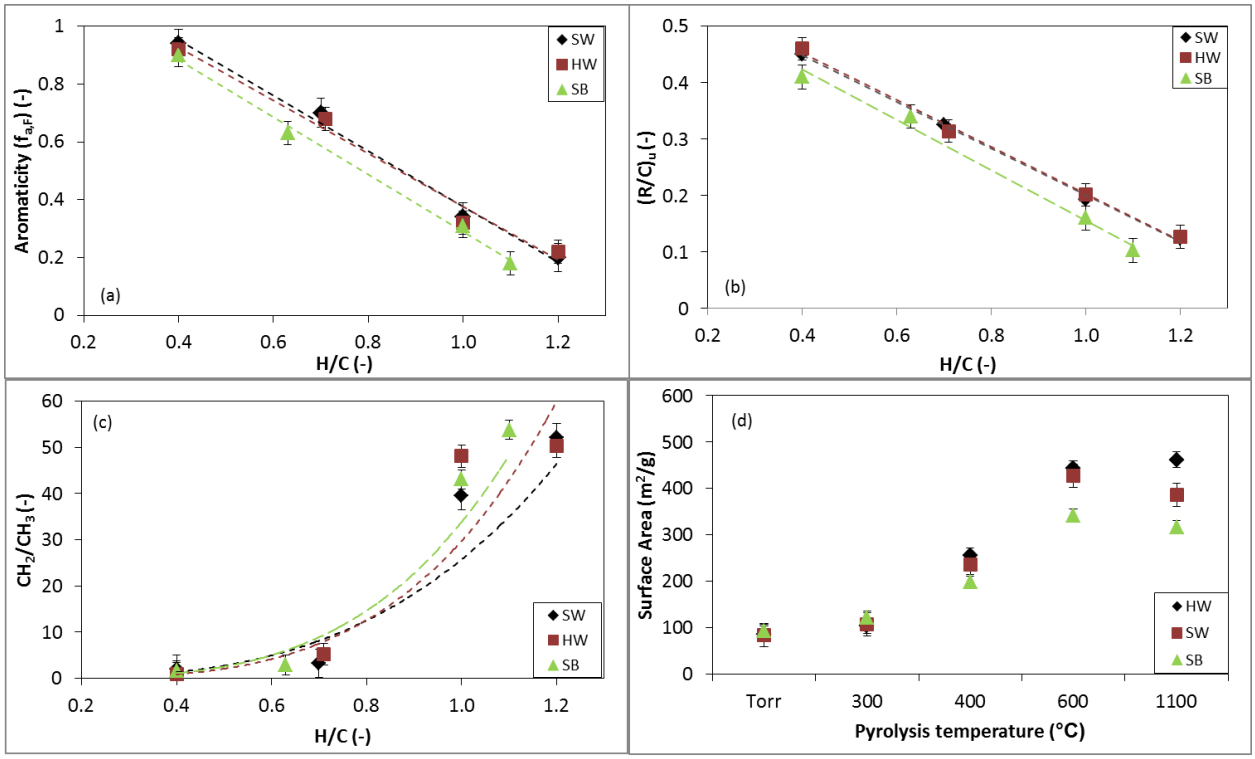

Figure 4-3: Correlations between the chemical characteristics of biomass and biomass chars

Table 4-4: Comparison equations of some properties of torrefied biomass and subsequent chars

Parameter	Sample ID	Correlation equation	R^2
$f_{a,F}$	**SW**	$f_{a,F} = -0.96(H/C) + 1.34$	0.991
	HW	$f_{a,F} = -0.92(H/C) + 1.30$	0.983
	SB	$f_{a,F} = -0.99(H/C) + 1.28$	0.995
$(R/C)_n$	**SW**	$(R/C)_n = -0.41(H/C) + 0.61$	0.998
	HW	$(R/C)_n = -0.42(H/C) + 0.62$	0.997
	SB	$(R/C)_n = -0.44(H/C) + 0.60$	0.990
CH_2/CH_3	**SW**	$CH_2/CH_3 = 26(H/C)^{3.23}$	0.858
	HW	$CH_2/CH_3 = 29.8(H/C)^{3.85}$	0.958
	SB	$CH_2/CH_3 = 33.8(H/C)^{3.74}$	0.924

4.4 Conclusion

Char development was found to be dependent on the pyrolysis conditions. There was an observed link between the proximate and ultimate analysis data with fibre degradation. Chemical properties of the chars can be extracted from ATR-FTIR data, complimenting results from other techniques. Gradual decrease in H/C and O/C ratios, and aliphatic chains with increasing pyrolysis temperature, resulted in increasing f_a and $(R/C)_u$ of the chars. While micropore development was observed up to 600 °C, pore coalescence was more significant for SW and SB at 1100 °C. Char development can be considered as a two steps process: < 600 °C where changes were attributed to fibre degradation, resulting in the removal of aliphatics, and > 600 °C where changes were as a result of hydrogen abstraction and aromatic ring condensation.

References

Anca-Couce, A., 2016. Reaction mechanisms and multi-scale modelling of lignocellulosic biomass pyrolysis. Prog. Energy Combust. Sci. 53, 41–79.

Angin, D., Sensoz, S., 2014. Effect of Pyrolysis Temperature on Chemical and Surface Properties of Biochar of Rapeseed (*Brassica napus L.*). Int. J. Phytoremediation 16, 684–693.

Antonio, W., Lenço, P.C., Carvalho, D.J., Paulo, J., Veiga, S., 2014. The generation of residual biomass during the production of bio-ethanol from sugarcane , its characterization and its use in energy production. Renew. Sustain. Energy Rev. 29, 589–603.

Anupam, K., Sharma, A.K., Lal, P.S., Dutta, S., Maity, S., 2016. Preparation, characterization and optimization for upgrading *Leucaena leucocephala* bark to biochar fuel with high energy yielding. Energy 106, 743–756.

Asadullah, M., Zhang, S., Min, Z., Yimsiri, P., Li, C.-Z., 2010. Effects of biomass char structure on its gasification reactivity. Bioresour. Technol. 101, 7935–43.

Azargohar, R., Nanda, S., Kozinski, J.A., Dalai, A.K., Sutarto, R., 2014. Effects of temperature on the physicochemical characteristics of fast pyrolysis bio-chars derived from Canadian waste biomass. Fuel 125, 90–100.

Bardet, M., Hediger, S., Gerbaud, G., Gambarelli, S., Jacquot, J.F., Foray, M.F., 2007. Investigation with ^{13}C NMR , EPR and magnetic susceptibility measurements of char residues obtained by pyrolysis of biomass. Fuel 86, 1966–1976.

Barnette, A.L., Lee, C., Bradley, L.C., Schreiner, E.P., Bum, Y., Shin, H., Cosgrove, D.J., Park, S., Kim, S.H., 2012. Quantification of crystalline cellulose in lignocellulosic biomass using sum frequency generation (SFG) vibration spectroscopy and comparison with other analytical methods. Carbohydr. Polym. 89, 802–809.

Cetin, E., Moghtaderi, B., Gupta, R., Wall, T.F., 2004. Influence of pyrolysis conditions on the structure and gasification reactivity of biomass chars. Fuel 83, 2139–2150.

Collard F., Blin, J., Benshakhria, A., Valette, J. (2012) Influence of impregnated metal on the pyrolysis conversion of biomass constituents. Journal of Analytical and Applied Pyrolysis 95, 213-226.

Cui, T., Fan, W., Dai, Z., Guo, Q., Yu, G., Wang, F., 2016. Variation of the coal chemical

structure and determination of the char molecular size at the early stage of rapid pyrolysis. Appl. Energy 179, 650–659.

Deng, J., Wang, G., Kuang, J-h., Zhang, Y., Luo, Y. 2009. Pre-treatment of agricultutal residues for co-gasification via torrefaction. Journal of Analytical and Applied Pyrolysis 86, 331-337.

Everson, R.C., Okolo, G.N., Neomagus, H.W.J.P., Santos, J., 2013. X-ray diffraction parameters and reaction rate modeling for gasification and combustion of chars derived from inertinite-rich coals. Fuel 109, 148–156.

Fisher, E.M., Dupont, C., Darvell, L.I., Commandré, J.M., Saddawi, A., Jones, J.M., Grateau, M., Nocquet, T., Salvador, S., 2012. Combustion and gasification characteristics of chars from raw and torrefied biomass. Bioresour. Technol. 119, 157–165.

Freitas, J.C.C., Bonagamba, T.J., Emmerich, F.G., 2001. Investigation of biomass- and polymer-based carbon materials using ^{13}C high-resolution solid-state NMR. Carbon. 39, 535–545.

Giudicianni, P., Cardone, G., Ragucci, R., 2013. Cellulose , hemicellulose and lignin slow steam pyrolysis : Thermal decomposition of biomass components mixtures. J. Anal. Appl. Pyrolysis 100, 213–222.

Huang, L., Chen, Y., Liu, G., Li, S., Liu, Y., Gao, X., 2015. Non-isothermal pyrolysis characteristics of giant reed (*Arundo donax L.*) using thermogravimetric analysis. Energy 87, 31–40.

Huang, Y., Yin, X., Wu, C., Wang, C., Xie, J., Zhou, Z., Ma, L., Li, H., 2009. Effects of metal catalysts on CO_2 gasification reactivity of biomass char. Biotechnol. Adv. 27, 568–72.

Kajitani, S., Zhang, Y., Umemoto, S., Ashizawa, M., Hara, S., 2010. Co-gasification reactivity of coal and woody biomass in high-temperature. Energy & Fuels 24, 145–151.

Kaudal, B.B., Chen, D., Madhavan, D.B., Downie, A., Weatherley, A., 2016. An examination of physical and chemical properties of urban biochar for use as growing media substrate. Biomass and Bioenergy 84, 49–58.

Liu, Z., Zhang, F., Wu, J., 2010. Characterization and application of chars produced from pinewood pyrolysis and hydrothermal treatment. Fuel 89, 510–514.

Mafu, L.D., Neomagus, H.W.J.P., Everson, R.C., Carrier, M., Strydom, C.A., Bunt, J.R., 2016. Structural and chemical modifications of typical South African biomasses during

torrefaction. Bioresour. Technol. 202, 192–197.

Mao, Y., Dong, L., Dong, Y., Liu, W., Chang, J., Yang, S., Lv, Z., Fan, P., 2015. Fast co-pyrolysis of biomass and lignite in a micro fluidized bed reactor analyzer. Bioresour. Technol. 181, 155–162.

McBeath, A. V, Smernik, R.J., Schneider, M.P.W., Schmidt, M.W.I., Plant, E.L., 2011. Determination of the aromaticity and the degree of aromatic condensation of a thermosequence of wood charcoal using NMR. Org. Geochem. 42, 1194–1202.

Melkior, T., Jacob, S., Gerbaud, G., Hediger, S., Pape, L. Le, Bonnefois, L., Bardet, M., 2012. NMR analysis of the transformation of wood constituents by torrefaction. Fuel 92, 271–280.

Mukome, F.N.D., Zhang, X., Silva, L.C.R., Six, J., Parikh, S.J., 2013. Use of chemical and physical characteristics to investigate trends in biochar feedstocks. J. Agric. Food Chem. 61, 2196–2204.

Murillo, J.D., Ware, E.A., Biernacki, J.J., 2014. Characterization of milling effects on the physical and chemical nature of herbaceous biomass with comparison of fast pyrolysis product distributions using Py-GC/MS. J. Anal. Appl. Pyrolysis 108, 234–247.

Okolo, G.N., Neomagus, H.W.J.P., Everson, R.C., Roberts, M.J., Bunt, J.R., Sakurovs, R., Mathews, J.P., 2015. Chemical–structural properties of South African bituminous coals: Insights from wide angle XRD–carbon fraction analysis, ATR–FTIR, solid state ^{13}C NMR, and HRTEM techniques. Fuel 158, 779–792.

Pimenidou, P., Dupont, V., 2012. Characterisation of palm empty fruit bunch (PEFB) and pinewood bio-oils and kinetics of their thermal degradation. Bioresour. Technol. 109, 198–205.

Roberts, M.J., Everson, R.C., Neomagus, H.W.J.P., Okolo, G.N., Van Niekerk, D., Mathews, J.P., 2015. The characterisation of slow-heated inertinite- and vitrinite-rich coals from the South African coalfields. Fuel 158, 591–601.

Rutherford, D.W., Wershaw, R.L., Rostad, C.E., Kelly, C.N., 2012. Effect of formation conditions on biochars : Compositional and structural properties of cellulose , lignin , and pine biochars. Biomass and Bioenergy 46, 693–701.

Skhonde, M.P., Matjie, R.H., Bunt, J.R., Strydom, A.C., Schobert, H., 2009. Sulfur Behavior in

the Sasol-Lurgi Fixed-Bed Dry-Bottom Gasification process. Energy & Fuels 23, 229–235.

Suggate, R.P., Dickinson, W.W., 2004. Carbon NMR of coals: The effects of coal type and rank. Int. J. Coal Geol. 57, 1–22.

Suliman, W., Harsh, J.B., Abu-Lail, N.I., Fortuna, A.M., Dallmeyer, I., Garcia-Perez, M., 2016. Influence of feedstock source and pyrolysis temperature on biochar bulk and surface properties. Biomass and Bioenergy 84, 37–48.

Trubetskaya, A., Jensen, P.A., Jensen, A.D., Garcia Llamas, A.D., Umeki, K., Glarborg, P., 2016a. Effect of fast pyrolysis conditions on biomass solid residues at high temperatures. Fuel Process. Technol. 143, 118–129.

Trubetskaya, A., Jensen, P.A., Jensen, A.D., Steibel, M., Spliethoff, H., Glarborg, P., Larsen, F.H., 2016b. Comparison of high temperature chars of wheat straw and rice husk with respect to chemistry, morphology and reactivity. Biomass and Bioenergy 86, 76–87.

Tumuluru, J.S., Sokhansanj, S., Hess, J.R., Wright, C.T., Boardman, R.D., 2011. A review on biomass torrefaction process and product properties for energy applications. Ind. Biotechnol. 7, 384–402.

Uzun, B.B., Putun, A.E., Ersan, P., 2006. Fast pyrolysis of soybean cake : Product yields and compositions. Bioresour. Technol. 97, 569–576.

Wannapeera, J., Worasuwannarak, N., 2012. Upgrading of woody biomass by torrefaction under pressure. J. Anal. Appl. Pyrolysis 96, 173–180.

Wei, L., Zhang, L., Xu, S., 2011. Effects of feedstock on co-pyrolysis of biomass and coal in a free-fall reactor. J. Fuel Chem. Technol. 39, 728–734.

Wen, J.-L., Sun, S.-L., Yuan, T.-Q., Xu, F., Sun, R.-C., 2014. Understanding the chemical and structural transformations of lignin macromolecule during torrefaction. Appl. Energy 121, 1–9.

Yang, D., Zhong, L., Yuan, T., Peng, X., Sun, R., 2013. Studies on the structural characterization of lignin , hemicelluloses and cellulose fractionated by ionic liquid followed by alkaline extraction from bamboo. Ind. Crop. Prod. 43, 141–149.

Yang, H., Yan, R., Chen, H., Lee, D.H., Zheng, C., 2007. Characteristics of hemicellulose , cellulose and lignin pyrolysis. Fuel 86, 1781–1788.

Yang, H., Yan, R., Chen, H., Zheng, C., Lee, D.H., Uni, V., V, N.D., March, R. V, Re, V., Recei,

M., September, V., 2006. In-depth investigation of biomass pyrolysis based on three major components : hemicellulose , cellulose and lignin. Energy and Fuels 388–393.

Zhang, Y., Zheng, Y., Yang, M., Song, Y., 2016. Effect of fuel origin on synergy during co-gasification of biomass and coal in CO_2. Bioresour. Technol. 200, 789–794.

Zhang, Li, L., Tong, D., Hu, C., 2016. Microwave-enhanced pyrolysis of natural algae from water blooms. Bioresour. Technol. 212, 311–317.

Zhao, X., Chen, J., Chen, F., Wang, X., Zhu, Q., Ao, Q., 2013. Surface characterization of corn stalk superfine powder studied by FTIR and XRD. Colloids Surfaces B Biointerfaces 104, 207–212.

Supplementary Information

S4 Supplementary data from the characterization of pyrolytic chars

From the published journal article of Chapter 4, only the results of one of the samples was presented and discussed and only reference to the rest of the samples were made as observed trends were similar. These supplementary results were discussed in Chapter 4 and are presented in this subsection. Presented supplementary data include the ATR-FTIR spectra, the SEM micropgraphs, and the WA-XRD-CFA diffractograms of the torrefied and pyrolysed biomass samples.

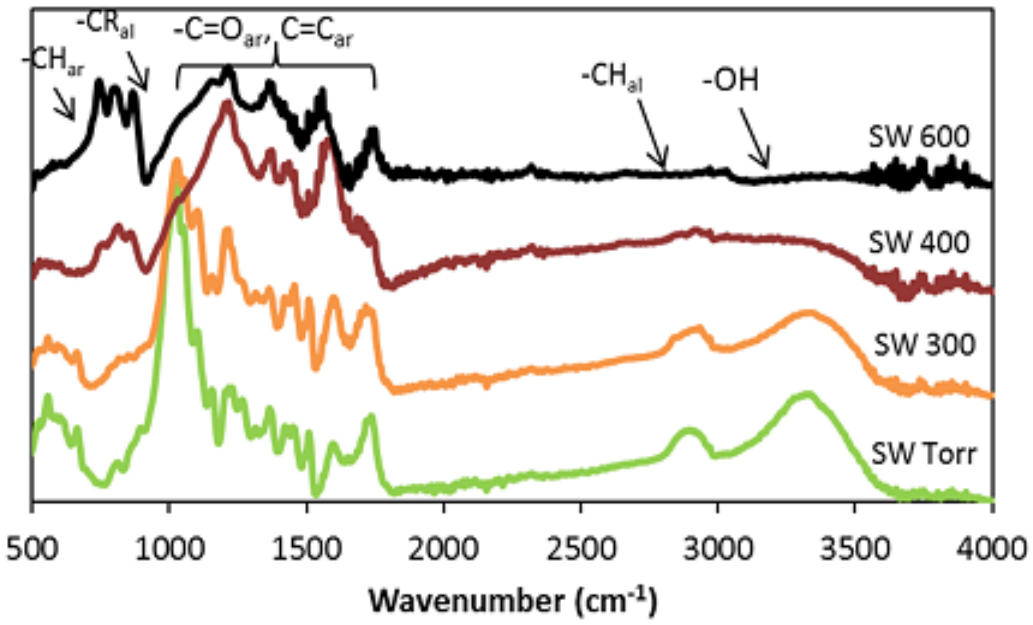

Figure S 4-4: ATR-FTIR spectra for chars prepared from SW

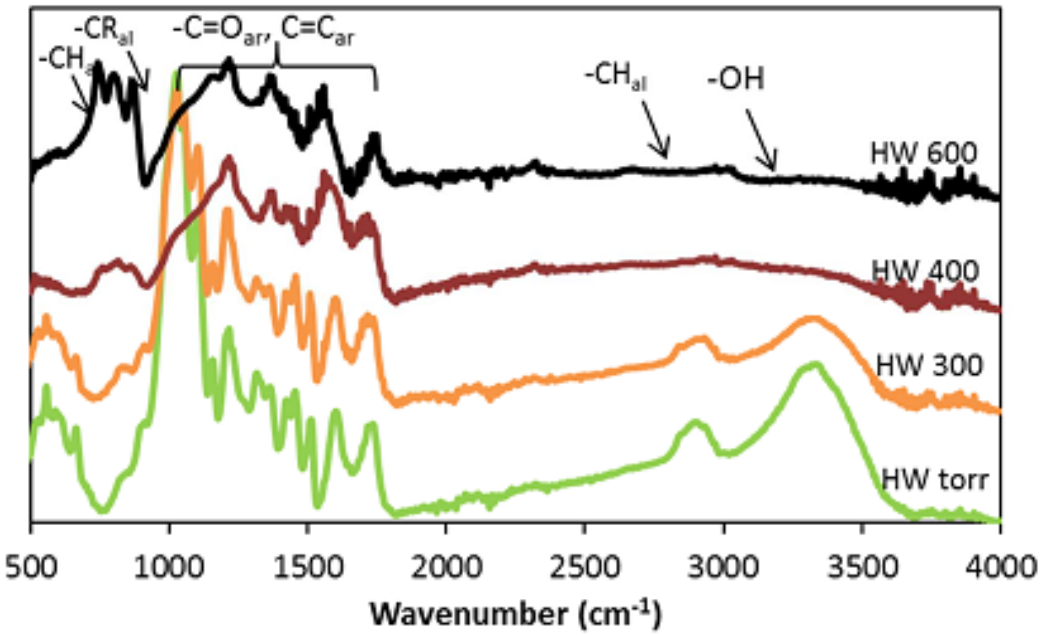

Figure S 4-2: ATR-FTIR spectra for chars prepared from HW

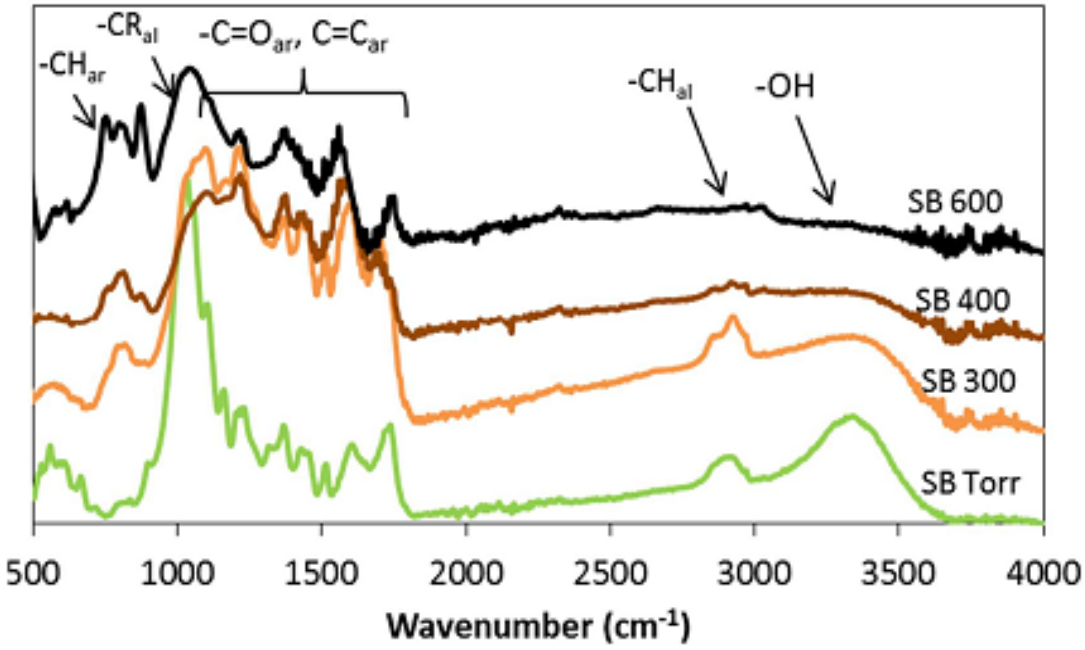

Figure S 4-3: ATR-FTIR spectra for chars prepared from SB

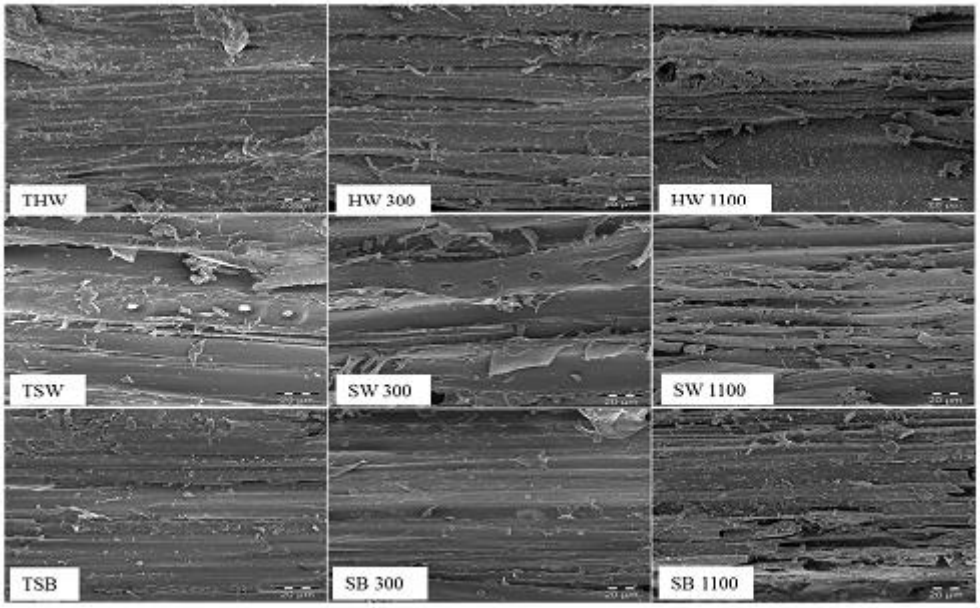

Figure S 4-4: SEM micrographs for torrefied biomass and chars prepared at 300 and 1100°C

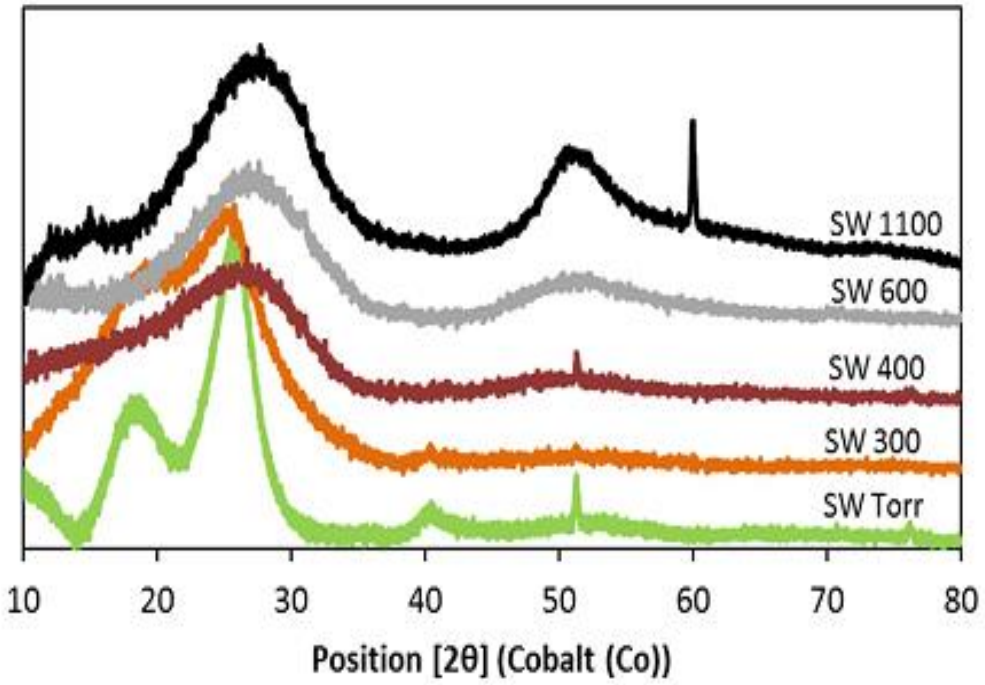

Figure S 4-5: WA-XRD-CFA diffractograms for chars prepared from SW

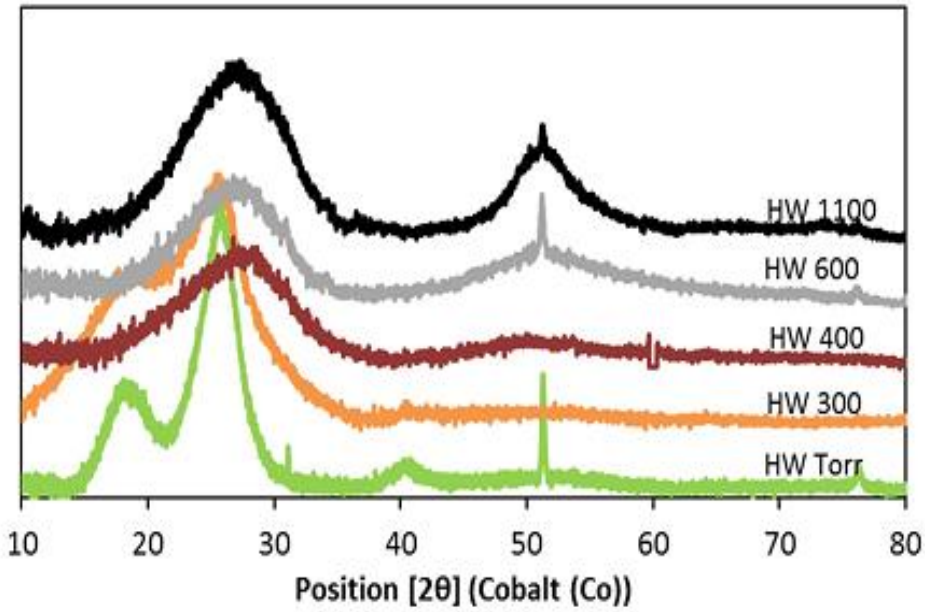

Figure S 4-6: WA-XRD-CFA diffractograms for chars prepared from HW

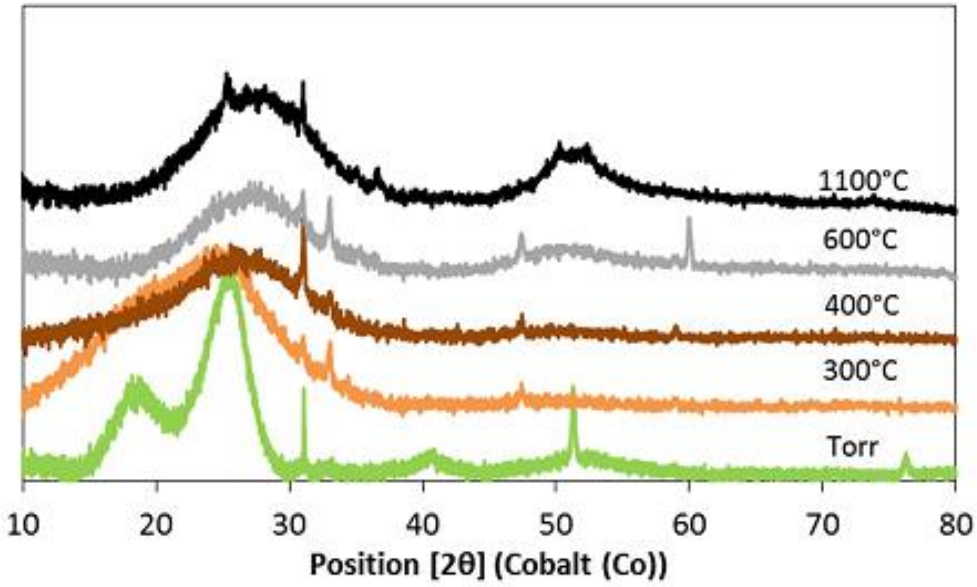

Figure S 4-7: WA-XRD-CFA diffractograms for chars prepared from SB

Chapter 5: The CO_2 char gasification characteristics of biomass and biomass-coal char blends

Findings reported in this chapter are published as: Mafu, L.D., Neomagus, H.W.J.P., Everson, R.C., Okolo, G.N., Strydom, C.A., Bunt, J.R. **2018**. The carbon dioxide gasification characteristics of biomass char samples and their effect on coal gasification reactivity during co-gasification. *Bioresource Technology*. **258**, 70-78. https://doi.org/10.1016/j.biortech.2017.12.053

Abstract

The CO_2 gasification characteristics of three biomass char samples (softwood chips - SW, hardwood chips - HW and sweet sorghum bagasse - SB) and bituminous coal char were investigated in a thermogravimetric analyser in the temperature range of 850 – 950 °C. SB exhibited higher reactivities (average initial reactivity (R_i), specific reactivity (R_s), and average final reactivity (R_f)) than SW and HW. Coal char gasification reactivities were observed to be lower than those of the three biomass chars. Correlations between the char reactivities and char characteristics show linear correlations between H/C, alkali index (AI_2), L_a, and L_c/d_{002} with the char reactivity; while the surface area exhibited a polynomial relationship with the char reactivity. The addition of 10% biomass had no significant impact on the coal char gasification reactivity. However, 20 and 30% biomass additions resulted in increased coal char gasification rate. HW and SW had similar effect on the coal char during co-gasification: increase in the gasification reactivity at lower conversions, while co-gasification of coal and SB chars resulted in increased gasification rates throughout the conversion range. Experimental data from biomass char gasification and biomass-coal char co-gasification were well described by the modified random pore model (MRPM), while coal char gasification was better described by the random pore model (RPM).

***Key Words**: Average initial reactivity, biomass-coal char blends, co-gasification and modified random pore model.*

5.1 Introduction

The use of biomass in energy applications has been receiving significant attention lately. Based on their chemical and structural characteristics, various biomass wastes and energy crops have been identified as possible feedstock for different energy applications (Mata et al., 2010). Woods, weeds, grasses, leaves, agricultural wastes and municipal wastes have found applications in the production of methane (Gunaseelan, 1997), fuel pellets (Liu et al., 2014), methanol and biodiesel (Fukuda et al., 2001) as well as electricity generation (Ruiz et al., 2013). There has been growing interest in lignocellulosic biomass for thermochemical applications, as it is cheap, abundantly available and considered to be carbon neutral (Ruiz et al., 2013). However, its characteristics' variability hinders progress towards stand-alone biomass gasifiers for electricity generation (Rosillo-Calle, 2016). To overcome source variability and fuel upgrade, torrefaction has been explored and it has been demonstrated that the characteristics of sweet sorghum bagasse, hardwood and softwood chips were comparable after torrefaction (Mafu et al., 2016).

In gasifiers, such as the fixed bed dry bottom (FBDB) gasifier, feedstock is processed at temperatures as high as 1000°C and at pressures up to 30 bar where it is subjected to different reaction zones: drying, pyrolysis, gasification and combustion zones (Bunt and Waanders, 2008). Pyrolysis, a pre-step to gasification, plays a significant role in the gasification reactivities of feedstocks as it influences the features of chars fed into the gasification zone (Bunt and Waanders, 2008). The characteristics of feedstock that affect its gasification reactivity may be divided into two: the structural and chemical characteristics (Cetin et al., 2004; Huo et al., 2014). The amount of potassium (K) and calcium (Ca) in the ash have been associated with higher gasification reactivities for biomass samples (Ding et al., 2014; Zhang et al., 2010). On the other hand, higher silicon (Si), aluminium (Al) and phosphorus (P) contents are reported to inhibit gasification (Ding et al., 2014; Min et al., 2011). The correlation of structural characteristics to the gasification reactivity has been limited in biomass studies. However, these have been considerably reported for coal gasification studies (Everson et al., 2013). The gasification reactivity has been reported to increase with decreasing aromaticity for various feedstocks including lignocellulosic biomass and coal (Ahmad et al., 2016; Everson et al., 2013). Huo et al. (2014) reported the relationship between the crystalline parameters and the gasification reactivity for various biomass char samples, where the reactivity index ($R_{0.5}$) increased with increasing interlayer spacing (d_{002}) and decreasing crystallite height (L_c). Zuo et al. (2015) investigated the effect of the degree of disorderliness of the carbon structures on the gasification reactivity by evaluating the ratio of the intensity of the V-band and the G-band (I_V/I_G) for biomass char and

coal char blends. They found that the gasification reactivity increased with increasing I_V/I_G, i.e. the gasification reactivity increased with increasing disorderliness of the carbon structures (Zuo et al., 2015).

Some of the shortcomings of biomass conversion may be overcome by biomass-coal co-gasification. Co-gasification of biomass and coal reduces the disadvantages of using the individual feedstock and exploits the advantages of the separate fuels (Taba et al., 2012). For instance, the relatively high amounts of alkali and alkali earth metals (AAEMs) in biomass may act as catalysts for coal gasification during co-gasification (Lahijani et al., 2013a). As co-gasification proceeds, a solid-solid interface between the AAEMs from biomass and the coal char may be formed, depending on the particle size/shape and gasification conditions, and this promotes the formation of intercalation compounds. These compounds increase the interlayer spacing, hence weakening the C-C bonds resulting in increased gasification reactivity (Huang et al., 2009; Jeong et al., 2014). However, the gasification rate may be inhibited by the formation of potassium silicate eutectics that are responsible for abstracting catalysts, thereby reducing the gasification reactivity (Ding et al., 2014). Co-gasification does not require new generation power plants, and is more efficient than biomass gasification in terms of energy conversion (Masnadi et al., 2015). It has the potential to reduce GHG emissions as well as act as a transition into the generation of electricity from biomass (Rosillo-Calle, 2016).

The CO_2-char gasification of lignocellulosic biomass and coal chars have been widely reported (Min et al., 2011; Wang et al., 2016; Xue et al., 2014; Zhang et al., 2010). However, analysis of the relationship between biomass char characteristics and the gasification reactivity, at different stages of conversion, has not been adequately studied. In this paper, we report the CO_2-char gasification of three waste biomass chars; prepared from softwood chips (SW), hardwood chips (HW) and sweet sorghum bagasse (SB). The char characteristics of these samples have been investigated at low temperature treatment i.e. torrefaction at 260 °C (Mafu et al., 2016) and at higher temperatures, up to 1100 °C (Mafu et al., 2017). The gasification reactivity was divided into three – the average initial reactivity (R_i), specific reactivity (R_s), and the average final reactivity (R_f). They are defined by the average reactivity at $0 \leq X \leq 0.1$, the reactivity at a gasification time where $X = 0.5$ and the average reactivity at $0.7 \leq X \leq 0.9$, respectively.

As the correlations of structural characteristics of biomass in relation to the gasification reactivity have not received considerable attention, this forms the main motivation of this study. In this paper, the relationship between the biomass- and coal-char characteristics and R_i, R_s, and

R_f were investigated. This was accomplished by determining the CO_2-char gasification rate of three waste biomass chars; softwood chips (SW), hardwood chips (HW) and sweet sorghum bagasse (SB). The char characteristics of these samples have been previously investigated at low temperature treatment i.e. torrefaction at 260 °C (Mafu et al., 2016) and at higher temperatures, up to 1100 °C (Mafu et al., 2017). The reactivity of the pure biomass char and coal char and blends of biomass and coal chars are reported and correlations are provided to relate the gasification rate and selected structural properties of the solid fuels.

5.2 Materials and methods

5.2.1 Preparation of char samples

The vitrinite-rich coal used in this study was a seam 4 bituminous coal from the Witbank coalfields, and is a typical coal used in the coal to liquid process in South Africa. Woody biomass samples (softwood chips – SW and hardwood chips – HW) were sourced from the South African Pulp and Paper Industries (SAPPI) Limited. Sweet sorghum bagasse (SB) was supplied by the Agricultural Research Council (ARC) of South Africa. These biomass samples are the most abundantly available in South Africa and therefore show potential as possible co-feed material in the coal to liquid processes. The preparation of the biomass samples was reported in a previous paper (Mafu et al., 2017). The bulk coal sample was air-dried until constant weight. To obtain a representative sample, standardised cone and quartering (DD CEN/TS 14780:2005) was performed on the sample three times. The obtained representative sample was then pre-crushed with a jaw crusher (Model No. 46-126) and further reduced to < 300 µm using a Fritsch P-14 ball mill (R-Mill). Torrefied biomass samples were prepared in a tube furnace, where approximately 10 g raw biomass samples (SW, HW and SW) were heated at 10 °C/min to 260 °C in N_2 flow of 100 mL/min (Mafu et al., 2016). The characteristics of the raw coal and torrefied biomass samples are presented in Table 5.1. Char samples were prepared from the raw coal and torrefied biomass by heating 10 g of sample in N_2 (100 mL/min) at 10 °C/min to a final temperature of 1100 °C and kept isothermal for 60 min. Blends were prepared by weight, blended, flushed with N_2, and stored in a desiccator.

Table 5-1: Characteristics of torrefied biomass and coal samples

Proximate analysis					
Properties	**Method**	**TSW***	**THW**	**TSB**	**Coal**
Volatile Matter (wt.%, mfb)	ISO 562:2010	76.5	77.3	69.8	33.6
Ash yield (wt.%, mfb)	ISO 1171:2010	0.6	0.6	6.5	12.1
Calorific Value (MJ/kg)	ISO 1928:2010	22.3	22.4	23.0	25.8
Fixed Carbon (wt.%, mfb)	By Difference	22.9	22.1	23.7	54.3
Ultimate analysis (wt.%, daf)					
C	ASTM D 5373	47.7	46.4	43.5	80.6
H	ASTM D 5373	5.7	5.5	5.6	5.5
N	ASTM D 5373	1.0	0.1	0.3	2.1
S	ASTM D 4239	0.16	0.01	0.13	0.91
O	by difference	45.5	48.0	50.5	11.0
Maceral composition (vol.%, mmb)					
Vitrinite	ISO 7404-3: 1994	-	-	-	62.9
Liptinite	ISO 7404-3: 1994	-	-	-	6.8
Total inertinite	ISO 7404-3: 1994	-	-	-	30.3

5.2.2 Char characterization

Conventional and advanced characterization techniques, including proximate and ultimate analysis, wide angle X-ray diffraction carbon fraction analyses (WA-XRD-CFA), X-ray fluorescence (XRF) analyses were performed using a PANalytical Epsilon 3 XL ED-XRF spectrometer, equipped with a 50kV Ag-anode X-ray tube, 6 filters, a helium purge facility and a high resolution silicon drift detector, calibrated using a number of international and national certified reference materials (CRMs). From the XRF data, the alkali index, often referred to as the catalytic index was determined using the different expressions; AI_1 (Equation 5.1a), AI_2 (Equation 5.1b) and AI_3 (Equation 5.1c) (Bouraoui et al., 2016). The surface area measurements were evaluated by CO_2 adsorption as outlined in Mafu et al., (2016).

$$AI_1 = Ash\ yield * \frac{Fe_2O+CaO+MgO+Na_2O+K_2O}{SiO_2+Al_2O_3+P_2O_5} \quad (5.1a)$$

$$AI_2 = Ash\ yield * \frac{K_2O}{SiO_2+Al_2O_3+P_2O_5} \quad (5.1b)$$

$$AI_3 = Ash\ yield * \frac{K_2O+CaO}{SiO_2+Al_2O_3+P_2O_5} \quad (5.1c)$$

5.2.3 Char reactivity

CO_2-char gasification and co-gasification experiments were performed at isothermal conditions in a thermogravimetric analyser (TGA) (SDQT - 600). Gasification experiments were carried out by heating up the char samples (approximately 15 mg) under N_2 at 50 °C/min to the desired isothermal temperatures (850, 875, 900, 925, and 950 °C), after which, the reactant gas (CO_2) was introduced and the experiments were allowed to proceed to completion. The gasification fractional conversion (X) and gasification rate (r) were determined using Equations 5.2a and 5.2b, respectively.

$$X = \frac{m_0-m_t}{m_0-m_{ash}} \quad (5.2a)$$

$$r = \frac{dX}{dt} \quad (5.2b)$$

where m_0 is the initial char mass, m_t, the weight of char at time, t and m_{ash}, the ash yield or the final weight after gasification has been completed. The average initial reactivity (R_i), the reactivity index (R_s), and the average final reactivity (R_f) were evaluated following Equations 5.3 – 5.5. A synergy factor (SF) was used to evaluate synergistic effect and/or inhibition effect during co-gasification, where SF > 1 indicated synergy, and SF < 1, inhibition. SF was determined using Equation 5.6. When SF is calculated using $R_{i,ave}$, SF is referred to as SFR_i, as was for R_s and R_f. R_{calc} was determined from Equation 5.7.

$$R_i = \frac{\sum_{X=0\%}^{X=10\%} r}{N} \quad (5.3)$$

$$R_s = \frac{0.5}{\tau_{50}} \quad (5.4)$$

$$R_f = \frac{\sum_{X=70\%}^{X=90\%} r}{N} \quad (5.5)$$

$$SF = \frac{R_{exp}}{R_{calc}} \quad (5.6)$$

$$R_{calc} = f_b R_b + f_c R_c \quad (5.7)$$

where X, N and τ_{50} denotes the conversion, number of data points and the time required for the conversion to reach 50%, respectively. R_{calc} and R_{exp} are the calculated and experimental reactivity, respectively. f_b, and f_c are the fractions of biomass- and coal-char, and R_b, and R_c are the reactivities of biomass- and coal-char, respectively.

5.2.4 Kinetic modelling

The model fitting of biomass char gasification and biomass-coal char co-gasification experimental data was done in two steps. In the first step, R_i (the reactivity at the beginning of the reaction) was used as the reaction constant, k_{RPM}, in the random pore model (RPM) equation (Equation 5.8). Through regression, the structural parameter, ψ, was obtained using Equation 8. These two parameters were then used, in the second step, where a stepwise regression was used to evaluate the empirical constants controlling the changes in the char structure, c and p, as discussed in Zhang et al. (2008). The variable function, θ, in Equation 5.9 may be equivalent to cX or c(1-X), depending on the most effective catalyst in the sample (Zhang et al., 2010). The model fitting for coal gasification was achieved following the first step only. The quality of fit (QOF), defined by Equation 5.10 was used to validate and determine the statistical significance and efficiency of the applied model.

The random pore model (RPM) (Equation 8) was early developed and used extensively to describe coal gasification (Everson et al., 2013). However, for brown coals, catalytic gasification and most biomass gasification, the RPM model shows shortcomings (Zhang et al., 2010), specifically at high conversions. This has resulted in the modification (Equation 9) for biomass with gasification maxima at higher conversions (Taba et al., 2012). For model fitting, the reactivity at X = 0 was used as the k_{RPM} in Equations 5.8 and 5.9 and the structural parameter, ψ, was obtained through regression. To fit the modified random pore model (MRPM), a procedure discussed by Zhang et al., (2008) was followed. The variable function, θ, in Equation 5.9 may be given by cX or c(1-X) depending on the effect of catalysis during gasification (Zhang et al., 2010). The quality of fit (QOF, Equation 5.10) has been a significant component of kinetic model fitting and it was used to determine the accuracy and efficiency of the applied model (Lahijani et al., 2013b; Jeong et al., 2014).

$$\frac{dX}{dt} = k_{RPM}(1-X)\sqrt{1-\psi ln(1-X)} \tag{5.8}$$

$$\frac{dX}{dt} = k_{RPM}(1-X)\sqrt{1-\psi Ln(1-X)}(1+\theta^{p}) \tag{5.9}$$

$$QOF\ (\%) = 100 * \left[1 - \frac{\sum_1^n \frac{|X_{calc}-X_{exp}|}{X_{exp}}}{N}\right] \tag{5.10}$$

where N is the number of data points, X_{calc} is the calculated conversion from the model equation and X_{exp} is the experimental conversion.

5.3 Results and discussion

5.3.1 Char characteristics

The characteristics of biomass and coal char samples are presented in Table 5.2. There were similarities in the proximate and ultimate analysis results of SW and HW char samples compared to SB and coal char samples. SB char sample exhibited the highest volatile matter and ash yield compared to SW and HW whilst having the lowest calorific value (26.6 MJ/kg against 32.3 and 32.1 for SW and HW, respectively) and fixed carbon (83.9 wt.% compared to 97.4 and 97.5 wt.%, respectively). Char derived from the coal sample had the lowest volatile matter and fixed carbon contents, while exhibiting the highest ash content. Using the Van Krevelen ranking, all char samples could be ranked with the coalification process up to anthracite, with biomass char samples having similar H/C ratios, and this was even lower for coal char. SW and HW chars exhibited similar O/C ratios, while SB char and coal char had higher O/C ratios. There were no significant differences in the d_{002} values for all samples. However, SB had bigger carbon lattice i.e. longer L_c and wider crystalline size (L_a) than the woody biomass and coal char samples. Coal char samples had the shortest carbon lattice. L_c decreased in magnitude in the order: SW ≈ HW < SB < coal. The number of aromatic rings per carbon crystallite, N_{ave}, was observed to increase with increasing L_c.

The micropore surface areas of chars were found to increase in the order: coal < SB < SW < HW, similar to the trend observed for the micropore volumes. These observations could be influenced by the degree of graphitization and amount of ash (Azargohar et al., 2014; Okolo et al., 2015; Suliman et al., 2016). From XRF spectroscopy, no oxides of Si and Al were detected for woody biomass char samples, while coal and SB char samples possessed the highest amounts of oxides of Si, Al, Ca and K species as observed by other researchers (Andersen et al., 2013; Niu et al., 2013).

Table 5-2: Char characteristics for biomass chars and coal char

Properties	SW char	HW char	SB char	Coal char
Proximate analysis results (wt.%, mfb)				
Volatile matter	1.3	1.2	3.2	0.6
Ash content	1.2	1.2	12.9	26.3
Calorific value (MJ/kg)	32.3	32.1	26.6	-
Fixed carbon	97.4	97.6	83.9	73.1
Ultimate analysis data (wt.%, daf)				
C	98.5	98.6	95.0	97.6
H	0.97	0.88	1.31	0.01
N	0.03	0.03	0.39	0.84
S	0.07	0.08	0.18	1.19
O	0.44	0.41	3.14	0.37
O/C (x10)	0.03	0.03	0.30	0.20
H/C	0.12	0.11	0.17	0.012
Lattice parameters from WA-XRD-CFA				
d_{002} (Å)	3.7	3.8	3.8	3.5
L_c (Å)	9.2	9.4	10.4	11.2
L_a (Å)	370	364	401	42
N_{ave} (-)	3.47	3.48	3.62	4.49
CO_2 low pressure gas adsorption measurements				
Micropore surface area (m^2/g)	387	462	316	41
Maximum pore volume (cm^3/g)	0.08	0.10	0.07	0.01
X-ray Fluorescence spectroscopy data (wt.%. LOI-free basis)				
SiO_2	nd	nd	36.4	46.7
TiO_2	nd	nd	nd	1.2
Al_2O_3	nd	nd	4.2	25.3
Fe_2O_3	3.4	5.2	3.2	6.7
MnO	2.8	1.5	0.3	0.2
MgO	9.0	nd	5.1	2.1
CaO	16.9	29.1	8.2	16.0
Na_2O	36.0	26.1	nd	nd
K_2O	17.4	20.1	38.4	0.7
P_2O_5	3.9	5.2	1.4	0.1
SO_3	10.7	12.7	2.7	1.1
Alkali Index (AI)				
AI_1	25	19	17	9
AI_2	5.4	4.6	11.8	0.3
AI_3	10.5	11.3	14.3	6.1

5.3.2 Biomass and coal CO2 – char gasification

The CO_2–char gasification rate of the three biomass samples increased with increasing gasification temperature. Figure 5.1(a) shows the reduction in gasification time as the gasification temperature increased, while Figure 5.1(b) shows the increase in the reactivity, R, with increasing temperature, as demonstrated for SW. Similar observations have been reported for CO_2 char gasification for various feedstocks (Bouraoui et al., 2015; Huo et al., 2014; Lahijani et al., 2013c). The CO_2 gasification of biomass chars resulted in higher reactivities than coal char, shown by the shorter gasification times for the biomass chars than for coal char. For the three biomass char samples, the reactivities were found to increase in magnitude in the order: HW < SW < SB. In Figure 5.1(d), the comparison between the reactivities of biomass and coal chars is presented by plotting the normalised reactivity (R/R_0) versus conversion (X). The reactivity of biomass char samples increased with increasing conversion, while coal char reactivity decreased (Figure 5.1(d)). There were differences, for biomass chars gasification, at conversions higher than X = 0.5. SB char gasification showed a decrease in the reactivity, while SW and HW gasification reactivity increased. These observations could be attributed to the inorganic constituents in the ash (higher Si, Al and P for SB char than SW and HW chars). Figure 5.1(e) shows a combined Arrhenius plot with parallel straight lines, with $R^2 \geq 0.98$, which is an indication that the investigated reactions were under chemical reaction control (Regime I). The gasification results of chars HW, SB, and coal char are presented in Figures S5.1 – S5.3 of the Supplementary information.

The gasification reactivities, R_i, R_s and R_f, are presented in Table 5.3. All the gasification reactivities investigated increased with increasing temperature for all the char samples. The gasification reactivities of the chars (R_i, R_s, R_f) increased in the order: coal < HW < SW < SB as also shown in Figure 5.1(d). With increasing conversion, only the gasification rates of HW and SW chars increased. On the other hand, the gasification reactivities of SB char increased in magnitude in the order: $R_i < R_f < R_s$, while the gasification of coal char resulted in the reactivities increasing in the order: $R_f < R_s < R_i$.

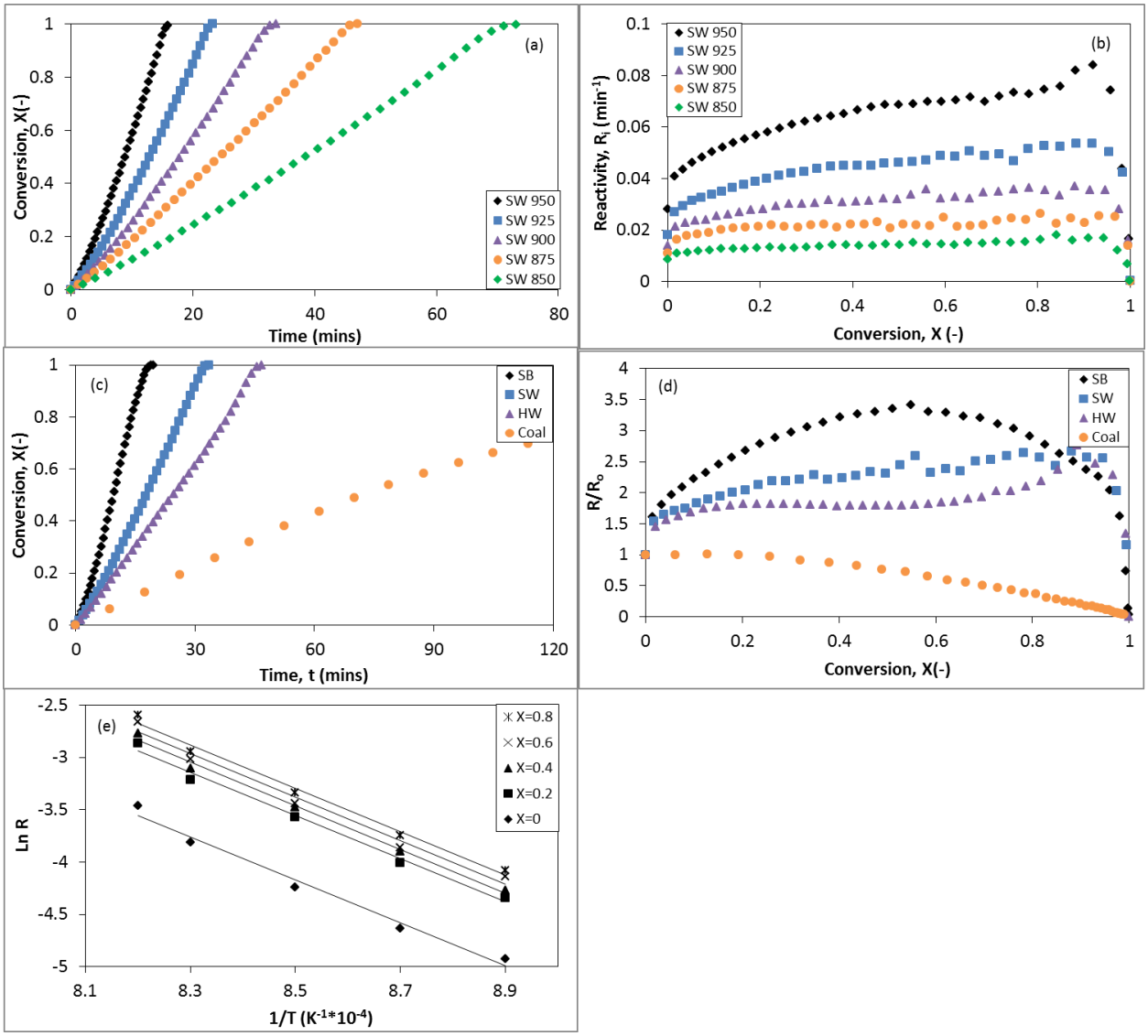

Figure 5-1: The char CO_2 - gasification plots for biomass and coal char samples

From these observations, it can be concluded that at higher conversion, the catalytic mineral species in SW and HW chars catalysed the gasification reactions more than SB. In contrast, the mineral species in SB and coal chars, resulted in the reduction and or inhibition of the gasification reactivity (Zhang et al 2010). This is supported by the char characteristics, more evidently, the ash compositions, where SW and HW chars possessed lesser amounts of Si, Al and P species, while having significant amounts of K, Ca and Na species. SB and coal showed larger contents of Si, Al and P species. Similar findings have been reported by Zhang et al., (2010).

Table 5-3: Gasification reactivity parameters and char characteristics of biomass and coal char samples

Sample	T (°C)	Reactivity (min^{-1}) ($x10^3$)		
		$R_{i,ave}$	R_s	$R_{f,ave}$
SW char	**850**	11.3	14.2	16.2
	875	17.0	22.3	24.1
	900	21.9	32.0	35.6
	925	29.6	46.3	51.4
	950	44.3	68.8	76.4
HW char	**850**	8.4	6.8	7.8
	875	13.2	13.9	17.5
	900	20.2	24.0	29.5
	925	24.7	31.2	39.1
	950	35.3	41.7	45.0
SB char	**850**	14.5	25.2	21.3
	875	18.5	43.4	38.6
	900	36.2	68.0	57.3
	925	58.4	102.6	79.9
	950	92.6	135.5	121.0
Coal char	**850**	2.5	1.9	0.8
	875	4.2	3.2	1.4
	900	7.5	5.7	2.6
	925	11.3	9.4	4.3
	950	18.2	15.9	7.6

The higher amounts of K in SW and HW char samples, in comparison to Si and Al, could be responsible for the observed maximums at higher conversion (X > 0.8) compared with SB and coal chars. Even though SB possessed the highest amount of K specie in the ash, the presence of relatively greater amounts of Si, Al and P species resulted in the observed decline in reactivity at higher conversions (Hognon et al., 2014; Masnadi et al., 2015). Coal char exhibited much lower K species in the ash in addition to possessing greatest amounts of Si and Al components, hence, the low gasification reactivity characteristics (Irfan et al., 2011; Zhang et al., 2010). Also, the presence of K, Al and Si species promotes the formation of potassium silicate eutectics reported to diminish gasification reactivity by K-inactivation (Howaniec and Smoliński, 2013; Kajitani et al., 2010; Lahijani et al., 2013a). The formation of the silicate compounds takes place as ash is formed with the progression of gasification. The influence of the inorganic species present in the ash of the chars on the gasification reactivities of the samples was evaluated by the catalytic

indices: AI_1, AI_2 and AI_3. The relationship between R_i, R_s and R_f is presented in Tables 5.2 and Table 5.3).

Graphical illustrations of the correlations between the char characteristics and the gasification reactivities (R_i, R_s, and R_f) are shown in Figures 5.2(a-e). The correlation equations and correlation coefficients, R^2, are presented in Table 5.4. The correlation between L_a and the ratio, L_c/d_{002}, with reactivity could be drawn for the biomass data, while the coal char data were outliers as a result of its lower L_a, reactivity, and micropore surface area. For biomass char samples, L_a showed linear correlations with R_i, R_s and R_f with $R^2 > 0.99$. The L_c/d_{002} also showed similar trends, with $R^2 > 0.9$. The gasification reactivity could also be predicted from the H/C ratio as well as the AI_2 as shown in Figures 5.2(a) and 5.2(b), respectively. From the correlation coefficients, the H/C ratio, and by extension aromaticity (Mafu et al., 2017), had more influence on the R_i and R_f than R_s, while the linear correlation for AI_2 had the least correlation coefficient for R_f. These observations imply that the lattice structure governed the initial reactivity, however, during the course of the gasification, more structural and chemical properties of the char sample contributed to the observed reactivities. For biomass char samples, a 2nd order polynomial correlation could be drawn between the micropore surface areas and the reactivities (Figure 5.2(e)). However, coal char correlation in this regard was an outlier due to their significantly lesser micropore surface areas and reactivities (see Tables 5.2 and 5.3). Summarily, the gasification reactivities of the investigated feedstocks can be predicted from the H/C ratio and the catalytic index, AI_2, irrespective of the nature of feedstock. However, L_a, L_c/d_{002} ratio, and the micropore surface area can only be used to predict the gasification reactivity of biomass samples with regards to this study.

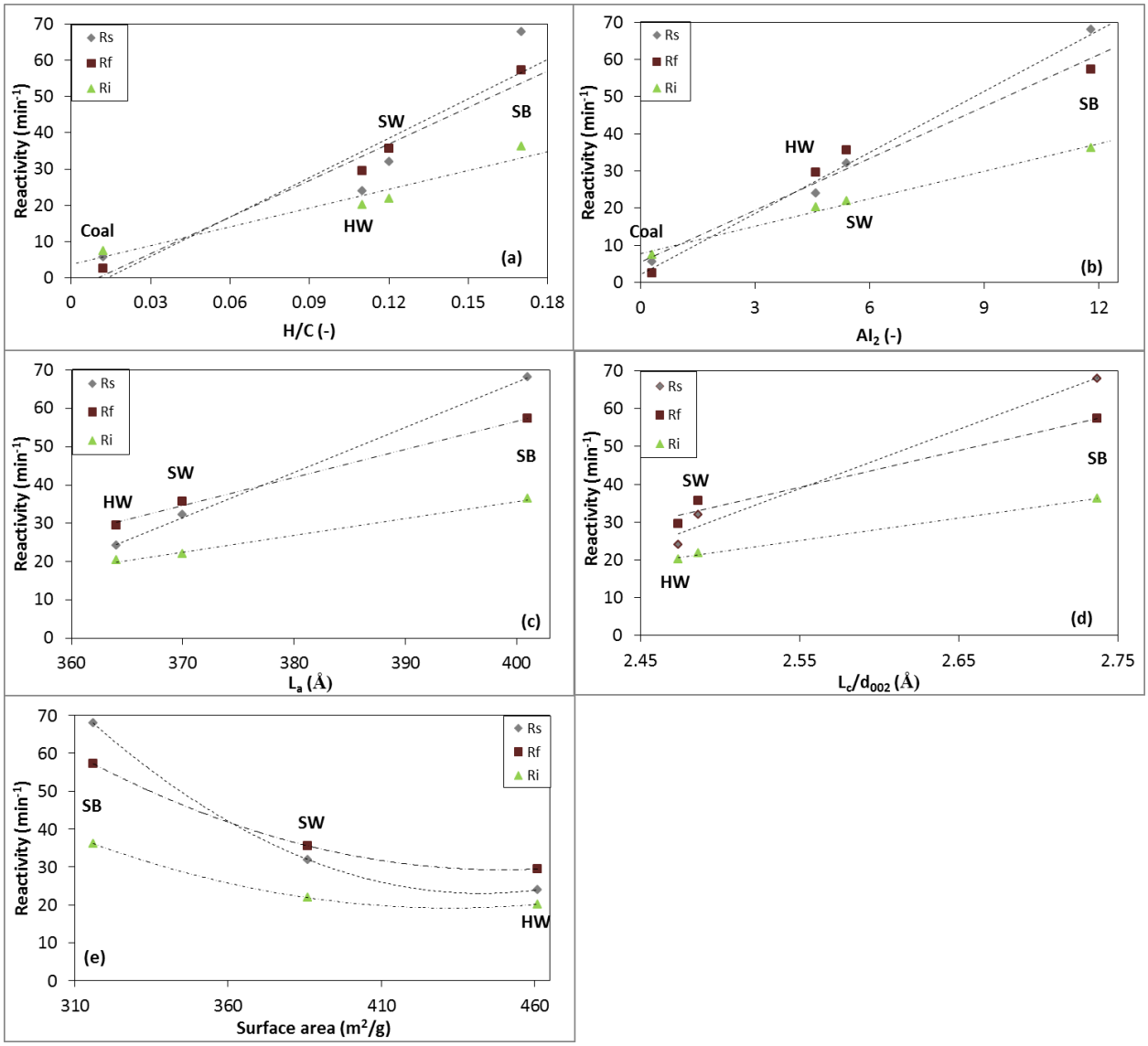

Figure 5-2: The correlation between various char characteristics with gasification reactivities

Table 5-4: Correlation equations between the reactivity and various char characteristics

Parameters	Correlation equation	R^2
L_a	$R_i = 0.44(L_a) - 141$	0.997
	$R_s = 1.18(L_a) - 405$	0.999
	$R_f = 0.735(L_a) - 237$	0.997
L_c/d_{002}	$R_i = 59.1(L_c/d_{002}) - 126$	0.997
	$R_s = 157(L_c/d_{002}) - 361$	0.984
	$R_f = 97.1(L_c/d_{002}) - 208$	0.972
H/C	$R_i = 172(H/C) + 3.71$	0.936
	$R_s = 362(H/C) - 4.89$	0.839
	$R_f = 336(H/C) - 3.44$	0.977
AI_2	$R_i = 2.47(AI_2) + 7.83$	0.992
	$R_s = 5.49(AI_2) + 2.16$	0.992
	$R_f = 4.65(AI_2) + 5.55$	0.961
S.A.	$R_i = 0.0013(SA)^2 - 1.08(SA) + 253$	1
	$R_s = 0.0028(SA)^2 - 2.49(SA) + 573$	1
	$R_f = 0.0016(SA)^2 - 1.42(SA) + 347$	1

SA – surface area

5.3.3 Biomass-coal char blends gasification

The co-gasification behaviour of biomass and coal char samples is presented in Figure 5.3. There was no significant change in the gasification reactivity with the addition of 10% biomass char samples to the coal char (Figure 5.3a). This may be due to the physical effect as discussed by Ding et al. (2014). However, further additions of the biomass char for co-gasification resulted in increased gasification reactivity, for all biomass char samples. There were more contributions of the catalytic mineral species from the biomass ash as the biomass fraction was increased, hence the increase in gasification reactivity. These observations are further confirmed by the reactivity

data presented in Table 5.5, where with increasing biomass fractions, R_i significantly increased, compared with R_s and R_f for SW and HW chars. There was significant increase in the value of R_s and R_f as the SB char fraction in the blends was increased. Biomass-coal char blends co-gasification for SW and HW chars resembled Ca-catalysed gasification reaction as shown by the reactivity maximum at lower conversion (Zhang et al., 2010). The co-gasification behaviour of SB and HW samples at 900 °C are shown in Figure S5.4 of the Supplementary data.

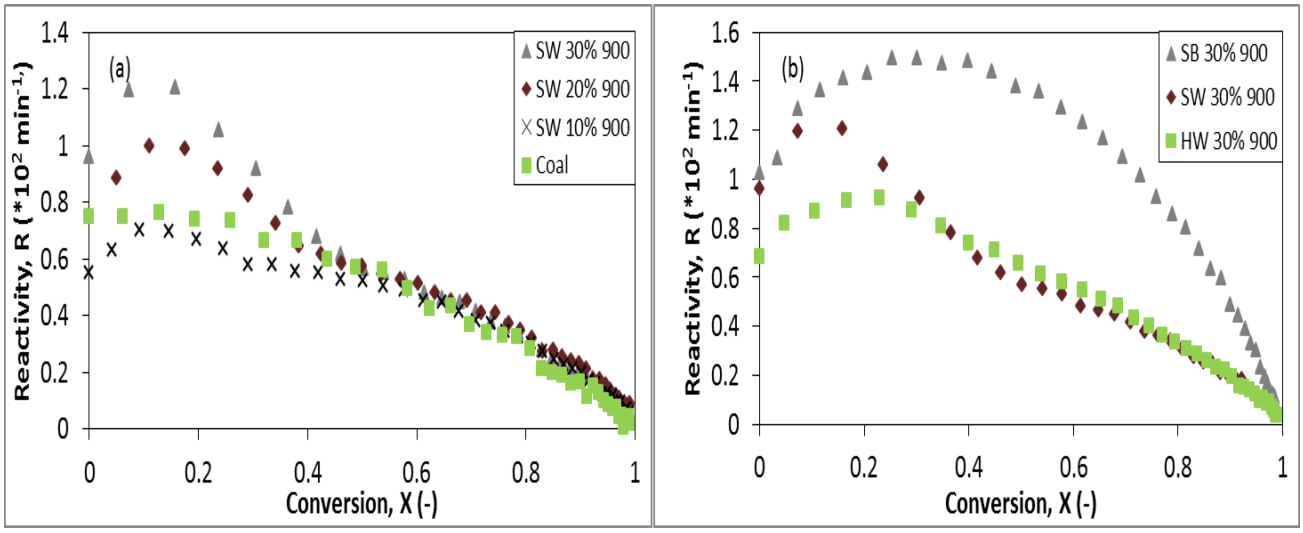

Figure 5-3: The biomass-coal char blends co-gasification behaviour

Table 5-5: Gasification parameters for the CO_2 co-gasification of biomass- and coal- char blends at 900°C

Parameter		Coal char	SW char			HW char			SB char		
			10%	20%	30%	10%	20%	30%	10%	20%	30%
Experimental Reactivity (min^{-1}) ($x10^3$)	$R_{i,ave}$	7.6	6.3	8.8	10.8	6.2	8.3	10.9	6.3	8.9	11.9
	R_s	5.5	6.0	7.9	9.0	5.3	7.1	7.6	7.3	10.2	14.1
	$R_{f,ave}$	2.5	2.9	3.1	2.9	2.5	2.7	2.8	3.6	5.7	7.6
Calculated Reactivity (min^{-1}) ($x10^{-3}$)	$R_{i,ave}$	-	9	10.4	11.8	8.7	10	11.2	10.4	13.3	16.1
	R_s	-	8.5	10.7	12.9	7.7	9.1	10.5	10.8	15.3	19.8
	$R_{f,ave}$	-	5.9	9.2	12.5	5.9	9.2	12.5	8.0	13.5	19.0
Synergy Factor (-)	$R_{i,ave}$	-	0.70	0.85	0.92	0.71	0.83	0.97	0.61	0.67	0.74
	R_s	-	0.71	0.74	0.70	0.69	0.78	0.72	0.68	0.67	0.71
	$R_{f,ave}$	-	0.49	0.34	0.23	0.42	0.29	0.22	0.45	0.42	0.40

SW and HW char samples had similar effect on the co-gasification reactivity, where an increase in the reactivity was observed at lower conversion, and beyond X = 0.4, the co-gasification reactivity was similar to the gasification reactivity of coal char (Figure 5.3a and 5.3b). This observation could be as result of the biomass fraction in the blends reacting preferably than coal, or a combination of the preferential reaction of the biomass and the catalysis by the biomass. Beyond X = 0.4, the catalysts in the biomass may be de-activated by the formation of silicate eutectics such as $KAlSiO_4$ (Ding et al., 2014). The addition of SB char to coal char for gasification resulted in the increase in the gasification reactivity throughout the conversion range, as shown in Figure 5.3b. The higher ash yield and the ash composition of SB char may have shielded the abstraction of K species.

The experimental and calculated biomass char gasification and biomass-coal chars co-gasification reactivity results for experiments at 900 °C are presented in Table 5.5, while data for 850 and 950 °C are given in Tables S5.1 and S5.2 of the supplementary information. The synergy factor (SF) was < 1 for all char-blends-CO_2 co-gasification reported in this study and at

all stages of conversion. Even though the co-gasification of biomass and coal chars resulted in increased reactivity compared to coal char, there was no synergy observed at any stage of gasification. These observations were made by other researchers for different biomass samples and coal (Jeong et al., 2015; Tursun et al., 2016). The lack of synergy may have been as a result of the high pyrolysis temperatures as well as the low biomass fractions used in this study. However, the lack of synergistic effect is not related to catalysis or inhibition in terms of the catalytic influence of the chemical species in the ash (Hu et al., 2013). SW and HW chars had similar SFs while SB char exhibited the highest SFs at all stages of conversion. There was an observed increase in the SF calculated from R_i (SFR_i) with increasing biomass char fraction in the blends, however, when calculated using R_f (SFR_f) and R_s (SFR_s), it decreased significantly with increasing biomass char fraction. There was also an observed decrease in the SF as conversion increased, as can be noted from the decreasing order of SF as conversion progressed: $SFR_i > SFR_s > SFR_f$, for all biomass char samples.

5.3.4 Kinetic modelling

The experimental data from coal gasification was well described by the RPM and this has been reported by other researchers (Ding et al., 2014; Lahijani et al., 2013b). Figure 5.4 shows the model fitting results of SW char gasification. For the gasification of SW and HW chars, the maximum reaction rate was at higher conversions, thus, the MRPM with the condition $\theta = c(1-X)$ fitted the experimental data. For SB char, the maximum reaction rate was neither at low conversion nor at higher conversion, as such, both conditions ($\theta = cX$ and $\theta = c(1 - X)$) could be satisfied. The structural parameters, ψ, ranging from 15 – 21, also decreased in the same order: SW > HW > SB and did not vary with the gasification temperature. These were similar to the reported results by Ding et al. (2014) for corn stalk chars, but differ in order of magnitude due to varying char characteristics. The value of c was found to be similar for the gasification of the different biomass char samples and were consistent with the findings of Zhang et al., (2008) for various saw dusts, barks and bagasse samples and Ding et al. (2014) for corn stalk chars. The value of p (4.4 – 8.7) decreased in the order: SW > HW > SB and were found to be within the range of values (3.3 – 9.0) reported for cryptomeria bark, ezo pine bark, corncob, bamboo, and various tea grounds by Zhang et al. (2008), and greater than the values (2.3 – 3.8) found for corn stalk chars by Ding et al., (2008). However, greater p values (11.6 – 13.2) have been reported for various saw dusts, chips and barks (Zhang et al., 2008). These differences may be attributed to the differing chemical and structural characteristics of the various biomass chars (Zhang et al., 2008; Jeong et al., 2014; Zuo et al., 2015). The Arrhenius plot for coal char gasification is given

in Figure S5.5 of the Supplementary information. The RPM and MRPM fitting for CO_2 char gasification of SB and HW chars and CO_2 co-gasification results of SB and HW samples at 900 °C are presented in Figures S5.6 and S5.7 of the Supplementary data, respectively.

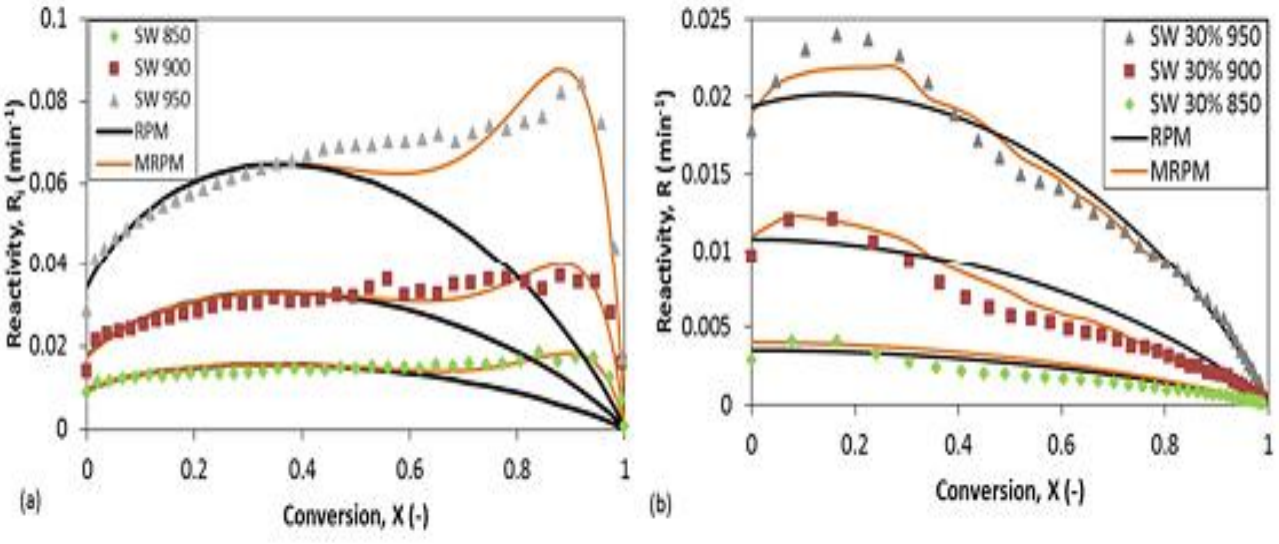

Figure 5-4: RPM and MRPM fitting for (a) SW char gasification and (b) SW-coal char blends co-gasification

Even though the co-gasification with SW and HW chars and coal char resulted in reactivity maximum at lower conversion, the MRPM with the condition, $\theta = c(1–X)$, fitted the experimental data. This was not the case for the co-gasification of corn stalk char with bituminous coal char (50:50% blend) reported by Ding et al. (2014) which fitted the RPM, and is comparable to the findings for the co-gasification of coal chars and SB chars for all SB char fractions. For all the co-gasification experiments at different biomass char to coal char ratios, quality of fits (QOF) > 90% were achieved (Table 5.6).

Table 5-6: Avarage model and kinetic parameters for the model fitting of biomass, coal and biomass-coal char blend samples[a] (850- 950°C)

Sample	**Coal**	**SW char**				**HW char**				**SB char**			
	char	**100%**	**10%**	**20%**	**30%**	**100%**	**10%**	**20%**	**30%**	**100%**	**10%**	**20%**	**30%**
ψ (-)	2.5	15	5.1	4.1	3.1	12	3.3	2.8	2.4	21	6.7	7.9	10.4
c (-)	-	1.20	0.32	0.38	0.41	1.21	0.38	0.40	0.43	1.22	-	-	-
p (-)	-	8.7	3.2	2.7	2.3	7.4	4.2	3.5	2.9	4.4	-	-	-
QOF (%)	97	90	91	91	93	91	94	93	94	91	95	94	95
E_a (kJ/mol)	241	146	232	222	212	128	230	218	207	178	235	228	222

[a]-For coal char samples, the RPM was fitted and for the biomass-coal char blends, the MRPM was fitted

For SW and HW chars co-gasification with coal char, the value of c increased with increasing biomass fraction in the blends. The value of p decreased in the order: SW > HW > SB and tended to increase with increasing biomass char fraction in the blends. There was also an observed decrease in the structural parameter as the biomass fraction increased for SW- and HW-coal chars co-gasification. An opposite trend was observed for SB-coal chars co-gasification. The obtained values of c from this investigation during co-gasification (0.32 – 0.42) were found to be comparatively lower to the reported data (0.90 – 1.91) of Lahijani et al. (2013b), while the p values (2.3 – 4.4) were relatively greater than the p values (1.12 – 3.58) of Lahijani et al. (2013b). The observation of the changes in the values of c, p and ψ are in line with the conclusion from Lahijani et al. (2013b), that all three parameters are linked to the char characteristics, including char structural evolution and inherent inorganic species. The activation energies (E_a) of the gasification reactions of the biomass char samples, coal char sample and biomass-coal char blends are given in Table 5.6. The E_a values for biomass samples in this study were comparable to those reported by Wang et al., (2015) for wheat stalk, rice lemma and pine saw dust. Ea was found to increase in magnitude in the order: HW < SW < SB < coal for the char gasification, and tended to increase with decreasing micropore surface area of the chars. The higher the surface area, the more readily it was for the reactant gas to access gasification reaction sites to initiate gasification. The effect of the biomass char additions on E_a was also evaluated (Table 5.6). For co-gasification, increasing biomass char fraction resulted in decreasing E_a for all

the biomass char samples. This is an indication that the addition of biomass chars improved the coal char gasification (Ding et al., 2014; Lahijani et al., 2013a).

5.4 Prospects

The findings from this investigation are important, since in previous studies in co-gasification of coal with alternative materials in a fixed bed gasifier, more carbon in ash was reported after co-feeding woody waste biomass with lignite due to the relative low reactivity of the blends (Straka and Bucko, 2009). A general disadvantage of the use of biomass in coal fed fixed bed gasifiers is the production of large amounts of tar (Higman and Tam, 2014). Our earlier findings (Mafu et al., 2017), has shown that pre-treatment of biomass at up to 400 °C replicates coal characteristics following the van Krevelen diagram. It has been demonstrated in this paper that, the reactivity of coal char and biomass char blends when compared to coal char gasification, and that blending ratios is an important factor. Thus, biomass char preparation and blending strategies can be formulated for stable gasifier operation. Further studies should however, be conducted at a fundamental level to verify tar formation and ash fusion temperatures on pre-treated biomass and coal blends as well as large scale testing for these blends.

5.5 Conclusions

Biomass gasification reactivity, decreased in the order: SB > SW > HW and were greater than that of coal. Char characteristics such as H/C, AI_2 and L_c/d_{002} and surface area impacted the reactivities of the sample with statistically significant correlation. However, coal properties were outliers in some cases. During co-gasification, R_i, R_s and R_f all increase for SB while for SW and HW, only R_i significantly increased. Biomass gasification and co-gasification with coal could be predicted by the MRPM. The amount of biomass in the blends impacted the kinetic parameters, and Ea decreased with increasing biomass fractions.

References

Ahmad, A.A., Zawawi, N.A., Kasim, F.H., Inayat, A., Khasri, A., 2016. Assessing the gasification performance of biomass: A review on biomass gasification process conditions, optimization and economic evaluation. Renew. Sustain. Energy Rev. 53, 1333–1347.

Andersen, L.K., Morgan, T.J., Boulamanti, A.K., Alvarez, P., Vassilev, S. V., Baxter, D., 2013. Quantitative X-ray fluorescence analysis of biomass: Objective evaluation of a typical commercial multi-element method on a WD-XRF spectrometer. Energy and Fuels 27, 7439–7454.

Azargohar, R., Nanda, S., Kozinski, J.A., Dalai, A.K., Sutarto, R., 2014. Effects of temperature on the physicochemical characteristics of fast pyrolysis bio-chars derived from Canadian waste biomass. Fuel 125, 90–100.

Bouraoui, Z., Dupont, C., Jeguirim, M., Limousy, L., Gadiou, R., 2016. CO_2 gasification of woody biomass chars: The influence of K and Si on char reactivity. Comptes Rendus Chim. 19, 457–465.

Bouraoui, Z., Jeguirim, M., Guizani, C., Limousy, L., Dupont, C., Gadiou, R., 2015. Thermogravimetric study on the influence of structural, textural and chemical properties of biomass chars on CO_2 gasification reactivity. Energy 88, 703–710.

Bunt, J.R., Waanders, F.B., 2008. Identification of the reaction zones occurring in a commercial-scale Sasol-Lurgi FBDB gasifier. Fuel 87, 1814–1823.

Cetin, E., Moghtaderi, B., Gupta, R., Wall, T.F., 2004. Influence of pyrolysis conditions on the structure and gasification reactivity of biomass chars. Fuel 83, 2139–2150.

Ding, L., Zhang, Y., Wang, Z., Huang, J., Fang, Y., 2014. Interaction and its induced inhibiting or synergistic effects during co-gasification of coal char and biomass char. Bioresour. Technol. 173C, 11–20.

Everson, R.C., Okolo, G.N., Neomagus, H.W.J.P., Santos, J., 2013. X-ray diffraction parameters and reaction rate modeling for gasification and combustion of chars derived from inertinite-rich coals. Fuel 109, 148–156.

Fukuda, H., Kondo, A., Noda, H., 2001. Biodiesel fuel production by transesterification of oils. J. Biosci. Bioeng. 92, 405–416.

Gunaseelan, V.N., 1997. Anaerobic digestion of biomass for methane production: A review.

Biomass and Bioenergy 13, 83–114.

Haykiri-Acma, H., Yaman, S., 2007. Synergy in devolatilization characteristics of lignite and hazelnut shell during co-pyrolysis. Fuel 86, 373–380.

Hognon, C., Dupont, C., Grateau, M., Delrue, F., 2014. Comparison of steam gasification reactivity of algal and lignocellulosic biomass: influence of inorganic elements. Bioresour. Technol. 164, 347–53.

Howaniec, N., Smoli, A., 2011. Steam co-gasification of coal and biomass derived chars with synergy effect as an innovative way of hydrogen-rich gas production. International journal of hydrogen energy 36, 14455 - 14463.

Howaniec, N., Smoliński, A., 2013. Steam co-gasification of coal and biomass - Synergy in reactivity of fuel blends chars. Int. J. Hydrogen Energy 38, 16152–16160.

Hu, J., Liu, L., Cui, M., Wang, J. 2013. Calcium-promoted catalytic activity of potassium carbonate for gasification of coal char: The synergistic effect unrelated to mineral matter in coal. Fuel 111, 628-635.

Huang, Y., Yin, X., Wu, C., Wang, C., Xie, J., Zhou, Z., Ma, L., Li, H., 2009. Effects of metal catalysts on CO_2 gasification reactivity of biomass char. Biotechnol. Adv. 27, 568–72.

Huo, W., Zhou, Z., Chen, X., Dai, Z., Yu, G., 2014. Study on CO_2 gasification reactivity and physical characteristics of biomass, petroleum coke and coal chars. Bioresour. Technol. 159, 143–9.

Irfan, M.F., Usman, M.R., Kusakabe, K., 2011. Coal gasification in CO_2 atmosphere and its kinetics since 1948 : A brief review. Energy 36, 12–40.

Jeong, H.J., Hwang, I.S., Hwang, J., 2015. Co-gasification of bituminous coal – pine sawdust blended char with H_2O at temperatures of 750 – 850°C. Fuel 156, 26–29.

Jeong, H.J., Park, S.S., Hwang, J., 2014. Co-gasification of coal – biomass blended char with CO_2 at temperatures of 900 – 1100°C. Fuel 116, 465–470.

Kajitani, S., Zhang, Y., Umemoto, S., Ashizawa, M., Hara, S., 2010. Co-gasification reactivity of coal and woody biomass in high-temperature. Energy & Fuels 24, 145–151.

Lahijani, P., Zainal, Z.A., Mohamed, A.R., Mohammadi, M., 2013a. CO_2 gasification reactivity of biomass char: catalytic influence of alkali, alkaline earth and transition metal salts. Bioresour. Technol. 144, 288–95.

Lahijani, P., Zainal, Z.A., Mohamed, A.R., Mohammadi, M., 2013b. Co-gasification of tire and biomass for enhancement of tire-char reactivity in CO_2 gasification process. Bioresour. Technol. 138, 124–130.

Lahijani, P., Zainal, Z.A., Mohamed, A.R., Mohammadi, M., 2013c. Ash of palm empty fruit bunch as a natural catalyst for promoting the CO_2 gasification reactivity of biomass char. Bioresour. Technol. 132, 351–355.

Liu, Z., Quek, A., Balasubramanian, R., 2014. Preparation and characterization of fuel pellets from woody biomass , agro-residues and their corresponding hydrochars. Appl. Energy 113, 1315–1322.

Mafu, L.D., Neomagus, H.W.J.P., Everson, R.C., Carrier, M., Strydom, C.A., Bunt, J.R., 2016. Structural and chemical modifications of typical South African biomasses during torrefaction. Bioresour. Technol. 202, 192–197.

Mafu, L.D., Neomagus, H.W.J.P., Everson, R.C., Strydom, C.A., Carrier, M., Okolo, G.N., Bunt, J.R., 2017. Chemical and structural characterization of char development during lignocellulosic biomass pyrolysis. Bioresour. Technol. 243, 941–948.

Masnadi, M.S., Grace, J.R., Bi, X.T., Lim, C.J., Ellis, N., 2015. From fossil fuels towards renewables: Inhibitory and catalytic effects on carbon thermochemical conversion during co-gasification of biomass with fossil fuels. Appl. Energy 140, 196–209.

Mata, T.M., Martins, A.A., Caetano, N.S., 2010. Microalgae for biodiesel production and other applications: A review. Renew. Sustain. Energy Rev. 14, 217–232.

Min, F., Zhang, M., Zhang, Y., Cao, Y., Pan, W.-P., 2011. An experimental investigation into the gasification reactivity and structure of agricultural waste chars. J. Anal. Appl. Pyrolysis 92, 250–257.

Niu, Y., Du, W., Tan, H., Xu, W., Liu, Y., Xiong, Y., Hui, S., 2013. Further study on biomass ash characteristics at elevated ashing temperatures: the evolution of K, Cl, S and the ash fusion characteristics. Bioresour. Technol. 129, 642–5.

Okolo, G.N., Everson, R.C., Neomagus, H.W.J.P., Roberts, M.J., Sakurovs, R., 2015. Comparing the porosity and surface areas of coal as measured by gas adsorption, mercury intrusion and SAXS techniques. Fuel 141, 293–304.

Rosillo-Calle, F., 2016. A review of biomass energy- shortcomings and concerns. J. Chem.

Technol. Biotechnol. 1933–1945.

Ruiz, J.A., Juarez, M.C., Morales, M.P., Munoz, P., Mendivil, M.A., 2013. Biomass gasification for electricity generation : Review of current technology barriers. Renew. Sustain. Energy Rev. 18, 174–183.

Suliman, W., Harsh, J.B., Abu-Lail, N.I., Fortuna, A.M., Dallmeyer, I., Garcia-Perez, M., 2016. Influence of feedstock source and pyrolysis temperature on biochar bulk and surface properties. Biomass and Bioenergy 84, 37–48.

Taba, L.E., Faisal, M., Ashri, W., Wan, M., Chakrabarti, M.H., 2012. The effect of temperature on various parameters in coal , biomass and Co-gasification : A review. Renew. Sustain. Energy Rev. 16, 5584–5596.

Tursun, Y., Xu, S., Wang, C., Xiao, Y., Wang, G., 2016. Steam co-gasification of biomass and coal in decoupled reactors. Fuel Process. Technol. 141, 61–67.

Wang, F., Zeng, X., Wang, Y., Su, H., Yu, J., Xu, G., 2016. Non-isothermal coal char gasification with CO_2 in a micro fluidized bed reaction analyzer and a thermogravimetric analyzer. Fuel 164, 403–409.

Weldemichael, Y., Assefa, G., 2015. Assessing the energy production and GHG (greenhouse gas) emissions mitigation potential of biomass resources for Alberta. J. Clean. Prod. 112, 4257–4264.

Xue, G., Kwapinska, M., Horvat, a, Kwapinski, W., Rabou, L.P.L.M., Dooley, S., Czajka, K.M., Leahy, J.J., 2014. Gasification of torrefied Miscanthus × giganteus in an air-blown bubbling fluidized bed gasifier. Bioresour. Technol. 159, 397–403.

Zhang, Y., Ashizawa, M., Kajitani, S., Miura, K., 2008. Proposal of a semi-empirical kinetic model to reconcile with gasification reactivity profiles of biomass chars. Fuel 87, 475–481.

Zhang, Y., Hara, S., Kajitani, S., Ashizawa, M., 2010. Modeling of catalytic gasification kinetics of coal char and carbon. Fuel 89, 152–157.

Zhang, Y., Zheng, Y., Yang, M., Song, Y., 2016. Effect of fuel origin on synergy during co-gasification of biomass and coal in CO_2. Bioresour. Technol. 200, 789–794.

Zuo, H., Geng, W., Zhang, J., Wang, G., 2015. Comparison of kinetic models for isothermal CO_2 gasification of coal char-biomass char blended char. Int. J. Miner. Metall. Mater. 22, 363–370.

Supplementary Information (SI)

S5 Supplementary data from char gasification and co-gasification

This subsection presents supplementary gasification data that were not presented in the accepted article from Chapter 5. This includes conversion, reactivity and Arrhenius plots. The explanations of these figures are similar to the ones given in the chapter.

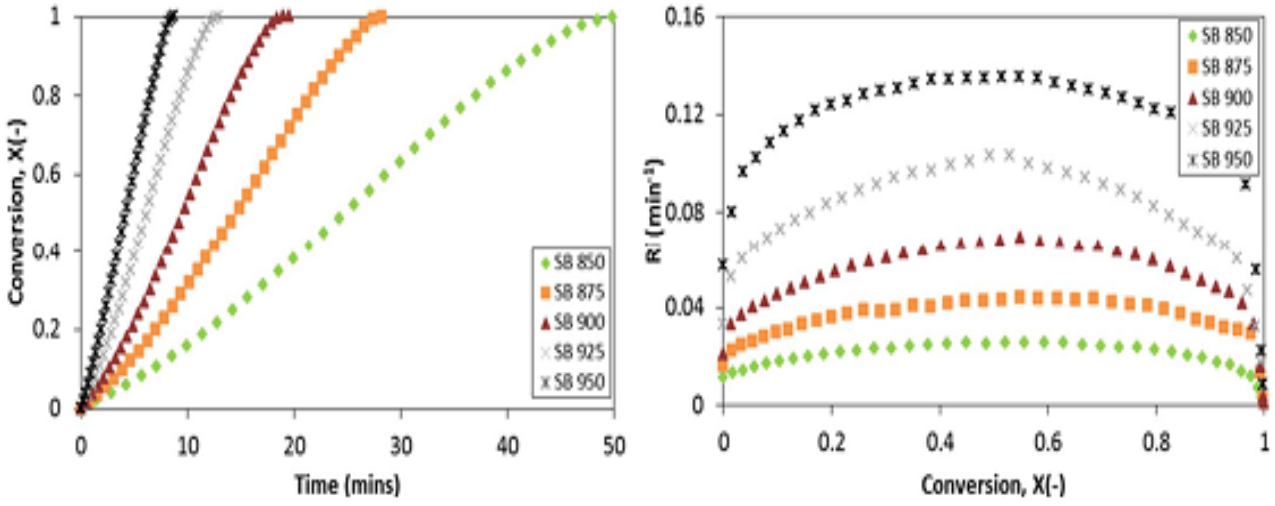

Figure S 5-5: CO_2 gasification results for SB char

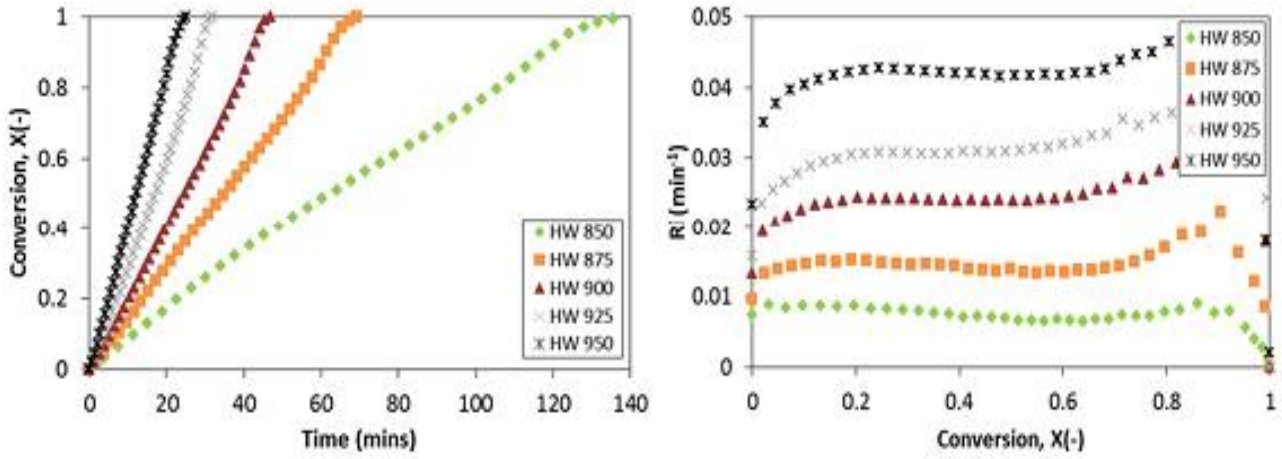

Figure S 5-2: CO_2 gasification results for HW char

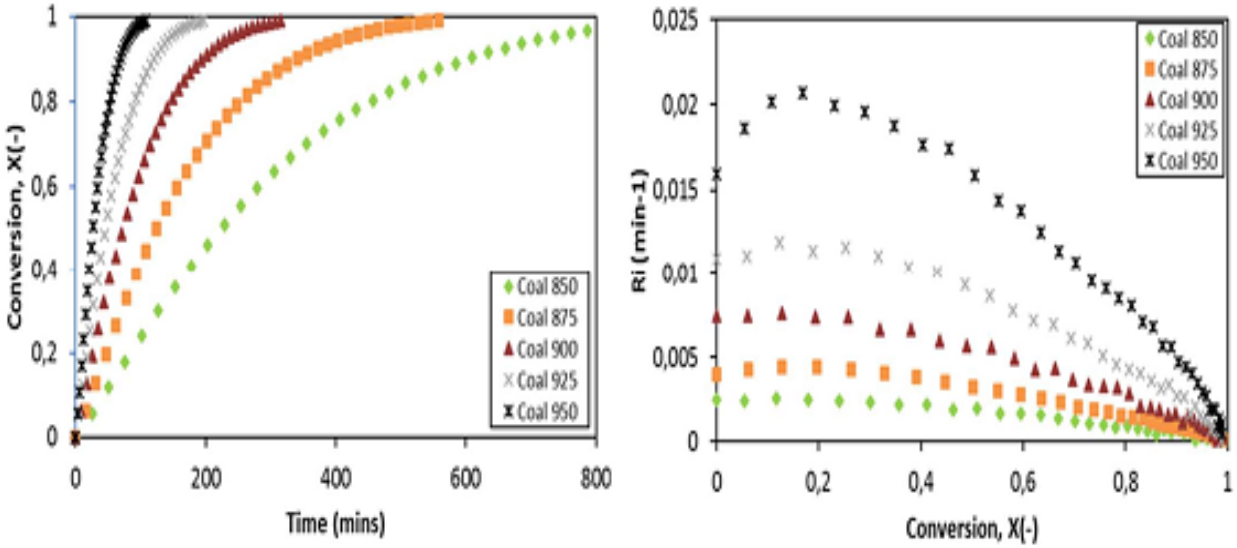

Figure S 5-3: CO_2 gasification results for HW char

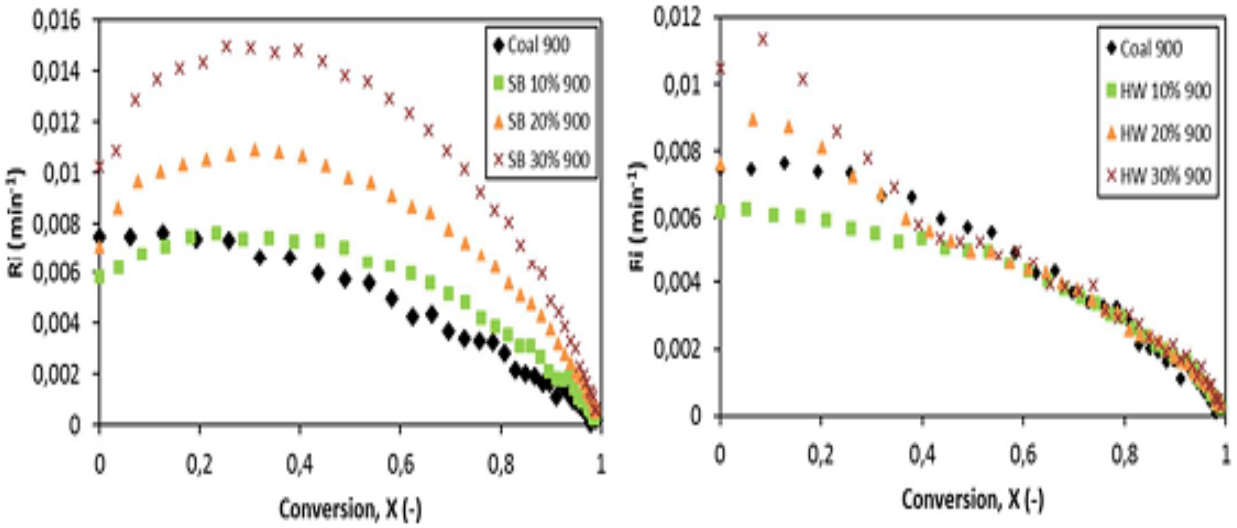

Figure S 5-4: Co-gasification results as shown for 900°C

Table S 5-7: Gasification parameters for the CO_2 co-gasification of biomass- and coal- char blends at 850 °C

Parameter		Coal char	SW char			HW char			SB char		
			10%	20%	30%	10%	20%	30%	10%	20%	30%
Experimental Reactivity (min^{-1}) ($x10^3$)	$R_{i,ave}$	7.6	2.2	3.0	3.4	2.6	3.6	4.3	2.4	2.9	4.0
	R_s	5.5	2.1	2.2	3.0	2.0	2.2	2.9	2.6	3.3	5.0
	$R_{f,ave}$	2.5	0.91	0.93	0.98	0.88	0.89	1.0	1.2	1.7	3.2
Calculated Reactivity (min^{-1}) ($x10^{-3}$)	$R_{i,ave}$	-	3.4	4.2	5.1	3.1	3.6	4.3	3.6	4.7	5.9
	R_s	-	3.3	4.3	5.4	2.8	3.3	3.9	4.0	5.9	7.7
	$R_{f,ave}$	-	2.3	3.8	5.4	2.3	3.9	5.4	2.9	4.9	6.9
Synergy Factor (-)	$R_{i,ave}$	-	0.65	0.71	0.67	0.84	1.0	1.0	0.67	0.62	0.68
	R_s	-	0.64	0.51	0.56	0.71	0.67	0.74	0.65	0.56	0.65
	$R_{f,ave}$	-	0.40	0.24	0.18	0.38	0.23	0.19	0.41	0.35	0.46

Table S 5-2: Gasification parameters for the CO2 co-gasification of biomass- and coal- char blends at 850 °C

Parameter		Coal char	SW char			HW char			SB char		
			10%	20%	30%	10%	20%	30%	10%	20%	30%
Experimental Reactivity (min^{-1}) ($x10^3$)	$R_{i,ave}$	7.6	16.3	18.1	20.6	16.5	20.4	23.5	15.7	21.3	22.9
	R_s	5.5	16.0	18.2	19.6	16.1	17.6	20.7	18.5	24.4	33.0
	$R_{f,ave}$	2.5	8.1	8.6	8.6	7.8	8.1	8.2	9.8	13.3	16.5
Calculated Reactivity (min^{-1}) ($x10^{-3}$)	$R_{i,ave}$	-	20.7	23.2	25.7	19.9	21.6	23.3	25.7	33.1	40.5
	R_s	-	22.3	26.1	29.9	20.6	22.8	25.0	28.1	37.8	47.5
	$R_{f,ave}$	-	14.5	21.4	28.2	14.5	21.4	28.2	18.9	30.3	41.7
Synergy Factor (-)	$R_{i,ave}$	-	0.79	0.78	0.80	0.83	0.94	1.01	0.61	0.64	0.57
	R_s	-	0.72	0.70	0.66	0.78	0.77	0.83	0.66	0.65	0.69
	$R_{f,ave}$	-	0.56	0.40	0.30	0.54	0.38	0.29	0.52	0.44	0.40

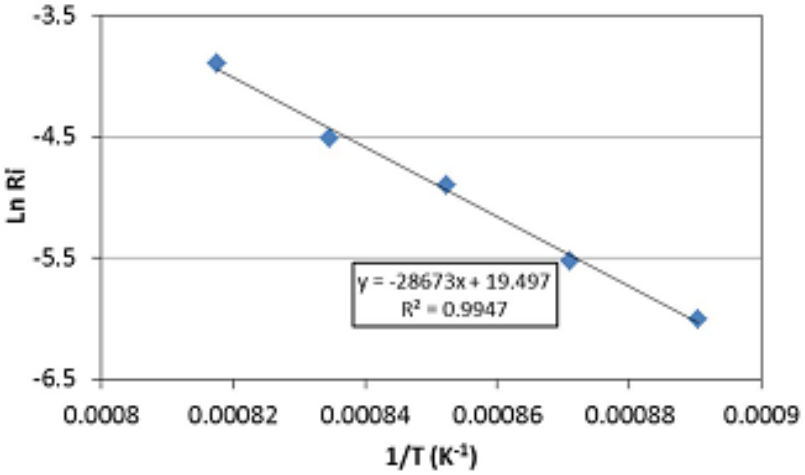

Figure S 5-5: Arrhenius plot for coal char gasification

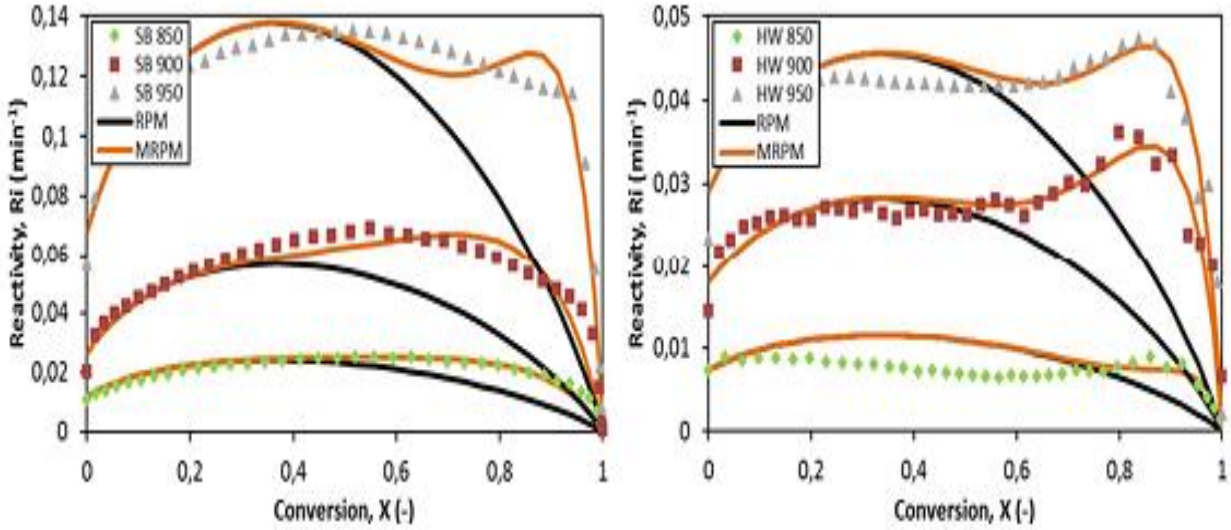

Figure S 5-6: RPM and MRPM fitting for CO_2 char gasification: (a) SB gasification (b) HW char gasification

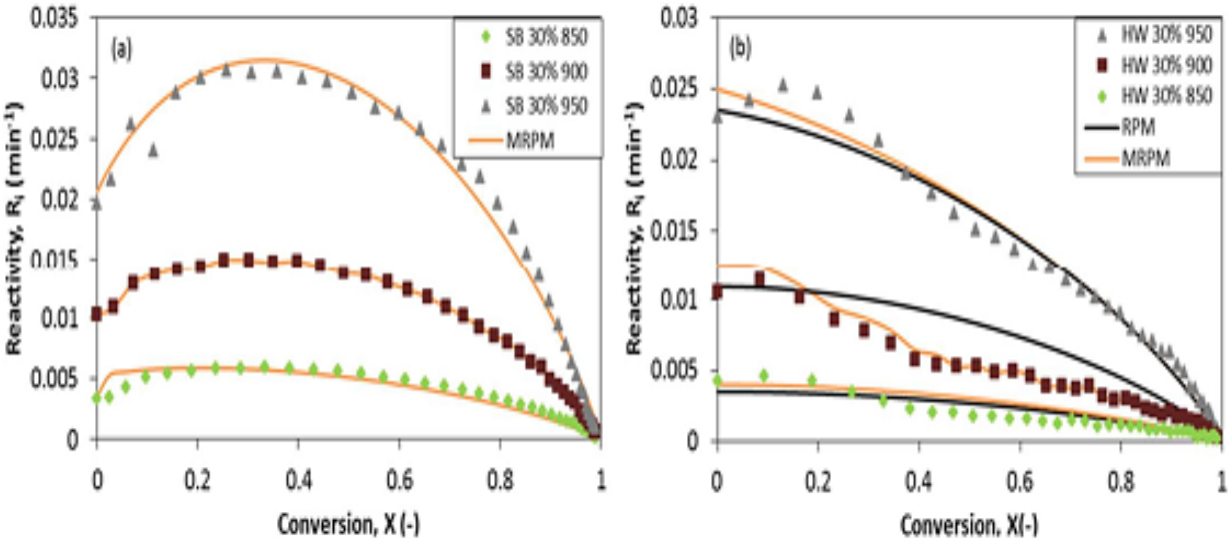

Figure S 5-7: Co-gasification results as shown for 900°C

Chapter 6: Conclusions and Recommendations

6.1 General conclusions

Softwood chips (SW) and hardwood chips (HW) had comparable characteristics, while sweet sorghum bagasse (SB) has significantly different features. Torrefaction improved the fuel properties of biomass, and the differences in characteristics resulted in different torrefaction times needed to achieve a 30% mass loss for the different biomass samples: 110, 100 and 20 minutes for SW, HW and SB respectively. At this torrefaction conditions, hemicelluloses were the most degraded and this resulted in an increase in aromaticity and reduction in the crystallite diameter. An increase in the surface area was only observed for SB due to the low lignin and high hemicellulose content when compared to the woody samples (Tripathi et al., 2016). The slight degradation of celluloses could be concluded from CPMAS ^{13}C NMR spectroscopy results and the peaks linked to the presence of lignin were useful in concluding that torrefaction did not increase the lignin amounts in biomass.

The pyrolysis of WH, HW and SB at 10°C/min in streaming N_2 was investigated. At low temperatures (< 600 °C) the degradation of fibre components was accompanied by the reduction of aliphatic groups and the conjugation of aromatic rings. This results in the loss of amorphous carbon whilst the aromaticity increased. These conclusions were drawn from ATR-FTIR, CPMAS ^{13}C NMR and WA-XRD-CFA. Further, a method developed for the determination of aromaticity using ATR-FTIR yielded results that are comparable to those of CPMAS ^{13}C NMR. The structural changes at the first stage of char formation was mostly the ordering and graphitization of the carbon lattice which, at this stage, allowed for pore development and consequently an increased in the surface area. The second stage of char formation (600 – 1100 °C) was mainly the reorganization of bonds as the biomass samples undergo structural core degradation (Link et al., 2008; Novak et al., 2009). However, more investigations are needed to ascertain the exact stages where the char formation mechanism changes (Varhegyi and Jakab, 1994; Giudicianni et al., 2013; Di Blasi and Lanzetta, 1997) The increase in aromaticity was as a result of the increase in the degree of aromatic ring condensation. The changes in elemental H, O and C at this stage are not as gradual as in the first stage. Proximate results also slightly changed at the second stage when compared to the first stage. The degree of graphitization at 1100 °C and possible coalescence of pores resulted in the reduction of the surface area, as carbon sheets were drawn into almost flat sheets at this pyrolysis temperature.

The CO_2-char gasification of biomass may be divided into three sections: (1) the initial stage (quantified by the average initial reactivity) where the surface area has the major effect, (2) the intermediate stage (quantified by the reactivity index) where the reactivity was related to the carbon structure (d_{002}/L_c) and finally the final stage where the mineral matter content played a dominant role. The absence of Si, Al and P in the chars of SW and HW resulted in an increase in the gasification rate at high conversions (R_f) and SB showed a decrease after X=0.6. This reduction was as a result of pore collapse and the formation of gasification retardants which captured K. The observed initial gasification rates (R_i) may be a result of the surface area and density of the chars. Coal char gasification recorded much lower reactivity than all biomass char samples.

The co-gasification of biomass and coal char resulted in improved gasification rates compared to coal. However, SW and HW improved the reactivity only for X=0-0.5 after which the reactivity of biomass coal blends was equal to the reactivity of coal. The addition of 10% biomass to coal char did not result in significant changes in the gasification rate due to the physical effect. With increase in the biomass fraction, the physical effect was overcome and the overall co-gasification reactivity increased until K-inactivation at X > 0.5. HW and SW showed almost similar gasification characteristics during co-gasification compared to SB. This was a result of the similarities in characteristics for HW and SW, which were different for SB. The MRPM better predicted biomass char gasification and SW/HW-coal char co-gasification, whilst SB-coal char co-gasification was described by RPM. An increase in the biomass fraction had the same impact on the reactivity, as did catalyst loading and this resulted in a slight change in the model parameters (ψ, c and p) (Zhang et al., 2010).

6.2 Contributions to the knowledge of biomass energy

The following are considered a valuable contribution to the knowledge in biomass energy:

- An elaborate chemical and structural characteristics' comparison of softwood chips, hardwood chips and sweet sorghum bagasse.
- The use of complimentary characterisation techniques (WA-XRD-CFA and CPMAS ^{13}C NMR) to track the effect of torrefaction of SW, HW and SB.
- The structural and chemical characteristics of the different biomass samples were related to the composition of the fibre components.

- As char formation proceeds, the aromaticity increased in two ways: at lower temperature charring through the elimination of aliphatic groups simultaneously with the conjugation of aromatic rings then the second step at higher temperatures where the main reaction is the conjugation of aromatic rings,
- The analysis of ATR-FTIR results to determine the aromaticity, the degree of cyclisation by determining the ratio CH_2/CH_3.
- The correlation of chemical and structural characteristics: H/C and aromaticity, H/C and the degree of aromatic ring condensation, the aromaticity and CH_2/CH_3 and lastly the pyrolysis temperature and the surface area.
- The analysis of gasification was segmented into three sections namely, initial reactivity ($0 \leq X \leq 0.3$), reactivity index (R at t_{50}) and final reactivity ($0.7 \leq X \leq 0.9$).
- The comparison of the gasification of the three biomass samples with coal.
- The gasification reactivity, at all stages of the conversion, were successfully linked to d_{002}/L_c, AI, L_a, H/C and $(R/C)_u$.
- Low biomass ratio addition during co-gasification resulted in improved gasification rates, however no synergetic effects were observed when blended with coal.

6.3 Recommendations for future work

The torrefaction step as a pre-step for gasification may improve the gasification efficiencies, and can further reduce logistic costs of biomass as a fuel source. As a result, a techno economic and energy balance evaluation is recommended, from which torrefaction may be carefully included in the net biomass conversion process, either at the point of source or as a pre-step in gasifiers. The characterization of lignocellulosic biomass and the chemical and structural changes during both torrefaction and pyrolysis may be elevated by the use of both high resolution transmission electron microscopy (HRTEM), density measurements and small angle X-ray scattering (SAXS). These techniques will complement the characterization results reported in literature and those presented in this work by providing more information on surface area and porosity of biomass samples, property ranges that are not covered by XRD and CO_2 gas adsorption. SAXS probes a wider range of pores even those of diameters between 5 and 17 Å. The investigation of particle size and shape during torrefaction and the char formation process is a need for this study. It is anticipated that different shapes and sizes of particles would result in different weight loss kinetics and characteristics changes because internal temperature gradient and temperature

overshoots towards the centre-line are dependent on particle size, shape and bulk density. The inclusions of more biomass samples, or different classes, would enrich the information on biomass characteristics' variability and this would be inform the beneficial biomass use in the fields of thermochemical conversion. Torrefaction kinetics is another area that needs attention. After adequate analysis of torrefaction characteristics, more elaborate kinetics may be extracted for both isothermal and non-isothermal conditions which should be an extension of the works by Prins et al (Prins et al., 2006) and (Hattingh et al., 2014).

Quench gasification for biomass and biomass-coal blends gasification may provide insights into pore development during gasification and the assumptions made in this study herein. It will monitor the formation of gasification retardants, pore development and ash formation during gasification. Quench gasification during co-gasification of biomass with coal may help in following the consumption of the different chars as the reaction progressed. It is further recommended that the comparison of the co-gasification of chars from co-pyrolysis and the co-gasification of char blends.

For techno economic evaluation of the torrefaction step to be included in the conversion of biomass for energy production, the torrefaction – grinding sequence would be important as this sequence will impact on the power generation efficiency. The investigation of particle size and shape would provide another dimension to the explanation of the trends observed for torrefaction, char formation and gasification kinetics. It is anticipated that different shapes and sizes of particles would result in different weight loss kinetics and characteristics changes because internal temperature gradient and temperature overshoots towards the centre-line are dependent on particle size, shape and bulk density (Bates and Gloniem, 2014).